Abstract

YEH, TING-FENG. Chemical and structural characterizations of juvenile wood, mature wood, and compression wood of loblolly pine (*Pinus taeda*). (Under the direction of Dr. Hou-min Chang and Dr. John F. Kadla)

In an effort to comprehensively study the wood property variation in juvenile wood, compression wood, and mature wood, and also to provide a rapid and cost-effective assessment tool to screening the wood chemical property variation, several loblolly pines (*Pinus tadea*), and transmittance near infrared spectroscopy were utilized in this study. The method development results show that a successful screening of wood chemical property variation, such as lignin and α-cellulose contents, could be adapted using stacked wood wafers microtomed from increment cores and combining with transmittance near infrared spectroscopy. The morphological, chemical, and metabolic analyses of juvenile wood and compression wood show that although compression wood and juvenile wood share some properties, they are actually distinct in their chemistry during development and in final wood chemistry and anatomy. The within tree variation analyses also show that juvenile wood from the top of the tree and that from the base of the tree are more different in morphological structures than in chemical structures. A similar pattern was found between juvenile wood and mature wood. The results obtained suggest that the within tree compression wood percentage and the fiber quality differences inherent in juvenile wood appear to have a greater influence on the final wood products.

Chemical and Structural Characterizations of Juvenile Wood, Mature Wood, and Compression Wood of Loblolly Pine (*Pinus taeda*)

by

Ting-Feng Yeh

A dissertation submitted to the Graduate Faculty of
North Carolina State University
In partial fulfillment of the
Requirements for the degree of
Doctor of Philosophy

Wood and Paper Science

Raleigh

2005

Approved by:

Dr. Hou-min Chang	Dr. John F. Kadla
Co-chair of Advisory Committee	Co-chair of Advisory Committee
Dr. Vincent L. Chiang	Dr. Barry Goldfarb

I would like to dedicate this dissertation to my parents

and my beloved, Riva, all of whom had a major influence

on my life, goals and ambitions.

Biography

Ting-Feng Yeh received his B.S. degree in Forest Science from National Taiwan University, Taiwan in 1995. He continued his graduate work in the same department and received his M.S. degree in Forest Product in 1997.

After graduation, he served in the army for two years till 1999, and after that he became a full-time teaching assistant in Department of Chemistry, National Taiwan University till 2001.

In the fall of 2001, the author began the Ph.D. curriculum in the Department of Wood and Paper Science under the direction of Dr. Hou-min Chang and Dr. John F. Kadla.

Acknowledgements

The author would like to express his sincere appreciation for the guidance and support from Dr. Hou-min Chang and Dr. John F. Kadla, co-chairmen of his advisory committee. Their constant encouragement, invaluable advice and constructive criticism were always available when any suggestions or discussions were needed. Their sincere friendship and guidance have made this study enjoyable and memorable.

Sincere gratitude is also extended to Dr. Barry Goldfarb and Dr. Vincent L. Chiang for their invaluable assistance, suggestions, discussion and guidance. The author would like to thank Drs. Tomoya Yokoyama, Satoshi Kubo, Tatsuhiko Yamada, Yuji Matsumoto, Ewellyn A. Capanema, Mikhail Yu. Balakshin, Takuya Akiyama, Chen-Loung Chen, Ilona Peszlen, Fikret Isik, Keiichi Koda, Jennifer L. Braun, Qizhou Dai, Kevin M. Holtman, Cameron R. Morris, Rui Katahira, Mr. Zhoujian Hu and Robert F. Sykes for their suggestions, discussions and friendships.

The author would also like to thank NCSU Phytotron for growth chamber utilization, Dr. Robert J. Downs for wind speed measurement, and US DOE and USDA for financial supports.

Special appreciation must also be given to the author's family and Riva for their constant patience, support, encouragement, and assistance, and have made this study a wonderful memory.

Finally, the author wishes to thank all those faculty members, colleagues and friends who in one way or another have contributed to making this study a successful experience.

Table of Contents

List of Figures

List of Tables

1. INTRODUCTION

1.1 Background

Increasing utilization of rapidly growing trees in plantations in the southeast US is shifting the raw materials for solid wood and pulp from predominately mature wood to a greater proportion of short-rotation juvenile wood [1,2]. Juvenile wood is the wood formed near the stem center and is formed by a young vascular cambium [3]. A typical 15-year-old loblolly pine contains as much as 85% juvenile wood by volume, as compared to only 20% in a 40-year-old tree [4]. Compared to mature wood, juvenile wood has lower wood density, shorter fiber length, higher lignin content, and higher compression wood content [5,6].

The percentage of compression wood in juvenile pine is on average about 18% by volume [7], but can be as high as 44% [8]. Compression wood, the tissue formed under leaning stems and branches in softwoods, arises from environmental disturbances, such as in gravitropic responses or in response to prevailing winds [9,10]. Its formation causes a "pushing" of the stems or branches back toward a vertical orientation [11]. Compression wood is generally considered to be inferior for both pulp and solid wood products. In chemical pulping, the utilization of juvenile and compression wood increases chemical consumption and decreases pulp yield, due to the higher lignin and lower cellulose content. As a result, increased usage of juvenile wood (and compression wood) from fast-growing plantation forests can significantly impact industrial production cost and product quality. A comprehensive study of wood property variation in juvenile wood (and compression wood) could help to utilized the material more efficiently.

It has been recognized that favorable wood properties may be obtained through tree breeding programs; for example, the wood density of juvenile pine can be increased by two pounds per cubic foot employing moderate selection of parents [12]. Wood properties, such as density, tracheid diameter and length, cell wall thickness and chemical composition, are closely related to product properties. Paper properties such as burst, tear strength and tensile strength are closely related to fiber morphology [13], while processing costs and resultant profitability are more significantly affected by chemical composition [14], specifically α-cellulose and lignin content.

Despite this, most operational breeding programs have placed limited emphasis on wood quality traits, especially chemical composition. Traditional wet chemistry methods for the determination of α-cellulose and lignin content are quite costly and time-consuming [15], where as the numbers of samples that must be assessed is large. As the global market places more emphasis on wood properties, rapid, precise, and cost-effective assessment tools need to be developed. This development will allow us to assess tree quality for a large number of samples, and select the best genetic traits (elite trees) suitable for different end-use products.

In the following section, a review of the literature on near-infrared spectrometry and its principles and application will be given. In addition, reviews of juvenile wood and compression wood, including formation, chemical and morphological property differences, and their influences on wood products will be presented. Finally, the utilization of metabolic profiling in plant science will be discussed. The followed sections are intended to provide rapid assessment tools of wood property variation and

assist in a better understanding the wood property variation between juvenile wood, mature wood, and compression wood.

1.2 Near-Infrared Analysis

1.2.1 Principles of Near-Infrared Spectroscopy

A near-infrared (NIR) spectrum is obtained when a sample absorbs radiation in the region of the electromagnetic spectrum known as the near infrared. The NIR spectral region is usually considered to include light of wavelength 800-2500 nm, or 12500-4000 cm^{-1} [16]. Figure 1.1 illustrates the relationship of the near-infrared region to others included in the electromagnetic spectrum. In this region, the absorption bands are the result of overtones or combinations originating in the fundamental mid-infrared (mid-IR) region (2.5-25μm, 4000-400 cm^{-1}) of the spectrum [17].

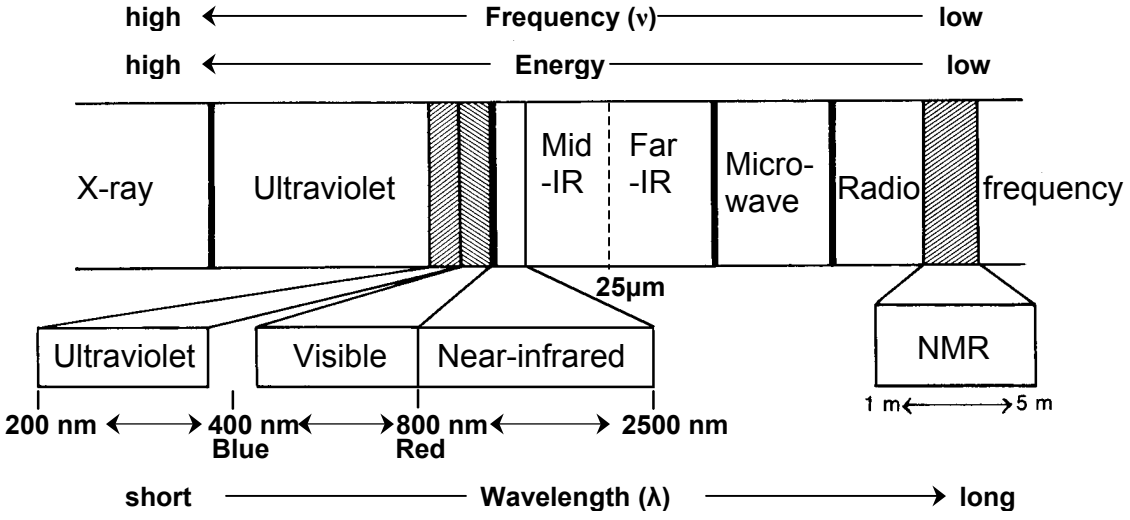

Figure 1.1 A portion of the electromagnetic spectrum, showing the relationship of the near-infrared to other types of radiation (modified from [18]).

In mid-IR absorption, energy is transferred from the incident radiation to the molecule, and a quantum mechanical transition occurs between two vibrational energy levels, E_1 and E_2. The energy differences (joules) between E_1 and E_2 is directly related to the frequency, ν (s^{-1}) of the electromaganetic radiation according to eq. 1-1, where h is Plank's constant (6.624×10^{-34} J s).

$$\Delta E = E_1 - E_2 = h\,\nu \qquad \text{(eq. 1-1)}$$

The quantity of energy, $h\,\nu$, is known as a photon, and the frequency of vibration of the molecule corresponds directly to the frequency of infrared radiation absorbed [19].

The simplest modes of vibrational motion in a molecule which give rise to fundamental absorptions in infrared region are the stretching (symmetric and asymmetric) and bending (scissoring, rocking, wagging, and twisting) modes. These fundamental absorption modes of $-CH_2-$ groups are illustrated in Figure 1.2. These fundamental transitions are from the vibrational ground state (all vibrational quantum numbers $\nu_i=0$) to the first excited levels (each $\nu_i=1$), as shown in Figure 1.3. A transition from the vibrational ground state to an excited vibrational level, $\nu_i=2$ or more, is known as an overtone. A transition to a level for which $\nu_i=1$ and $\nu_j=1$ (where i and j are two different vibrations) is known as a combination [19]. Overtones and combinations are forbidden by simple harmonic oscillator theory of molecular vibrations, but they become weakly allowed and of low probabilities when anharmonicity is taken into account [17].

In contrast to the fundamental bands of mid-IR spectroscopy, the absorption bands in the NIR region are mainly overtones or combinations. Due to the complex structures of the material measured, the bands usually overlay each other, and the degree of complexity of spectra is obvious. The majority of overtone bands seen arise from R-H

stretching modes (O-H, C-H, S-H, N-H, etc.) because of energy considerations. In other words, as "forbidden" transitions, the overtones are routinely between 10 and 1000 times weaker than the fundamental bands. Thus, a band arising from bending or rotating atoms (weaker than stretching modes to begin with) would have to be in their third or forth overtone to be seen in the near-infrared region of the spectrum [17].

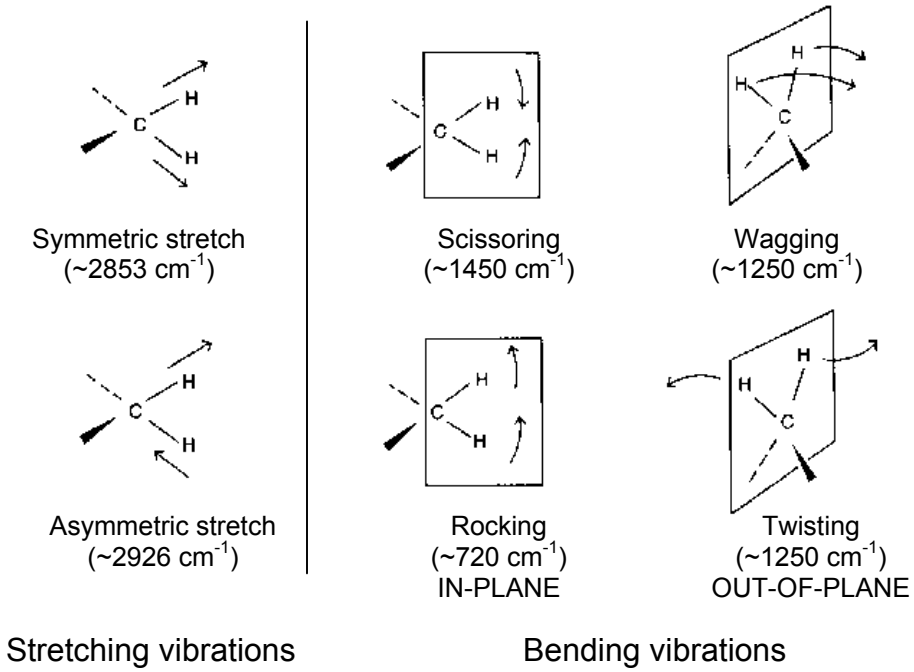

Figure 1.2 Fundamental IR vibration modes of $-CH_2-$ groups [18].

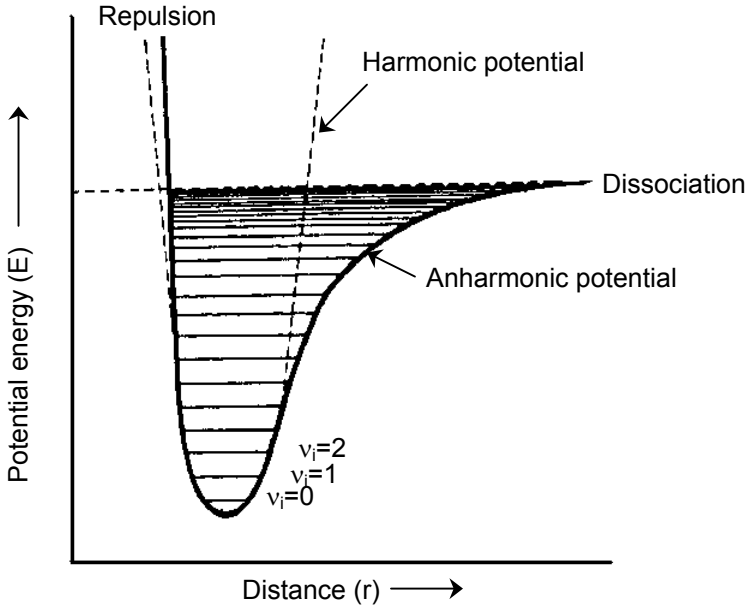

Figure 1.3 Energy potential diagram of diatom vibrational mode as an ideal harmonic oscillator and as an actual anharmonic oscillator [17].

1.2.2 NIR Instrumentations and Comparisons

An NIR instrument normally includes the following parts: the light source, monochromator or wavelength selector, sampling area, detector system, and data readout unit. Although the arrangement of these components differs between instruments, the basic configurations for transmittance and reflectance modes are shown schematically in Figure 1.4.

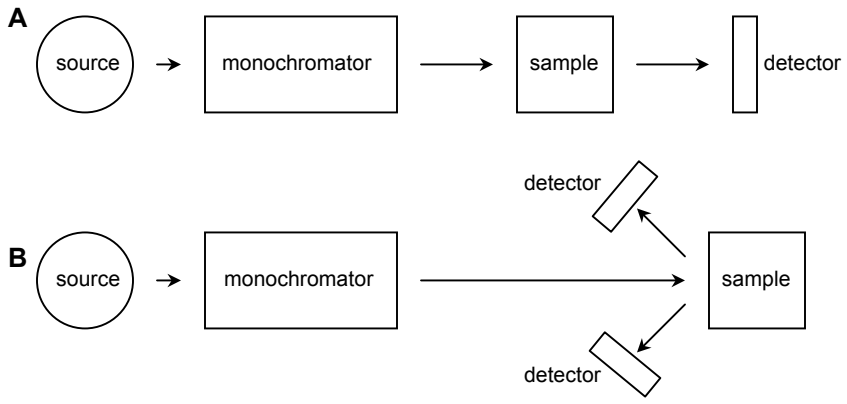

Figure 1.4 Basic NIR instrument configurations: (A) transmittance type; (B) reflectance type [20].

Reflectance NIR is the most widely used instrument configuration. However, reflectance measurements generally suffer from several limitations, the most serious being the small penetration depth (1-4 mm) of the incident beam [20]. For nonhomogeneous samples such as wood, this limited penetration leads to a large variation in the results obtained and a strong dependence on sample size and preparation technique. Thus, large sample sizes are typically utilized to better represent the sample of interest. By contrast, transmittance techniques, which penetrate fully through the sample [20], are less sensitive to sample preparation and homogeneity, and permit analysis of smaller quantities of samples.

Although NIR spectroscopy yields spectra less readily interpretable than mid-IR spectroscopy, the general advantages of NIR spectroscopy over mid-IR spectroscopy are the very low noise detectors and higher energy so that longer path lengths are possible [16,21]. The penetration depth of mid-IR radiation is about 10-100 μm, whereas for NIR

radiation it is several millimeters [16]. This permits little or no sample preparation. Also, quartz fiber optic cables, not practical for mid-IR measurements as they absorb strongly at about 2200 nm, may be used in the NIR region. As a result, the probe of the NIR spectrometer is comparably easier to design and fit to on-site environments as compared to mid-IR spectrometers [22].

The use of NIR technology in analytical and process applications is increasing due to the speed of analysis (typically less than 30 seconds), the minimal sample preparation, the overall simplicity of the technique, and the improved repeatability in comparison to traditional chemical methods [16]. Cost savings due to the speed of the analysis alone can often justify the purchase of the equipment [16].

1.2.3 NIR Calibration Development

One of the inherent features of NIR analysis is that it is a correlative technique. NIR relies upon a calibration developed using data acquired with another method, termed the "primary or direct method". The NIR calibration accuracy depends on the precision of the primary method. NIR is then used as the secondary method to predict the properties of unknown samples [23].

NIR spectra are mainly composed of overtones and combination bands, and these bands are commonly overlaid with each other. Calculating the second order derivative of a spectrum is a common technique to resolve overlapping peaks, and can remove both slope and offset [24]. Figure 1.5A shows an absorbance band as a function of wavelength λ involving two overlapped peaks. By calculating the second order derivative, a clear separation between the two peaks can be made (Figure 1.5B).

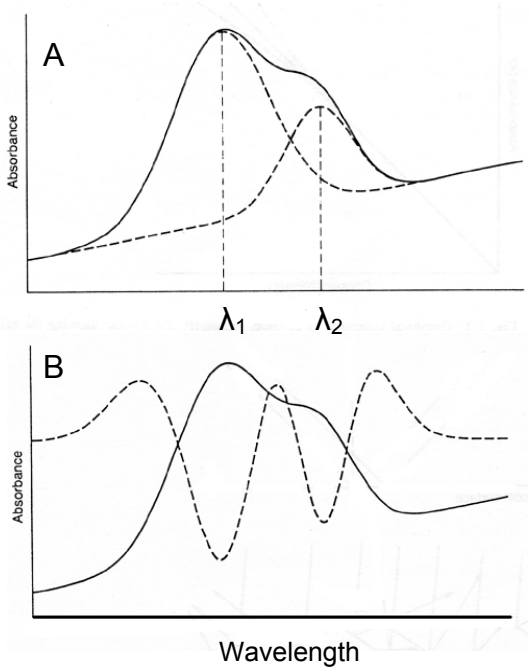

Figure 1.5 Deconvolution of bands by 2nd order differentiation: (A) original spectrum; (B) 2nd derivative resolved spectrum [25].

NIR predictive models are generated using single or multiple variable analysis of NIR results obtained from a known calibration set. Using linear regression algorithms, changes in NIR response are correlated with the results of the primary method. In simple linear regression (SLR), changes in absorbance intensity at a single wavelength are correlated with the analytical values or concentrations according to Beer-Lambert Law (eq. 1-2), where A is the absorbance, ε is the absorptivity coefficient, l is path length of light, and c is the concentration or the analytical value.

$$A = \varepsilon c l \quad \text{for a given wavelength} \qquad \text{(eq. 1-2)}$$

In multiple linear regression (MLR), changes in absorbance intensity at several wavelengths are correlated with changing analytical values. A regression equation will be established as eq. 1-3, where a, b_1, b_2,…, b_n are constant, x_1, x_2,…, x_n are absorbance intensity in n different wavelengths, and y is the analytical value.

$$y=a+b_1x_1+b_2x_2+\ldots+b_nx_n \qquad \text{(eq. 1-3)}$$

In simple chemical systems, typically one wavelength is required for each independently varying component of the chemical matrix. However, in more complex or full-spectrum system, other methods of linear analysis, termed chemometrics, are typically applied. Among these, Partial Least Square (PLS) regression is commonly used in NIR regression.

The essence of PLS regression lies in its construction of factors from the original spectral data. The aim is to reduce the quantity of spectral data, and, thus, avoid overfitting problems, without discarding any useful information [25]. Figure 1.6 illustrates how a regression model is produced by PLS regression. In a system with two different spectral measurements (x_1 and x_2), two axes are required to produce a scatter plot in which each point represents a sample (Figure 1.6A). However, in an actual transmittance NIR measurement, more than 500 spectral measurements will be recorded. That is, if the spectrum is collected from 700-1900 nm with a 2 nm increment, a total of 600 axes will be needed to describe the sample. One easy way of reducing the dimension is to project the points onto a smaller dimensional subspace. Figure 1.6A shows a projection from two dimensions (plane "x_1 vs x_2") onto one dimension (line "z"), with one point on the line for each of the original points. Performing this projection has created a new and much simpler spectral variable z. The value of z can also be established by measuring the angle between the new line and the two axes; a new

equation is produced for the value of z (Figure 1.6A, $z = w_1x_1+w_2x_2$), where w_1 and w_2 are the cosines of the corresponding angles, and x_1 and x_2 are the original spectral measurements.

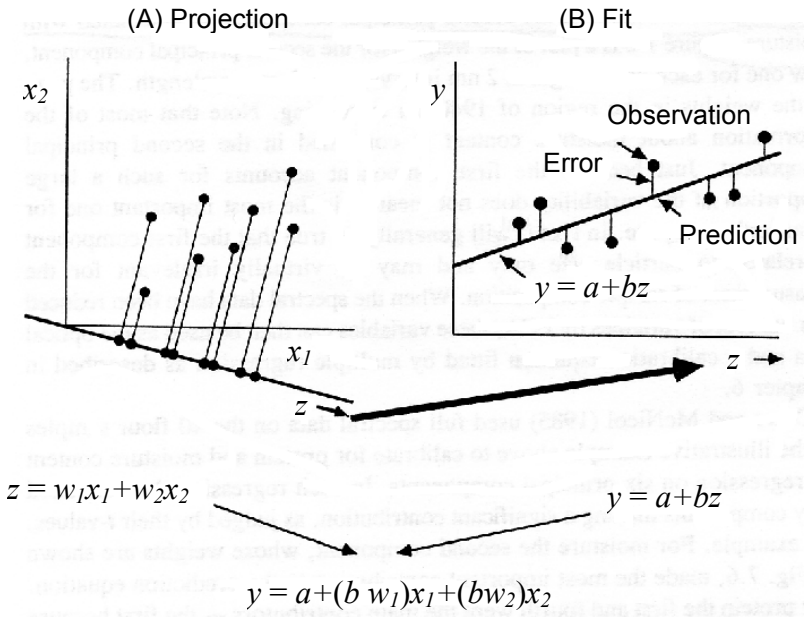

Figure 1.6 Illustration of PLS regression: (A) data projection (B) simple linear regression (modified from [25]).

The key point is the new variable z, referred to as **factor**, is a linear combination of the original data. In PLS, the values of z are the **scores** of the samples for this factor, and w_1 and w_2 are the **weights**. However, this projection must capture most of the variability in the original data points and retain most of the information, hence we can also call this projection selection step as Principal Component Analysis (PCA) [26,27].

To give relevance to this data projection, let's consider a calibration set of n samples or observations (n=8 in Figure 1.6), and each sample has one laboratory measurement (y)

and two spectral measurements (x_1 and x_2). By fitting a straight line between laboratory measurement (y) and new spectral variable z by least square, a linear equation ($y = a+bz$, a and b are constants) is obtained (Figure 1.6B). Since z is a linear combination of x_1 and x_2, substituting for z gives a new linear prediction equation for y in terms of x_1 and x_2 (Figure 1.6, $y = a+(b\ w_1)x_1+(bw_2)x_2$). By choosing the best projection that gives maximum variability to create z, this gives the one-factor PLS solution. In a practical NIR measurement, it usually starts with more than two spectral variables and constructs more than one factor, and this heavily involves matrices and computer calculation [26,27].

1.2.4 Evaluation of NIR Calibration model

There are three criteria to evaluate the suitability of a calibration: coefficient of determination (R^2), the standard error of calibration (SEC), and the standard error of cross validation (SECV). R^2 is interpreted as the fraction of the variation of the calibration set which is explained by the model. SEC is the standard deviation for the residuals due to the difference between the actual lab values and the fitted values of samples within the calibration set [28,29]. SECV is an indication of how well an equation will predict samples which were not used to generate the calibration equation in cross validation [22,26,27].

Cross validation avoids the need to set aside samples for the validation set. The original idea was to drop one sample (or one group of samples) from the calibration set, perform an entire calibration with the remaining samples, and make a prediction for the sample(s) left out. This exercise is repeated for each individual sample, which in turn

enables an average squared prediction error to be calculated. Thus, the sample being predicted has played no part in the calibration predicting it. This allows one set of samples to act as both calibration and validation sets, and protects against overfitting of the calibration model [24,25].

The standard error of prediction (SEP) is used to evaluate how well the calibration predicts the interested constituent values for a set of unknown samples, normally known as the validation set, that are different from the calibration set [30]. The predictability of the calibration is evaluated by the ratio of the performance to the deviation (RPD). The RPD is calculated from the ratio of the standard deviation of the reference data of the prediction data set to the SEP [31]. The RPD should be as high as possible; values between 5-10 are adequate for quality control, values > 2.5 are satisfactory for screening tree breeding programs [28,31], and values of ~1.5 can be used as an initial screening tool [30,32,33].

1.2.5 Application of NIR in Forest Products

By incorporating fiber optics and chemometrics, NIR has been extensively used both quantitative and qualitative in food science [24,34,35], polymer science [36], and the pharmaceutical industry [37].

In the forest product sector, NIR has been used extensively in the analysis of foliar nitrogen [38], extractive content [30,39,40], chemical composition [41], and wood chemistry characteristics [23,28], as well as estimating the tracheid morphology and wood density [32,33,42,43]. NIR has also been used to estimate microfibril angle [44], predict pulp properties such as kappa number, degree of polymerization, pulp yield

[21,45-48], assess wood mechanical properties such as stiffness, MOE, and MOR [49-52], and identify wood species [53,54].

In all these studies, reflectance mode NIR spectroscopy was utilized. However, as stated in section 1.2.2, reflectance spectra measure only the surface properties of the samples and required larger quantities of samples in order to get representative spectra. This limits the utilization of reflectance mode NIR if only limited amounts of samples are available, such as seedlings and young growth transgenic tree tissues. For whatever reason, the utilization of transmittance NIR in the analysis of forest products has been limited despite the fact that it can utilize small amounts of samples. Hence, a new methodology using transmittance NIR to assess wood chemical properties will be developed and presented.

1.3 Juvenile Wood

1.3.1 General Concept of Juvenile Wood

Wood formed near the pith of a tree has certain characteristics strikingly different from wood formed some distance away. This interior zone has often been referred to as core wood or juvenile wood, a name that accurately describes its physiological development [55]. More accurately, it is not related to the age of the tree but to the age of the cambium. The age of the cambium at the point of wood formation in any given year determines whether juvenile, transition or mature wood will be formed. Thus, in an old tree, in any given year, mature wood is produced near the stem base, but in the same year juvenile wood is also formed near the top of the tree [56]. The location of juvenile wood within a tree is shown schematically in Figure 1.7.

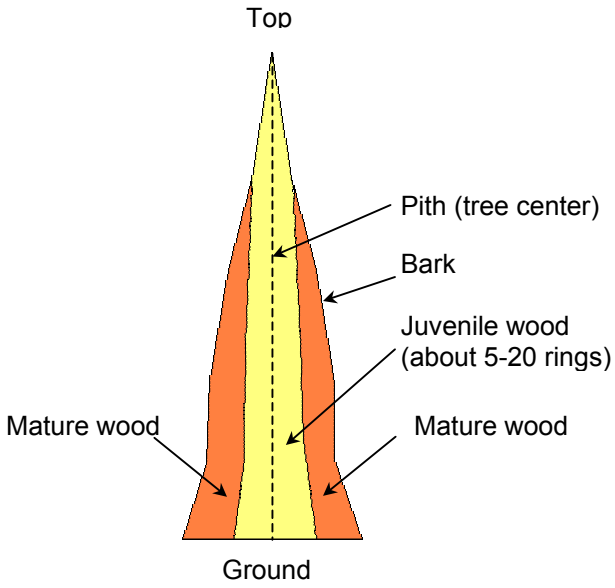

Figure 1.7 The location of juvenile wood within a tree, side view.

In old-growth forests, juvenile wood normally makes up only a small proportion of the total volume of wood furnish, whereas in fast-growing short rotation plantations, the amount of juvenile wood is greater. For example, a 15-year-old loblolly pine contains as much as 85% juvenile wood by volume (Table 1.1), whereas a 40-year-old tree contains only 19% juvenile wood by volume [57].

Table 1.1 Amount of juvenile wood by dry weight and volume in the merchantable bole of loblolly pine stands of different ages [57].

	Amount of juvenile wood	
Age of stand	Dry weight, %	Volume, %
15	76	85
25	50	55
40	15	19

1.3.2 Formation of Juvenile Wood

Surprisingly, there is a lack of information on juvenile wood formation, its function in living trees, or the biological mechanism that induces its formation. Most research on juvenile and mature wood has focused on how these zones influence the properties and quality of various forest products. One theory surrounding juvenile wood formation is the crown-formed wood theory [3,58]. In the growing season, radial growth starts at the apex of the tree in the vigorous crown, resulting in a larger proportion of thin-walled earlywood tissue in the top than in the bottom of the tree. The transition to thick-walled latewood tissue occurs first near the bottom, farthest from the source of auxins, and proceeds upward as moisture stress increases and translocation of auxins down the tree decreases. As trees grow older, lower branches cease to be vigorous, and the active crown region moves up the stem. Therefore, there is a core of crown-formed wood surrounded by a band of transition wood from the bottom to the top of the tree [58].

A new theory has been proposed by Yang et al. [59,60] in which the transition from juvenile wood to mature wood is associated with the age of cambial initials. The width of the juvenile zone, both by year ring and by volume, decreases with the age of cambium initials, which is defined as the number of years between the formation of the cambium initials and the year the seed germinated. The juvenile wood zone within a tree is also reported to be positively related to fertilization and the length of the growth season [58,61].

A recent study by Gartner [62] reported that the presence of juvenile wood is related to the photosynthetic bark, which refers to the green tissues immediately underneath the surface of the younger part of trunks and branches. This study hypothesized that a

photosynthetic layer in the periderm, only millimeters from the vascular cambium and connected to it through ray cells, influences the type of wood produced through a chemical reaction, such as using auxins [62]. However, this concept does not apply to all tree species.

1.3.3 Juvenile versus Mature Wood

The mechanism of juvenile wood formation is unsettled. However, based on different properties, juvenile wood can be distinguished from mature wood. Figure 1.8 shows the gradual change in properties from juvenile wood to mature wood in softwood. Juvenile wood, especially in hard pines, is generally characterized by lower specific gravity, shorter tracheid length, lower latewood percentage, thinner cell wall, lower cellulose content, lower strength, higher longitudinal shrinkage, higher microfibril angles, larger cell lumens, higher lignin content, and higher percentage of compression wood as compared to mature wood [3,63]. Table 1.2 shows some of the reported values for the various wood properties of juvenile wood as compared to mature wood.

Table 1.2 Comparison of wood properties between juvenile wood and mature wood.

Property	Juvenile wood	Mature wood	Reference
Specific gravity	~0.40	0.53	[64]
Fiber length, nm	3.3	4.3	[65]
Microfibril angle, °	~30	~15	[66]
Lignin, % (w/w)	29.4	27.8	[67]
α-cellulsoe, % (w/w)	50.9	54.7	[67]
Hemicellulose, % (w/w)	28.2	25.3	[67]

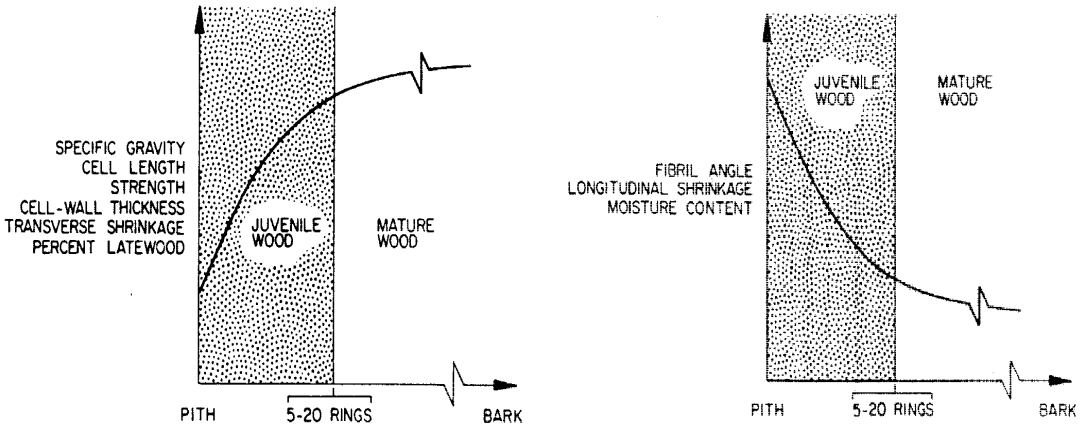

Figure 1.8 Schematic representation of the change in wood properties in going from the pith to bark differentiating between juvenile wood and mature wood in softwood [7].

Larger microfibril angles have been reported for juvenile wood as compared to mature wood [66,68-71] (Figure 1.9). Juvenile wood has a greater percentage of lignin, xylan, and extractives, higher moisture content, and lower holocellulose and α-cellulose content [55,72-76]. Analysis of the chemical composition variation in *Pinus resinosa* by age shows that the lignin content in juvenile wood is about 2% higher than that in mature wood (Figure 1.10A) [76]. Glucose and mannose residues are lower in juvenile wood, but xylose, galactose, and arabinose residues are higher (Figure 1.10B). Cellulose crystallinity of juvenile wood is also lower than that of mature wood [77,78].

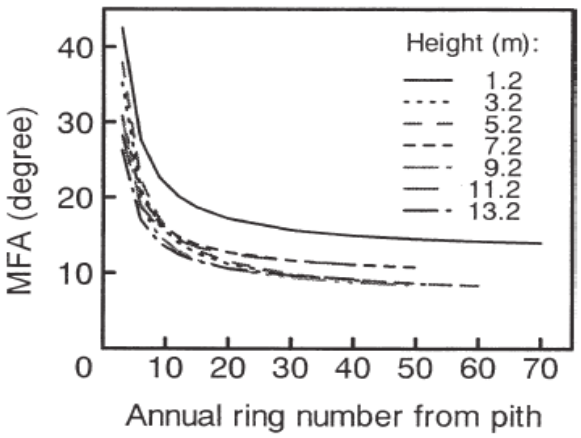

Figure 1.9 Fitted regression curves of microfibril angles in different height and year ring of *Cryptomeria japonica* [66].

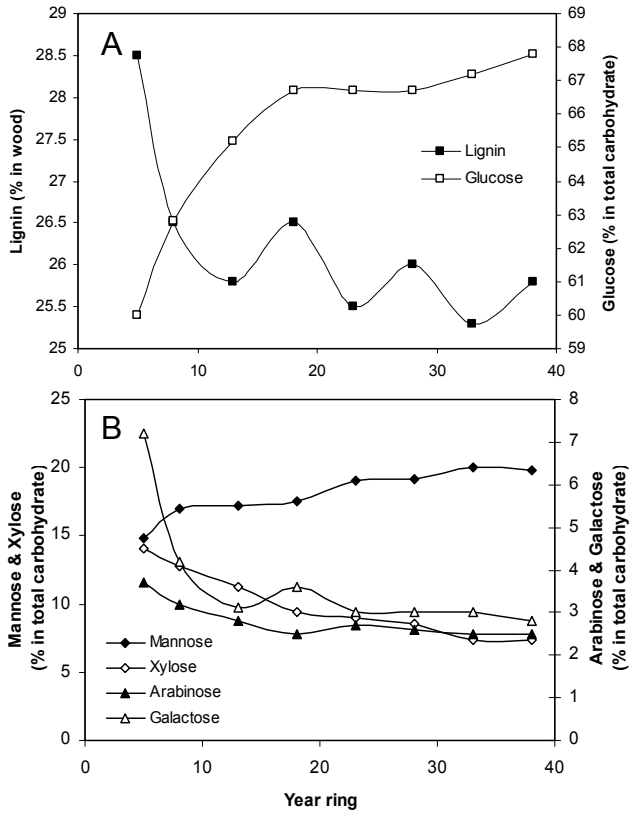

Figure 1.10 Changes in chemical composition of wood cell wall associated with age in *Pinus resinosa* (redraw from [76]).

In general, juvenile wood in softwood varies considerably by species. However, in most hardwoods, especially in diffuse porous hardwoods, the differences in properties between juvenile and mature wood are often quite small, and considered to be only of minor importance with respect to its effects on subsequent product properties [3,79].

1.3.4 Tree Top Juvenile Wood versus Bottom Juvenile Wood

As the distribution of juvenile wood within a tree is not uniform with tree height (see Figure 1.7), the vertical distribution of juvenile wood has been extensively studied both within and between species. In loblolly pine, the specific gravity of juvenile wood is typically the same at the top of the tree as at the bottom [3]. A similar pattern has been observed in radiata pine [63]. However, tracheid length and microfibril angle are frequently different in the juvenile wood at the top of the tree as compared with that at the bottom. Figure 1.11 shows the fiber length as a function of height and ring position. Fiber length increases from the bottom upward, reaching a maximum at a certain height, then decreasing [3,66,71]. By contrast, microfibril angle declines continuously with height in the stem [3,66,68,69], i.e. tree bottom juvenile wood has higher microfibril angle than tree top juvenile wood (Figure 1.9).

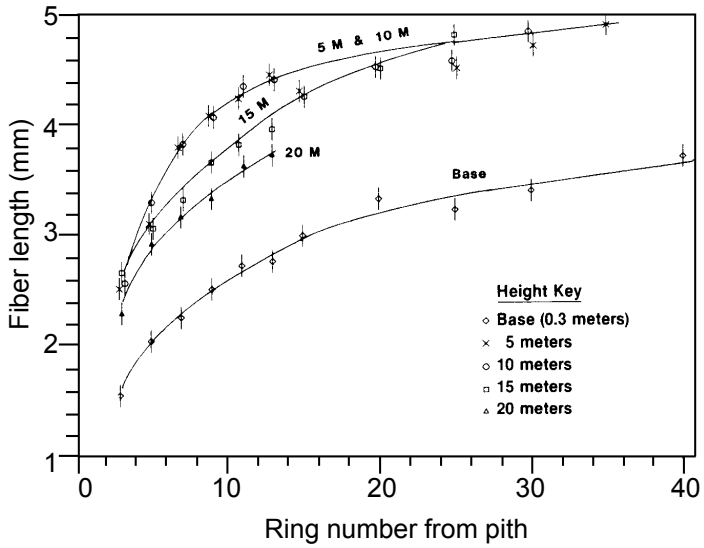

Figure 1.11 Fiber length as a function of height and ring position from the pith of a loblolly pine stand [71].

Very little has been reported on the differences in chemical constituents between juvenile wood at the top of the tree and juvenile wood from the bottom. In radiata pine, it was found that less lignin and more pentosans were in the juvenile wood near the top of the tree as compared with that near the bottom [80]. In lodgepole pine, juvenile wood near the top of the tree was reported to have a "significantly" higher lignin content than that near the bottom [72]. However, as the lignin contents were only 27.7% versus 27.0% with standard deviation in the range of 0.7~0.8 [72,73], no statistical difference in lignin content is present. Similarly, the alpha-cellulose content has been reported to be nearly constant between the bottom and the top of the tree in both slash and loblolly pines [55].

1.3.5 Influence of Juvenile Wood

Wood uniformity is considered one of the most important wood properties; differences between juvenile and mature wood are the main reason for the diversity in wood quality, both among and within trees [79]. The shorter and thinner tracheid walls of juvenile wood in hard pines and Douglas fir result in weak solid wood products and low tear-strength paper [81]. The larger or flatter fibril angle of juvenile wood makes for poor solid wood products, such as higher longitudinal shrinkage, lower modulus of elasticity (MOE), and lower modulus of rupture (MOR) as compared to products from mature wood [64,74].

The chemical and morphological differences between juvenile and mature wood cause slightly greater chemical consumption and higher manufacturing costs (+10%) during Kraft pulping [82]. However, the chemical differences between juvenile and mature wood appear to be of less importance in affecting product quality than the anatomical differences [67]. Pulp yields per unit volume of juvenile wood are 5~15% lower than those of mature wood, and the corresponding paper quality is quite different, such as lower tear strength, higher burst, tensile index, and apparent density [4,57,73,74,83-86].

It is important to recognize that juvenile wood is not necessarily an inferior wood for specific paper products but a different wood [82]. It produces paper that is weak for products requiring high tearing strength, but produces papers that bond well and have good burst, tensile strength, and fold. Some tissue grades made from juvenile wood are

excellent. The large surface caused by fiber collapse and the close chemical bonding yields paper with satisfactory printability and bendability [79]. Juvenile wood is, however, still a major problem for most solid wood products due to higher percentages of compression wood present when young trees or top wood are harvested. Generally, compression wood is considered to be inferior for both pulp and solid wood products.

1.4 Compression wood

1.4.1 General Concept of Reaction Wood

Trees have the natural tendency to grow upright. If this is disturbed, the vascular cambium of the leaning stem will respond by developing abnormal wood, known as reaction wood. The formation of reaction wood provides the woody stems with a mechanism by which they can realign their orientation to the vertical axis [79]. Branches also form such tissues, providing the means for continual reorientation of branch angles [87].

Reaction wood is known as compression wood in softwoods (gymnosperms) and tension wood in hardwoods (angiosperms). Tension wood is formed on the upper side of branches and leaning stems and functions by "pulling" the branches and stems to the needed orientation. On the other hand, compression wood is formed on the underside of leaning stems and branches and manifests its effect by slowly "pushing" the stems or branches until the requisite orientation is achieved [11,88].

Tension wood differs less from normal wood than compression wood. The secondary wall in tension wood has a characteristic gelatinous layer [89,90]. In normal wood, the secondary wall has three layers, i.e. S_1, S_2 and S_3 (Figure 1.12A, idealized). In tension

wood, three types of secondary wall structures (Figure 1.12B-D, idealized) have been reported [90]. The G- or gelatinous layer is rich in cellulose and is exists in all three types of tension wood fibre structures. Due to this gelatinous layer, tension wood has higher cellulose content and lower lignin content as compared to normal wood [89]. Compression wood, on the other hand, does not have a gelatinous layer, it is heavier, harder, and denser than normal wood, and has a higher lignin content.

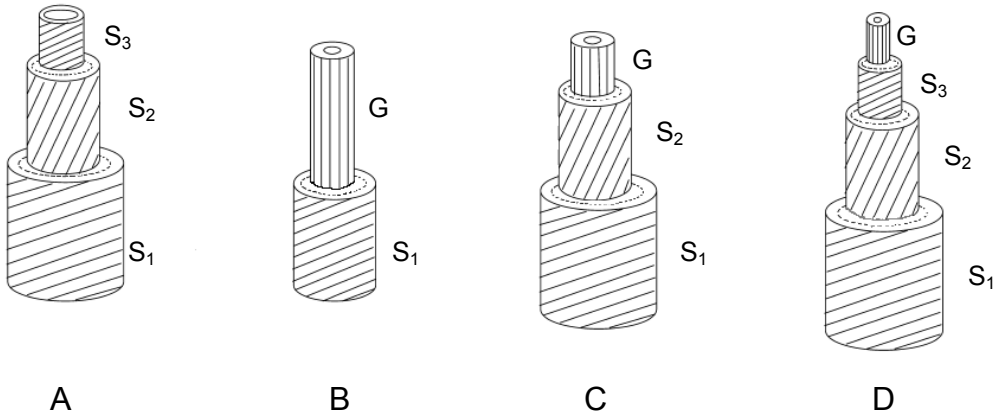

Figure 1.12 Idealized diagrammatic representation of the organization of the secondary wall in (A) normal wood, and (B), (C), and (D) types of tension wood. Abbreviations: S_1, outer layer; S_2, middle layer; S_3, inner layer; G, gelatinous layer of tension wood fiber [90].

1.4.2 Characteristics of Compression Wood

1.4.2.1 Structure

Compression wood occurs as brown or reddish-brown wood on the lower side of the leaning stem in gymnosperms (Figure 1.13). The area opposite to the compression wood

region is termed “opposite wood”, and the two sides of the eccentric trunk “side wood” [5,91]. In gymnosperms, the opposite wood has normal tracheids of rectangular shape, with no significant difference to those of normal wood xylem [5]. However, compression wood often has different tracheid characteristics and chemical composition [79].

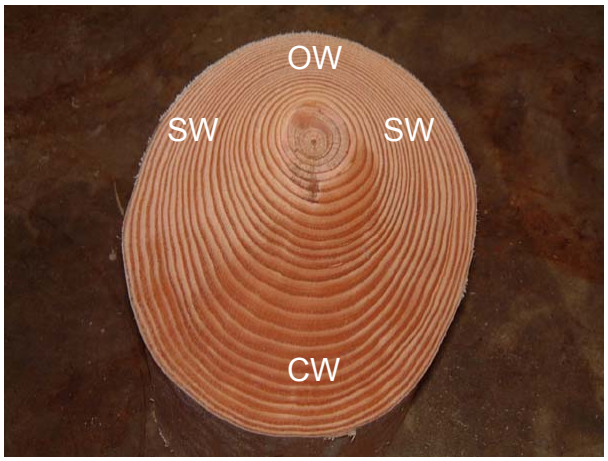

Figure 1.13 Cross section of a mature bent loblolly pine (*Pinus taeda*): CW, compression wood; OW, opposite wood; SW, side wood.

When compared to normal wood tracheids, the compression wood tracheids of pines are shorter [92], and the microfibril angle is much flatter (Figure 1.14 C & D), about 45° (vs. ~10°) in relation to the fiber axis [15]. Tracheids of the compression wood (Figure 1.14B) have a rounded shape with large intercellular spaces in the cell corners, as compared to normal wood which has a rectangular shape with no intercellular spaces (Figure 1.14A). The secondary walls of compression wood tracheids (Figure 1.14D) are thicker than those of normal wood (Figure 1.14C), and do not have an S_3 layer [11,87]. The lumen side (S_2 layer) of compression wood tracheids is ribbed (Figure 1.15), and the ribs form helices which run in the same direction as the cellulose microfibrils [93].

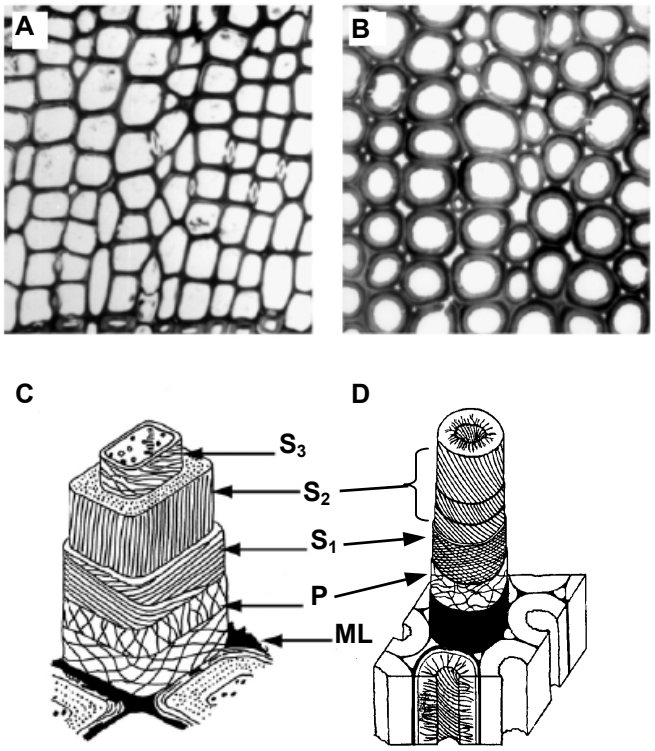

Figure 1.14 Cross section of Douglas fir cell wall and tracheid structures of normal wood (A & C) and compression wood (B & D) (modified from [11,15,87]).

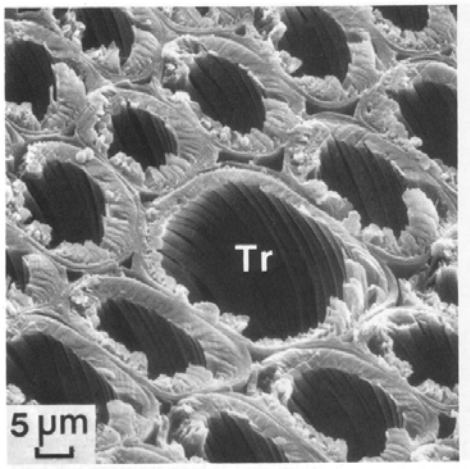

Figure 1.15 Helical ribs and cavities in the inner surface of compression wood tracheids (Tr) in *Cryptomeria japonica* [5].

1.4.2.2 General Chemical Composition

Table 1.3 lists the averaged chemical composition of normal wood and compression wood from 27 softwood species. One noticeable characteristic of compression wood is the lignin, galactose, and cellulose contents [91,94-96]. The lignin and galactose content of compression wood are about 1.3 and 5 times higher than that of normal wood, respectively. The cellulose content (determined as glucose residues) of compression wood is only 75% that of normal wood [94].

Table 1.3 Averaged chemical composition of normal and compression wood from 27 softwood species [94].

Constituent*	Normal wood	Compression wood
Lignin	30.1	38.9
Acetyl	1.3	0.8
Uronic anhydride	4.7	4.5
Residues of:		
Galactose	2.1	10.3
Glucose	43.0	32.5
Mannose	9.8	5.3
Arabinose	1.6	0.9
Xylose	7.1	6.6

*: % based on extractive-free wood.

1.4.2.3 Lignin

Figure 1.16 shows the structure model of normal wood lignin in softwood, and the types and frequencies of lignin interunit linkages are listed in Table 1.4. Lignin interunit linkages, such as 5-5, β-5, β-1, β-6, and β-β, are generally considered as condensed type lignin structures.

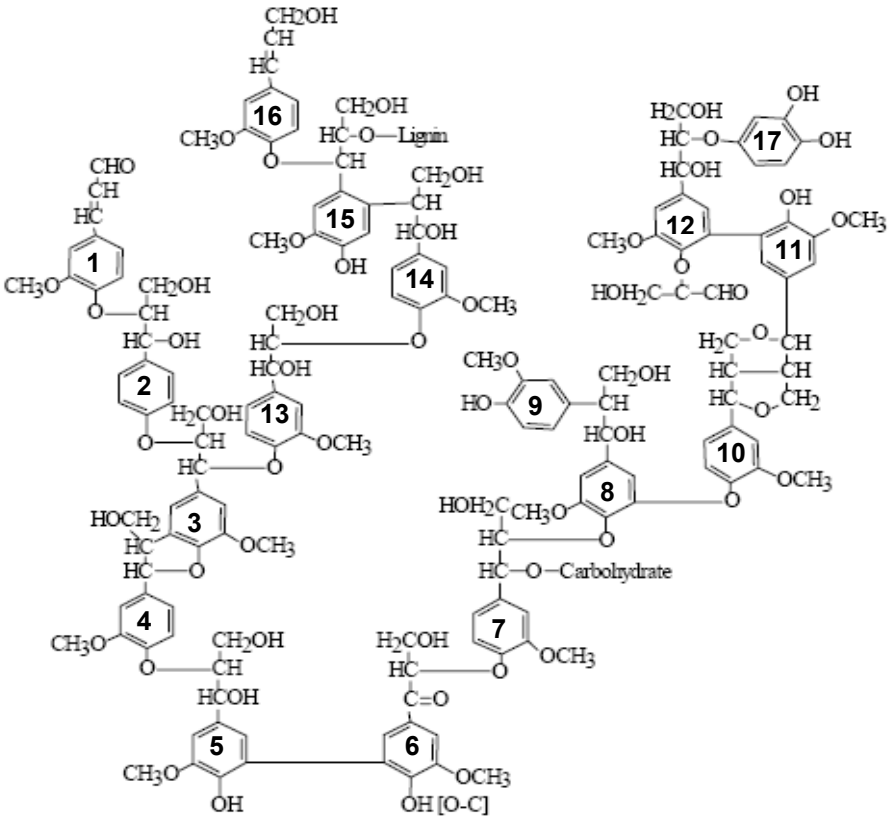

Figure 1.16 Proposed model structure of softwood lignin [97].

Table 1.4 Types and frequencies of interunit linkages in softwood lignin [98].

Linkages	Number per 100 C_9-units	Unit # in Figure 1.16
β-O-4	49-51	1/2, 2/3, 4/5, 6/7, 7/8, 13/1, 13/14
α-O-4	6-8	3/4, 3/13, 15/16
β-5	9-15	3/4
β-1	2	8/9
5-5	9.5	5/6, 11/12
4-O-5	3.5	8/10
β-β	2	10/11
β-6	-*	14/15
β-O-1	-*	12/17

*: Not reported in [98].

The lignin in compression wood has been extensively studied [91,96,99-105]. Compression wood lignin has been found to be different from normal wood lignin in: (1) the content of lignin (in *Larix* , 39.27% lignin in compression wood vs. 28.05% lignin in normal wood, Table 1.5). (2) the content of *p*-hydroxyphenyl propane units (H-units) which corresponds to methoxyl content (in *Larix*, 12.64% (w/w) methoxyl groups in compression wood milled-wood lignin (MWL) vs. 15.19% (w/w) in MWL from normal wood, Table 1.5). (3) the degree of condensed units (in *Larix*, 0.84/C_9 unit in compression wood lignin and 0.56/C_9 unit in normal wood lignin, Table 1.5).

Table 1.5 Chemical constituent differences between normal wood and compression wood of *Larix leptolepis* Gord (adapted from [100]).

Sample	% lignin	% OCH_3 in MWL* (w/w)	Degree of condensed unit (per C_9 unit)
Compression wood	39.27	12.64	0.84
Normal wood	28.05	15.19	0.56

*: MWL, milled wood lignin.

The condensed lignin structures of *Larix leptolepis* compression wood has been thoroughly studied by hydrogenolysis [106-111]. The results reveal the presence of β-5, β-6, β-β, 5-5, β-3, and γ-lactone type interunit linkages. The degree of condensation was also determined by gel permeation chromatography (GPC) of thioacidolysis degradation products. [96,104]. The GPC traces of thioacidolysis products from *Pinus radiata* compression wood show a higher proportion of oligomers/condensed units (earlier elution time) than that of normal wood (Figure 1.17). Similar results were also found from spruce [96], where a relatively lower amount of monomers and a higher amount of

oligomers were obtained from the thioacidolysis products. The low thioacidolysis yields indicate a relatively lower percentage of uncondensed β-O-4 linkages [96]. Consistent with this are the results from ethanolysis which show compression wood lignin to have less β-O-4 linkages than normal wood lignin [99,100].

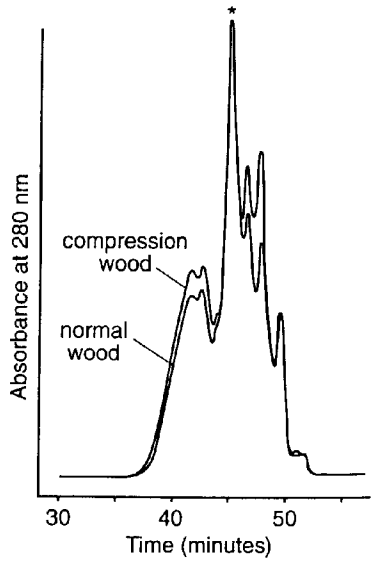

Figure 1.17 GPC traces of thioacidolysis products of normal and compression wood increment cores of *Pinus radiata* [104].

Details of β-aryl ether structures were studied by thioacidolysis coupled with diazomethane-methylated pine compression wood lignin [102,103]. The results showed that ca. 91% of the β-aryl ether-linked H units and ca. 22% of the β-aryl ether-linked G units (guaiacyl unit) were actually free phenolic end-groups in the pine compression wood lignin (Table 1.6).

Table 1.6 Frequency of the free phenolic groups within the degraded H and G structures of pine compression wood (modified from [102]).

Samples	H ($\frac{c}{a+c}$) %*	G ($\frac{d}{b+d}$) %*
Isolated and methylated MWL	90±1	33±0.5
In situ methylated lignin	91±1	22±1

*: a, b, c, d refer to the structures below.

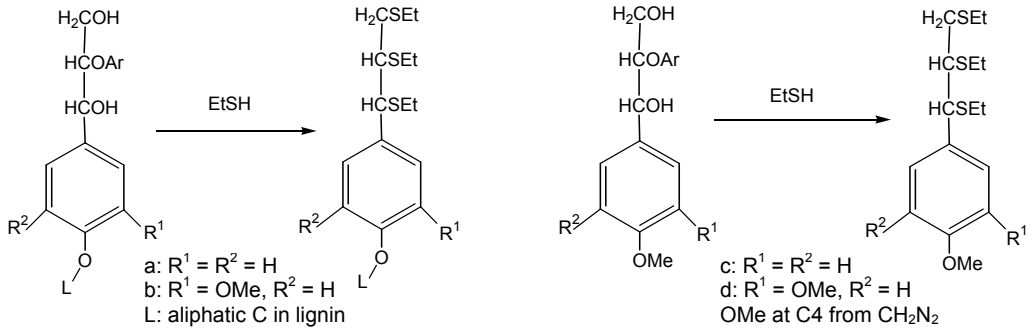

1.4.2.4 Cellulose

The percentage of cellulose in black spruce compression wood has been reported to be a 37.3% (w/w), which is about 20% lower than that in the normal wood (44.4%, w/w) [112]. Analysis of pulp and holocellulose isolated from Douglas fir normal and compression wood showed that the crystallinity indexes were significantly lower in the compression wood sample [77]. Similar results were obtained by Tanaka and Koshijima [113], who measured the crystallinity of *Pinus densiflora* wood meal (40~80 mesh) by X-ray diffraction. They reported that the degree of crystallinity of cellulose was 45~50% in compression wood, about 50% in normal wood, and 50~60% in opposite wood (Figure 1.18).

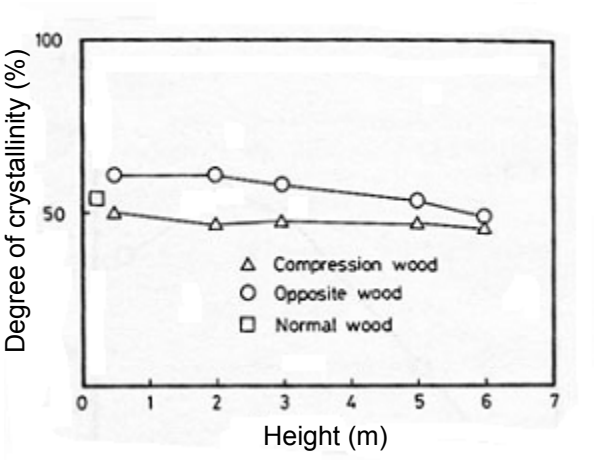

Figure 1.18 Crystallinity index for cellulose crystallites in *Pinus densiflora* [113].

1.4.2.5 Galactan

It has been reported [76,96,114-117], that compression wood contains significantly more galactan (~10%, w/w) in the cell wall than normal wood (see Table 1.3). This polysaccharide was first isolated by Bouveng and Meier [118] from compression wood of *Picea abies* in 1959. It has been found that most of this galactan dissolves in the chlorite liquor when compression wood is deligninfied with chlorous acid. Two additional galactans were later isolated by Schreuder et al. [119] from *Picea rubens* and by Jiang and Timell [120] from *Larix laricina* compression wood.

The structure of galactan was determined by the standard technique involving methylation of the free OH groups, followed by partial acid hydrolysis to simple sugars, and subsequently acetylation and analysis by paper or gas chromatography [115,120,121]. This polysaccharide consists of a main chain of (1 → 4)-linked β-D-

galactopyranose residues with some branching at the C-6 and C-2 positions [119,121]. It has been shown that in linkages with lignin, the lignin is predominately bound to galactan at the C-6 position [121]. It has also been shown that the galactan in *Picea rubens* contains a single, terminal β-D-galacturonic acid residue attached to the C-6 position of the main chain at 20 galactose residue intervals (Figure 1.19) [120].

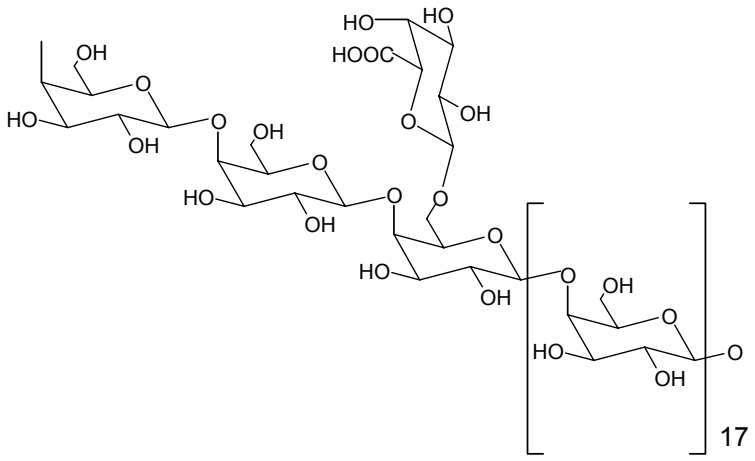

Figure 1.19 Representation of a branched portion of the galactan backbone in *Picea rubens* [120].

1.4.3 Formation of Compression Wood

Since compression wood has higher lignin content than normal wood, much of the work on compression wood formation has focused on lignin biosynthesis and cell wall deposition. Kutsuki and Higuchi [122] demonstrated that the enzyme activity of phenylalanine ammonia lyase (PAL), caffeate 3-*O*-methyltransferase (COMT), 4-coumarate:CoA ligase (4CL), and cinnamyl alcohol dehydrogenase (CAD) are marginally higher in compression wood than opposite wood. The lignin biosynthetic steps related to these enzymes are shown in Figure 1.20.

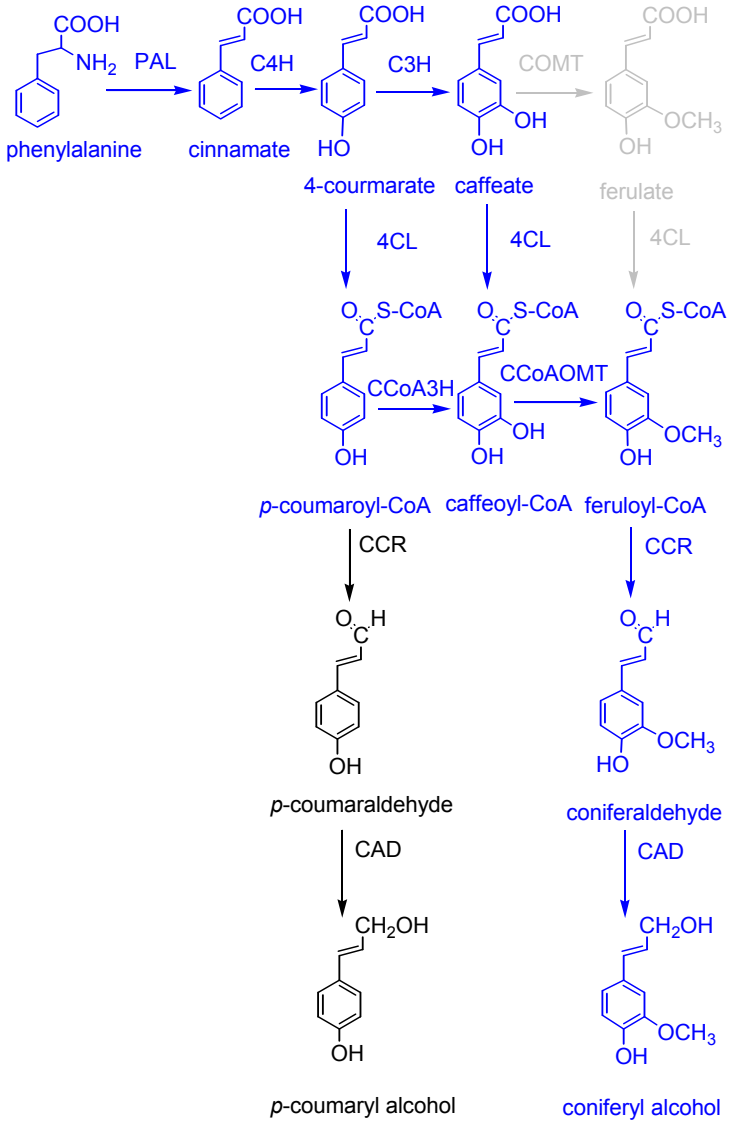

Figure 1.20 The proposed pathway of lignin biosynthesis in gymnosperm (only pathway leading to H and G lignin is showed), adapted from [123,124]: (PAL) phenylalanine ammonia lyase; (C4H) cinnamate-4-hydroxylase; (C3H) 4-coumarate-3-hydroxylase; (CCoA3H) *p*-coumaroyl CoA 3-hydroxylase; (COMT) caffeate 3-*O*-methyltransferase; (CCoAOMT) caffeoyl-CoA *O*-methyltransferase; (4CL) 4-coumarate:CoA ligase; (CCR) cinnamoyl CoA reductase; (CAD) cinnamyl alcohol dehydrogenase.

Elevated activity and amount of 4CL and CCR (cinnamoyl CoA reductase) were also found in the xylem of compression wood in loblolly pine [125]. Together, these results

suggest that larger amounts of lignin precursors should result in compression wood, as compared to opposite wood, and therefore lead to the high lignin content in compression wood. Zhang and Chiang [123] further demonstrated that compression stress affects the activity of 4CL enzyme in loblolly pine compression wood xylem. It increases the activity towards 4-coumarate, inhibits the activity with caffeate, and has no effect on the activity with ferulate. They propose that the specific catalytic function of 4CL toward different substrates is likely modulated by pathway intermediates induced under compressional stress. Therefore, the 4CL enzyme, with altered activities toward different substrates, could act as a regulator for the distribution of cinnamate derivatives into various phenylpropanoid pathways, favoring a characteristic flux of precursors for the formation of 4-coumaryl-enriched lignin (H-unit) required in compression wood tissue.

Another possible explanation for the noted increases in the H-unit content in compression wood lignin was put forth using loblolly pine cell cultures [126]. Increasing addition of phenylalanine to the cell suspension lead to a differential induction in monolignol formation. The formation of coniferyl and *p*-coumaryl alcohols was differentially induced, with their ratios changing from ca. 8:1 to 1:1, respectively [126].

Whetten et al. [127] reported a pioneering first-generation microarray study on the differences in gene expression between normal and compression wood formation in loblolly pine. The results showed that 156 out of the targeted 2300 genes were differentially expressed, 85 up-regulated and 71-down-regulated. Gene expression related to PAL (phenylalanine ammonia lyase, Figure 1.20) was significantly elevated in the compression wood xylem tissue leading to the high lignin content in compression wood.

The lignification processes in compression wood and normal wood have been studied in detail using radiolabeled precursors [128-131]. Figure 1.21 illustrates the lignin deposition processes.

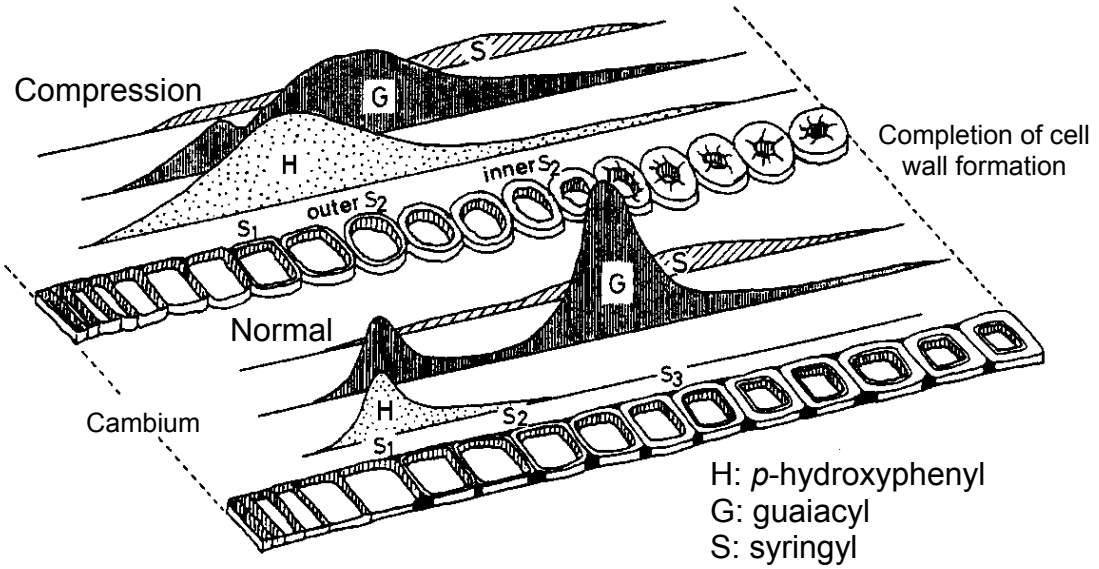

Figure 1.21 A schematic representation of the process of deposition of three kinds of lignin building units [131].

The deposition order of lignin precursors was the same in compression wood as in normal wood: *p*-hydroxyphenyl, guaiacyl, and syringyl lignin (if any). The *p*-hydroxyphenyl units are deposited mainly in the early stages of cell wall formation. In normal and opposite wood, this occurs in the compound middle lamella, whereas in compression wood, the *p*-hydroxyphenyl units are formed in both the compound middle lamella and the secondary wall. In compression wood, the most intensive lignification starts during the S_2 layer formation, proceeding from the outer to inner layers. By

contrast, lignification is most active during S_3 layer formation in normal or opposite wood. In normal wood, the occurrence of condensed guaiacyl units is preferentially in the compound middle lamella, with very little in the secondary wall. However, in compression wood, condensed guaiacyl units are homogenously distributed through all morphological regions [130,131].

1.4.4 Factors Causing Compression Wood Formation

There are many factors that might stimulate the formation of compression wood, and include light, gravity, auxin, compressive stress, and wind action [10,79]. However, each factor alone might not cause compression wood formation, rather it is a combination of several factors.

1.4.4.1 Light

It is a common observation that plant shoots grow (or bend) toward a light source, whereas roots grow away from it. This growth movement, phototropism, which occurs in response to light (especially sunlight), can indirectly be responsible for compression wood formation. Arboreal angiosperms are generally much more phototropic than gymnosperms. Timell [10] pointed out that *Pinus* and *Larix* are more phototropic than *Abies* and *Picea*. Phototropic bending of shoots, like all movements of orientation in gymnosperms, is associated with the formation of compression wood

1.4.4.2 Gravity

Gravity-directed growth processes, called gravitropism, affect both shoots and roots. Roots are considered positively gravitropic because of growing toward the direction of the gravity force, whereas stems are considered negatively gravitropic [132]. As early as in 1889, Mer [10] suggested the formation of compression wood must be stimulated by gravity. This is due to the fact that most compression wood, both from leaning stems and branches, is always found in the undersides of stem, and possibly in response to perception of their own weight.

If compression wood is a strictly gravitropic phenomenon, the amount of compression wood produced is expected to increase with the sine angle of displacement within the range 0º to 90º. However, the linkage between sine angle and the amount of compression wood is weak [10].

To investigate whether gravity is the key factor to trigger compression wood formation, Kwon et al. [87] measured compression wood formation in a microgravity environment. One-year-old Douglas fir and loblolly pine trees were taken into space for two weeks, where mechanical harnesses were utilized to induce compression wood formation. Trees planted on earth (1 *g* gravity) during the same time period were used as controls. The results revealed that compression wood development was able to occur under the mechanical stress in the near absence of gravity (round and thick wall tracheids in Figure 1.22C). There was actually no difference between compression wood formed in microgravity and that formed in 1 *g* gravity (round and thick wall tracheids in Figure 1.22D). No compression wood was detected in the upright microgravity control (Figure 1.22A) or upright 1 *g* control (Figure 1.22B).

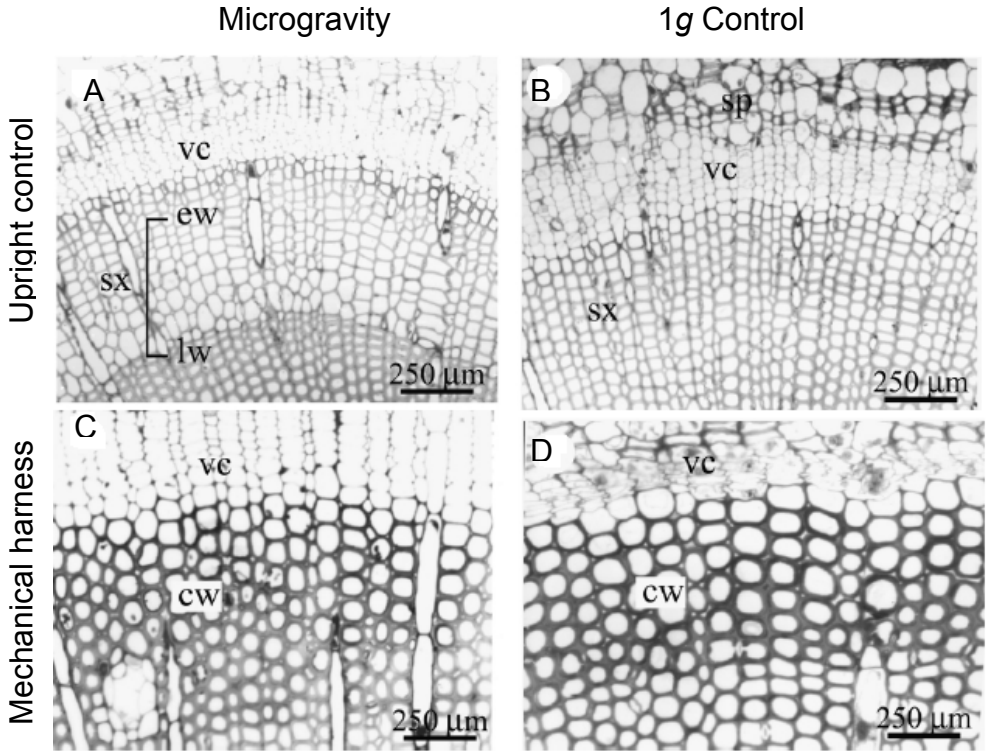

Figure 1.22 Cross-sections of Douglas fir seedlings grown in microgravity (A,C) and at 1 *g* (B, D): (vc) vascular cambium; (cw) compression wood; (sx) secondary xylem; (ew) early wood; (lw) late wood; (sp) secondary phloem [87].

Two scenarios can be considered from this space experiment: First, the microgravity environment was still sufficient for the plants to respond with compression wood formation. Second, the induced stress through mechanical loading (harnessing at 45º) overrides the gravitactic responses due to overlapping signal transduction, perception, and response mechanisms. The plants then compensated to the effect of the mechanical stresses, and underwent compression wood formation [87]. Thus, further research is still needed to clarify the gravitropic effect in compression wood formation.

1.4.4.3 Auxin

The formation of compression wood is often accompanied by a stimulation of cambial cell division, with cell division at the opposite side more or less inhibited [133]. Since auxin, indole-3-acetic acid (IAA), plays an important role in the promotion of cell division, considerable research has been done to establish the connection between IAA and compression wood formation [134]. The external application of a high concentration of IAA to a vertical stem of Douglas fir induced compression wood formation at the application point [135]. Likewise, the external application of morphactin or 1-N-naphthylthalamic acid (NPA), inhibitors of the basipetal transport of IAA, to vertical stems also induced compression wood formation just above the treatment point [136,137]. These finding suggest that a high concentration of IAA is probably correlated with compression wood formation.

Unfortunately, inconsistent results have been reported in studies investigating the relationship between the level of endogenous IAA and the formation of compression wood. An elevated endogenous IAA concentration was reported in two inclined stems of *Cryptomeria japonica* [138], but not in reoriented branches of Douglas fir [139]. Similarly, the induction of compression wood formation above an NPA application point was not accompanied by an increase in the concentration of endogenous IAA [140].

Recently, a comprehensive study on the distribution of IAA across cambium regions in gravistimulated pine trees were presented [133]. By continuously sectioning the cambium tissue, the distributions of IAA concentration across compression and opposite side tissues were obtained. In Figure 1.23, each dot represents the IAA concentration of the slice section, and the area under the dots is the total amount of IAA in the tissue

sectioned. Most of the trees were found to have similar concentrations and amounts of IAA. It was suggested that environmental modification of cambial growth pattern, such as reaction wood formation, is not mediated by changes in the IAA level in the cambial tissues [133]. This suggests that factors other than auxin might play a role in mediating compression wood formation.

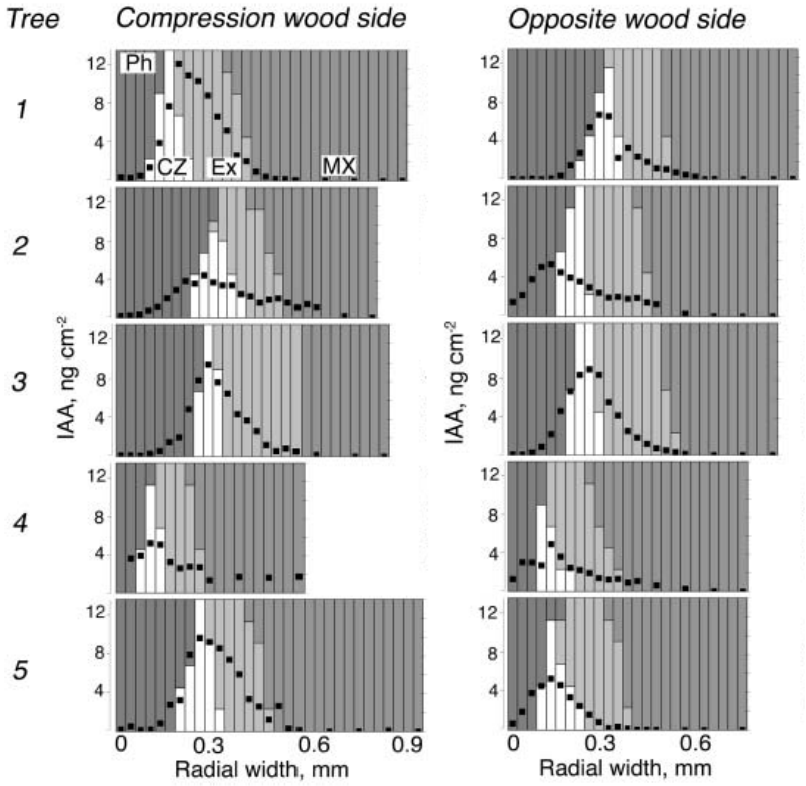

Figure 1.23 Levels and distribution patterns of IAA across the cambial region in compression and opposite wood tissues in gravistimulated pine trees. Each dot represents the amount of IAA in that section. (Ph) phloem; (CZ) cambial zone; (Ex) expending fibers; (MX) maturing and mature xylem [133].

1.4.4.4 Compressive Stress

Formation of compression wood has probably been more often attributed to compressive stress than to any other cause. Plants have the ability to react anatomically when subjected to compression or tension stress [10]. The vascular cambium responds to resulting asymmetrical distribution of stresses in the leaning stem by accelerated wood cell formation [88]. According to Fengel and Wegener [15], softwood reacts to mechanical, compressive forces by forming compression wood in the zone of compression.

Compressive stresses were detected using strain-gauge measurements [141,142] under the lower side of a leaning sugi trees (*Cryptomeria japonica* D. Don). The tree was bent in the lower 1.3m section of the tree (total height 8.3m). The high compressive stress (negative growth stress in Figure 1.24A) corresponded to the compression wood region, which exerted a positive release strain. The compressive stress correlated to a high Klason lignin content (Figure 1.24B) [141]. Similar results were also reported in hinoki (*Chamaecyparis obutusa* Endl.) by Yamamoto et al. [143]. In addition to lignin, a correlation between high compressive stress and high microfibril angle in the compression wood was also observed.

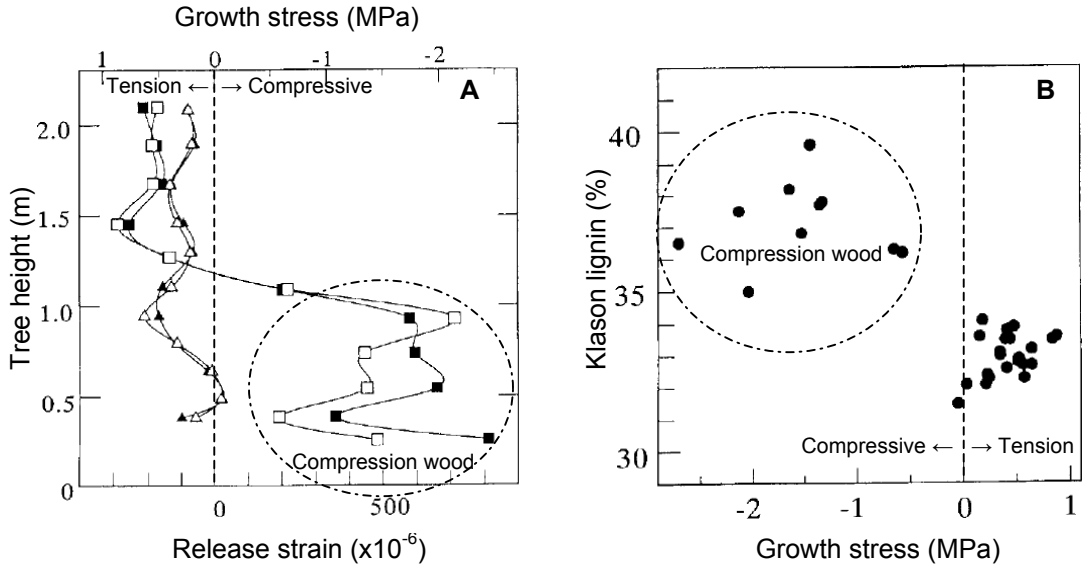

Figure 1.24 Distribution of growth stress (A), and the relationship between Klason lignin content and growth stress (B) in the longitudinal direction of a bent sugi tree (modified from [141]). (▲,△) stress and strain from opposite site of the tree; (■,□) stress and strain from compression site of the tree.

1.4.4.5 Wind Action

Wind-induced sway, or flexure, initiates a dynamic loading in stem tissues under turbulent or gusty conditions. The stem moves back and forth through the vertical position, returning to vertical after the stress has been removed. Under these conditions the tree is experiencing only dynamic bending, alternating between compression and tension, as it moves back and forth. This is considered the primary stress [9].

If the conditions occur long enough, e.g. constant wind flow from one direction, stem displacement and branch development on the leeward side can occur. Under such static loading, the stem may sway but never moves back through the vertical position, a

permanent displacement occurs and compression wood is formed on the lower side. This is considered secondary wind-induced mechanical stress [9].

Nicholls [144] reported that the action of prevailing winds on *Pinus radiata* plantations in Australia generally causes trees to lean on average up to ~5°, with some plantations showing about 70% of the trees being affected. Besides the obvious malformed stem shape, the crooked stems contained severe compression wood.

1.4.5 Influence of Compression Wood

Young trees (saplings) are lissome and easily bent under the influence of wind or snow in the field. At the same time, however, a young stem is usually able to right itself quickly with the aid of appropriately located compression wood. As a result, regions of compression wood are often observed surrounding the pith long after the trunk has resumed a vertical orientation [10]. The amount of compression wood in the tree can vary. For example, a typical black spruce (*Picea mariana* L.) contains about 15% (v/v) compression wood [112]. The percentage of compression wood in Caribbean pine stem is about an average 18% (v/v) [7]. In radiata pine (*Pinus radiata* D. Don), compression wood is most commonly found in juvenile wood, partly because of the high growth rate in this region of the stem [145]. In general, compression wood in pine varies from 5.4% to 57.1% of the commercial volume [79,84].

A large amount of compression wood can have a major effect on the pulping process. Compression wood fibers are short, round with thick cell walls and fewer and smaller pits. These features make them less permeable to the penetration of pulping liquor and water. The large amount of compression wood within black spruce stems and branches

result in a 6~20 % decrease in pulp yield from the kraft process, this corresponds to over 2.3 tons of usable pulp reduction per hectare [86,112].

An increased amount of compression wood in the furnish can lead to an increased lignin content pulp. Higher amounts of residual lignin were reported in compression wood kraft pulp produced under the industrial cooking conditions [112]. The residual lignin within compression wood kraft pulp is expected to have a higher molecular weight and lower reactivity towards bleaching agents, and hence this will increase bleaching requirements [146]. In fact, the final brightness of compression wood pulp was lower than that of normal wood pulp [95].

The inflexibility and rigidity of compression wood fibers lead to pulps that are difficult to improve by beating or refining, and result in pulps with low fibrillation and freeness. However, prolonged beating breaks the weak fibers into short fragments and fines. This causes low tensile strength, and contributes to poor quality pulp and paper. The presence of undercooked bundles of fibers, i.e. shives, originating from stem compression wood and knots, also adversely affects the runnability during papermaking and printing [146].

The presence of compression wood can also cause the downgrading of solid wood products. The flat fibril angles of compression wood tracheids result in excessive shrinkage along the grain, and reduced shrinkage in the radial and tangential directions. Normally, wood shrinks very little longitudinally (generally 0.1% to 0.3%), but compression wood can have in excess of 3% shrinkage upon drying [79]. The real problem occurs when part of a board is compression wood and part is normal wood. The

different amounts in shrinkage result in dimensional instability and all kinds of defects, such as warping and checking [146].

1.4.6 Similarity of Compression Wood and Juvenile Wood

Compression wood in softwood is often associated with juvenile wood [3]. Both juvenile wood and compression wood have short fibers with flat microfibril angles, higher longitudinal shrinkage, higher lignin content, lower cellulose content, lower cellulose crystallinity, and low pulp yield. Subsequently, it is generally considered that the juvenile wood is the same as compression wood [3,77,82,147].

As a result, the increased usage of juvenile wood (compression wood) from fast-growing plantation forests can significantly impact industrial production costs and product quality. Extensive research has been done on comparing the differences between mature wood and juvenile wood, or between normal wood and compression wood; however, the systematic comparison of juvenile wood and compression wood has been limited. Hence, a systematic comparison of the chemical and morphological differences between juvenile wood and compression wood will be proposed.

1.5 Metabolic Profiling

1.5.1 Definition

Metabolic profiling is a relative new and valuable technique being applied in the plant genomic community. Metabolic profiling is the characteristic measurement of a group of related metabolites using chromatographic profiles to determine the function of an interested biosynthetic pathway [148,149]. Metabolic profiling by definition must

embrace a wide range of compounds in a single measurement and given the inevitable biological variability, a somewhat lower degree of precision in quantification can be tolerated [148].

1.5.2 Metabolic Profiling in Plant Science

The first significant metabolic profiling publication on plants was the study by Sauter et al. [148-150]. Gas chromatography–mass spectrometry (GC/MS) was used to study the effect of various herbicides on barley leaves. They chose peaks that represented major compounds in the GC/MS chromatograms to get an overview of the major events in metabolism before and after pesticide application. They concluded that changes in peak profiles following herbicide application were a valuable tool in locating the biochemical site of action of novel herbicides.

The adoption of this technique (metabolic profiling coupled with GC/MS) was further optimized and used to simultaneously profile polar organic metabolites (sugars, sugar alcohols, acid and amino acids) extracted from apricots [151]. Roessner et al. [152] applied the technique to systematically analyze the number of metabolites involved in potato tuber primary metabolism, and ~150 metabolites were identified. Metabolic profiling has been utilized to study metabolite differences and biochemical phenotyping in different transgenic plants, such as *Arabidopsis thaliana* [153] and *Lycopersicon esculentum* [154]. Utilizing the distinct metabolic profile (metabolites data) generated by each genotype in combination with data mining tools such as principal component analysis (PCA, section 1.2.3) has enabled the assignment of "metabolic phenotypes" (Figure 1.25) and the interpretation of the consequences of genetic modification [153].

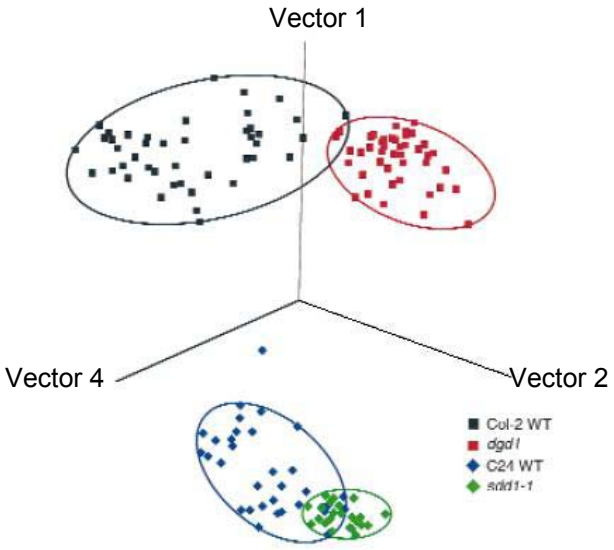

Figure 1.25 Metabolic phenotype clustering found after principal component analysis (PCA) of log-scaled polar metabolite data of 151 samples originating from four *Arabidopsis thaliana* genotypes (two wild types and two genome-modified) [153].

Recently, the first application of metabolic profiling on wood forming tissue in trees was reported [155]. To facilitate the specific analysis of differentiating xylem, Morris et al. [155] optimized the protocol of Fiehn et al. [156], whose original protocol was designed specifically for plant leaf tissue. Sixty metabolites from xylem tissues of loblolly pine were identified by GC and GC/MS [155]. This technique was further applied to wood formation studies [157], including metabolite analysis related to α-cellulose content and growth variations in loblolly pine, and to Balsam Woolly Adelgid (BWA) infestation of Fraser fir. The observed metabolite differences were well correlated to the specific phenotypic trait and response, and provided valuable evidence of correlations between metabolite pools and subsequent wood formation.

1.5.3 Sample Preparation and Analysis

Metabolic profiling using GC/MS can be separated into three major or primary steps: (1) tissue collection and metabolites extraction, (2) chromatographic separation and metabolite identification, and (3) statistical analysis. During tissue collection, it is crucial to immediately stop enzyme activity and any metabolic activity. This can be achieved by immediate immersion of the sample into liquid nitrogen, or acidic treatment using perchloric or nitric acid [149]. Further, it is important to avoid partial thawing of tissue before extracting metabolites.

Prior to metabolite extraction, the tissue is ground into a fine powder to increase extraction efficiency. This is accomplished using a pestle and mortar with liquid nitrogen, or a regular coffee grinder with dry ice [153,155]. The metabolites within the frozen tissue powder are then immediately extracted with organic solvents with heating. In addition to extracting specific metabolites, depending on the solvent used, it also inhibits enzyme activities [158]. Depending on the target compounds groups, different solvents can be used for extraction. Polar metabolites are exacted using methanol, ethanol, or ethyl acetate, while non-polar metabolites are extracted with ether or chloroform [151,153,155,158].

Gas chromatography (GC) separates volatile compounds based on their relative vapor pressure and affinity for the chromatography column. However, many metabolites are not volatile enough or have a high affinity to be separated by GC for typical GC columns, and hence they must be derivatized prior to GC separation. To facilitate GC analysis, metabolites such as alcohols, amines, and acids are derivatized with trimethylsilyl groups,

or in the case of fatty acids with methyl groups [151,153,159]. This technique greatly expands the range of compounds that can be detected and analyzed by GC/MS.

After separation by GC, the metabolites are sent to the mass detector or mass spectrometer. Mass spectrometers (MS) are generally more sensitive and selective than other detectors for small-molecule analysis [160]. In a mass spectrometer, ionized molecules are separated based on their mass-to-charge (m/z) ratio. Each molecule has a distinct m/z ratio and fragment pattern, which when combined with the retention time (or elution time) from the GC, enables successful compound identification (using direct comparison with standard compounds or against mass spectra databases.

For most applications of metabolic profiling, the relative values of metabolites is more important than the absolute values [153]. To enable a comprehensive analysis of the GC data and extract information relative to the different samples, two statistical methods are commonly applied: principal component analysis (PCA) and hierarchical cluster analysis (HCA). Both methods use all the metabolic data from a tissue sample to compute an individual metabolic profile and simultaneously compare this profile with all other metabolic profiles. Once the samples accumulate in the same cluster, this cluster can be viewed as a specific "metabolic phenotype" [149,153,158,161,162], as showed in Figure 1.25.

1.5.4 Alternative Instrumentation for Metabolic Profiling

Although GC/MS is the most established technique utilized in the metabolic profiling of plants [162], not all compounds can be well quantified by GC/MS. Thermolabile or large molecules such as bis- and trisphosphates, Co-enzyme A adducts or lipids can only be

detected after liquid chromatography (LC) separation [149]. High-performance liquid chromatography coupled with photodiode array detector (HPLC/PDA or HPLC/ UV-Vis) has successfully been used to characterize isoprenoids, such as carotenoids (thermallabile in GC analysis), tocopherols, quinines, and chlorophylls, in *Arabidopsis* and *Lycopersicon esculentum* [163,164]. Recently, an application of HPLC/MS in metabolic profiling was introduced in clinical studies of urine samples obtained from rodents [165], and the results successfully showed improved phenotypic classification to probe the different tryptophan biosynthesis activity. HPLC/MS based profiling can identify higher molecular weight compounds that cannot be detected by GC/MS, and also no derivatization is required for HPLC/MS detection [166]. Therefore, combining both GC/MS and HPLC/MS would provide thorough biochemical information of tree metabolite analysis.

1.6 Literature Cited

[1] Prestemon, J.P.; Abt, R.C. Timber products supply and demand. In *Southern Forest Resource Assessment. Gen. Tech. Rep. SRS-53*; D.N. Wear and J.G. Greis, Eds.; Department of Agriculture, Forest Service, Southern Research Station: Asheville, 2002; pp 299-325.

[2] Siry, J.P. Intensive timber management practices. In *Southern Forest Resource Assessment. Gen. Tech. Rep. SRS-53*; D.N. Wear and J.G. Greis, Eds.; Department of Agriculture, Forest Service, Southern Research Station: Asheville, 2002; pp 327-340.

[3] Zobel, B.J.; Sprague, J.R. *Juvenile Wood in Forest Trees*; Springer: New York, 1998.

[4] Zobel, B.J. Using the juvenile wood concept in the southern pines. *South. Pulp Paper Mfg.* **1975**, 14-16.

[5] Timell, T.E. *Compression Wood in Gymnosperms*,Vol.1; Springer-Verlag: New York, 1986.

[6] Zobel, B.J. Wood quality from fast-grown plantation. *TAPPI J.* **1981**, *64*, 71-74.

[7] Bendtsen, B.A. Properties of wood from improved and intensively managed trees. *Forest Prod. J.* **1978**, *28*, 61-72.

[8] Zobel, B.J.; McElwee, R.L. Variation of cellulose in loblolly pine. *TAPPI J.* **1958**, *41*, 167-170.

[9] Telewski, F.W. Wind-induced physiological and developmental responses in trees. In *Wind and Trees*; M.P. Coutts and J. Grace, Eds.; Cambridge University Press: New York, 1995; pp 237-263.
[10] Timell, T.E. *Compression Wood in Gymnosperms*,Vol.2; Springer-Verlag: New York, 1986.
[11] Scurfield, G. Reaction wood: its structure and function. *Science* **1973**, *179*, 647-655.
[12] Zobel, B.J.; Jett, J.B.; Hutto, R. Improving the density of short-rotation loblolly pine. *TAPPI J.* **1978**, *61*, 41-44.
[13] Kellog, R.M.; Thykeson, E. Influence of wood and fiber properties on kraft converting-paper quality. *TAPPI J.* **1975**, *58*, 131-135.
[14] Michell, A.J.; Schimleck, L.R. Developing a method for the rapid assessment of pulp yield of plantation eucalypt trees beyond the year 2000. *Appita J.* **1998**, *51*, 428-432.
[15] Fengel, D.; Wegener, G. Structure and ultrastructure. In *Wood Chemistry, Ultrastructure, Reactions*; Walter de Gruyter: New York, 1989; pp 6-25.
[16] Pope, J.M. Near-infrared spectroscopy of wood products. In *Surface Analysis of Paper*; T.E. Conners and S. Banerjee, Eds.; CRC Press: New York, 1995; pp 142-151.
[17] Ciurczak, E.W. Principles of near-infrared spectroscopy. In *HandBook of Near-Infrared Analysis*; D.A. Burns and E.W. Ciurczak, Eds.; Marcel Dekker: New York, 1992; pp 7-11.
[18] Pavia, D.L.; Lampman, G.M.; Kriz, G.S. *Introduction to Spectroscopy*; Saunders College Publishing: Orlando, 1996.
[19] Lambert, J.B.; Shurvell, H.F.; Lightner, D.A.; Cooks, R.G. *Organic Structural Spectroscopy*; Prentice Hall: New Jersey, 1998.
[20] Workman, J.J.; Burns, D.A. Commercial NIR instrumentation. In *Handbook of Near-Infrared analysis*; D.A. Burns and E.W. Ciurczak, Eds.; Marcel Dekker: New York, 1992; pp 37-51.
[21] Michell, A.J. Pulpwood quality estimation by near-infrared spectroscopic measurements on eucalypt woods. *Appita J.* **1995**, *48*, 425-428.
[22] NIRSystems, F. *Manuual for VISION software*: Silver Spring, Maryland, 2001.
[23] Schultz, T.P.; Burns, D.A. Rapid secondary analysis of lignocellulose: comparison of near infrared (NIR) and Fourier transform infrared (FTIR). *TAPPI J.* **1990**, *73*, 209-212.
[24] McClure, W.F. Near-infrared spectroscopy. In *Spectroscopic Techniques for Food Analysis*; R.H. Wilson, Ed.; VCH Publishers, Inc.: New York, 1994; pp 13-57.
[25] Osborne, B.G.; Fearn, T.; Hindle, P.H. *Practical NIR Spectroscopy: with Applications in Food and Beverage Analysis*. 2nd ed.; Longman Scientific & Technical: London, 1993.
[26] Beebe, K.R.; Pell, R.J.; Seasholtz, M.B. *Chemometrics: a practical guide*; John Wiley & Sons: New York, 1998.
[27] Kramer, R. *Chemometric Techniques for Quantitative Analysis*; Marcel Dekker: New York, 1998.
[28] Bailleres, H.; Davrieus, F.; Ham-Pichavant, F. Near infrared analysis as a tool for rapid screening of some major wood characteristics in a eucalyptus breeding program. *Ann. For. Sci.* **2002**, *59*, 479-490.

[29] Mark, H.; Workman, J. Statistics in Spectroscopy. Academic Press: San Diego, California, 1991; pp 287-302.
[30] Schimleck, L.R.; Doran, J.C.; Rimbawanto, A. Near infrared spectroscopy for cost effective screening of foliar oil characteristics in a *Melaleuca cajuputi* breeding population. *J. Agric. Food Chem.* **2003**, *51*, 2433-2437.
[31] Williams, P.C.; Sobering, D.C. Comparison of commercial near infrared transmittance and reflectance instruments for the analysis of whole grains and seeds. *J. Near Infrared Spec.* **1993**, *1*, 25-33.
[32] Schimleck, L.R.; David Jones, P.; Peter, G.F.; Daniels, R.F.; Clarklll, A. Nondestructive estimation of tracheid length from sections of radial wood strips by near infrared spectroscopy. *Holzforschung* **2004**, *58*, 375-381.
[33] Schimleck, L.R.; Evans, R. Estimation of *Pinus radiata* D. Don tracheid morphological characteristics by near infrared spectroscopy. *Holzforschung* **2004**, *58*, 66-73.
[34] Frankhuizen, R. NIR analysis of dairy products. In *Handbook of Near-Infrared Analysis*; D.A. Burns and E.W. Ciurczak, Eds.; Marcel Dekker: New York, 1992; pp 609-641.
[35] Kays, S.E.; Barton, F.E.I. Near-infrared analysis of soluble and insoluble dietary fiber fractions of cereal food products. *J Agric. Food Chem.* **2002**, *50*, 3024-3029.
[36] Camacho, W.; Valles-Lluch, A.; Ribes-Greus, A.; Karlsson, S. Determination of moisture content in Nylon 6,6 by near-infrared spectroscopy and chemometrics. *J. Appl. Polym. Sci.* **2003**, *87*, 2165-2170.
[37] Svensson, O.; Josefson, M.; Langkilde, W. Classification of chemistry modified celluloses using a near-infrared spectrometer and soft independent modeling of class analogies. *Appl. Spectrosc.* **1997**, *51*, 1826-1835.
[38] Wessman, C.A.; Aber, J.D.; Peterson, D.L.; Melillo, J.M. Foliar analysis using near-infrared reflectance spectroscopy. *Can. J. For. Res.* **1988**, *18*, 6-11.
[39] Gierlinger, N.; Schwanninger, M.; Hinterstoisser, B.; Wimmer, R. Rapid determination of heartwood extractives in *Larix sp.* by means of Fourier transform near infrared spectroscopy. *J. Near Infrared Spec.* **2002**, *10*, 203-214.
[40] Poke, F.S.; Wright, J.K.; Raymond, C.A. Predicting extractives and lignin contents in *Eucalyptus globulus* using near infrared reflectance analysis. *J. Wood Chem. Technol.* **2004**, *24*, 55-67.
[41] Schimleck, L.R.; Wright, P.J.; Michell, A.J.; Wallis, A.F.A. Near-infrared spectra and chemical compositions of *E. globulus* and *E. nitens* plantation woods. *Appita J.* **1997**, *50*, 40-46.
[42] Schimleck, L.R.; Michell, A.J.; Raymond, C.A.; Muneri, A. Estimation of basic density of *Eucalyptus globulus* using near-infrared spectroscopy. *Can. J. For. Res.* **1999**, *29*, 194-201.
[43] Hauksson, J.B.; Bergqvist, G.; Bergsten, U.; Sjostrom, M.; Edlund, U. Prediction of basic wood properties for Norway spruce. Interpretation of near infrared spectroscopy data using partial least squares regression. *Wood Sci. Technol.* **2001**, *35*, 475-485.
[44] Schimleck, L.R.; Evans, R. Estimation of microfibril angle of increment cores by near infrared spectroscopy. *IAWA J.* **2002**, *23*, 225-234.

[45] Raymond, C.A.; Schimleck, L.R.; Muneri, A.; Michell, A.J. Nondestructive sampling of *Eucalyptus globulus* and *E. nitens* for wood properties. III. Predicted pulp yield using near infrared reflectance analysis. *Wood Sci. Technol.* **2001**, *35*, 203-215.
[46] Fardim, P.; Ferreira, M.M.C.; Duran, N. Multivariate calibration for quantitative analysis of eucalypt kraft pulp by NIR spectrometry. *J. Wood Chem. Technol.* **2002**, *22*, 67-81.
[47] Wright, J.A.; Birkett, M.D.; Gambino, M.J.T. Prediction of pulp yield and cellulose content from wood samples using near infrared reflectance. *TAPPI J.* **1990**, *73*, 164-166.
[48] Easty, D.B.; Berben, S.A. Near-infrared spectroscopy for the analysis of wood pulp: quantifying hardwood-softwood mixtures and estimating lignin content. *TAPPI J.* **1990**, *73*, 257-261.
[49] Rials, T.G.; Kelley, S.S.; So, C.-L. Use of advanced spectroscopic techniques for predicting the mechanical properties of wood composites. *Wood Fiber Sci.* **2002**, *34*, 398-407.
[50] Kelley, S.S.; Rials, T.G.; Groom, L.R.; So, C.-L. Use of near infrared spectroscopy to predict the mechanical properties of six softwoods. *Holzforschung* **2004**, *58*, 252-260.
[51] Schimleck, L.R.; Evans, R.; Llic, J. Estimation of *Eucalyptus delegatensis* wood properties by near infrared spectroscopy. *Can. J. For. Res.* **2001**, *31*, 1671-1675.
[52] Schimleck, L.R.; Evans, R.; Ilic, J.; Matheson, A.C. Estimation of wood stiffness of increment cores by near-infrared spectroscopy. *Can. J. For. Res.* **2002**, *32*, 129-135.
[53] Brunner, M.; Eugster, R.; Trenka, E.; BerganminStrotz, L. FT-NIR spectroscopy and wood identification. *Holzforschung* **1996**, *50*, 130-134.
[54] Tsuchikawa, S.; Inoue, K.; Noma, J.; Hayashi, K. Application of near-infrared spectroscopy to wood discrimination. *J. Wood Sci.* **2003**, *49*, 29-35.
[55] Zobel, B.J.; Webb, C.; Henson, F. Core or juvenile wood of loblolly and slash pine trees. *TAPPI J.* **1959**, *42*, 345-356.
[56] Zobel, B.J.; Jett, J.B. Tree form and internal tree characteristics. In *Genetics of Wood Production*; Springer-Verlag: New Yok, 1995; pp 166-198.
[57] Zobel, B.J.; Blair, R. Wood and pulp properties of juvenile wood and topwood of the southern pines. *Appl. Polym. Symp.* **1976**, *28*, 421-433.
[58] Clark III, A.; Saucier, J.R. Influence of initial planting density, geographic location, and species on juvenile wood formation in southern pine. *Forest Prod. J.* **1989**, *39*, 42-48.
[59] Yang, K.C.; Benson, C.A.; Wong, J.K. Distribution of juvenile wood in two stems of *Larix laricina*. *Can. J. For. Res.* **1986**, *16*, 1041-1049.
[60] Harding, F. Juvenile wood formation theory. *Forest. Chron.* **2004**, *80*, 9.
[61] Yang, K.C. Impact of spacing on width and basal area of juvenile wood and mature wood in *Picea mariana* and *Picea Glauca*. *Wood Fiber Sci.* **1994**, *26*, 479-488.
[62] Gartner, B.L. Does photosynthetic bark have a role in the production of core vs. outer wood? *Wood Fiber Sci.* **1996**, *1996*, 53-61.
[63] Wilkes, J. Review of the significance of variations in wood structure in the utilization of *Pinus radiata*. *Aust. For. Res.* **1987**, *17*, 215-232.

[64] McAlister, R.H.; Clark III, A. Effect of geographic location and seed source on the bending properties of juvenile and mature loblolly pine. *Forest Prod. J.* **1991**, *41*, 39-42.
[65] Harris, G. Comparison of northern softwood and southern pine fiber characteristics for groundwood publication papers. *TAPPI J.* **1993**, *76*, 55-61.
[66] Zhu, J.; Tadooka, N.; Takata, K. Growth and wood quality of sugi (*Cryptomeria japonica*) planted in Akita prefecture (II). juvenile/mature wood determination of aged trees. *J. Wood Sci.* **2005**, *51*, 95-101.
[67] Byrd, V.L. Wood characteristics and kraft paper properties of four selected loblolly pines. *Forest Prod. J.* **1965**, *15*, 313-320.
[68] Sahlberg, U.; Salmen, L.; Oscarsson, A. The fibrillar orientation in the S2-layer of wood fibres as determined by X-ray diffraction analysis. *Wood Sci. Technol.* **1997**, *31*, 77-86.
[69] Donaldson, L.A. Within-and between-tree variation in microfibril angle in *Pinus radiata*. *New Zeal. J. For. Sci.* **1992**, *22*, 77-86.
[70] Donaldson, L.A.; Burdon, R.D. Clonal variation and repeatability of microfibril angle in *Pinus radiata*. *New Zeal. J. For. Sci.* **1995**, *25*, 164-174.
[71] Megraw, R.A. *Wood Qualitiy Factors in Loblolly Pine*; TAPPI Press: Atlanta, GA, USA, 1985.
[72] Hatton, J.V.; Hunt, K. Wood density and chemical properties of second-growth lodgepole pine. *Pulp Pap. Can.* **1993**, *94*, 140-146.
[73] Hatton, J.V. Pulping and papermaking properties of managed second-growth softwoods. *TAPPI J.* **1997**, *80*, 178-184.
[74] Bao, F.C.; Jiang, Z.H.; Jiang, X.M.; Lu, X.X.; Luo, X.Q.; Zhang, S.Y. Differences in wood properties between juvenile wood and mature wood in 10 species grown in China. *Wood Sci. Technol.* **2001**, *35*, 363-375.
[75] Shupe, T.F.; Choong, E.T.; Yang, C.H. The effects of silvicultural treatments on the chemical composition of plantation-grown loblolly pine wood. *Wood Fiber Sci.* **1996**, *28*, 295-300.
[76] Larson, P.R. Changes in chemical composition of wood cell walls associated with age. *Forest Prod. J.* **1966**, *16*, 37-45.
[77] Lee, C.L. Crystallinity of wood cellulose fibers. *Forest Prod. J.* **1961**, *11*, 108-112.
[78] Newman, R.H. Homogeneity in cellulose crystallinity between samples of *Pinus radiata* wood. *Holzforschung* **2004**, *58*, 91-96.
[79] Zobel, B.J.; Van Buijtenen, J.P. *Wood Variation: Its Causes and Control*; Springer-verlag, Berlin-Heidelberg-New York, 1989.
[80] Harwood, V.D. Variation in carbohydrate analyses in relation to wood age in *Pinus radiata*. *Holzforschung* **1971**, *25*, 73-77.
[81] Kirk, D.G.; Breeman, L.G.; Zobel, B.J. A pulping evaluation of juvenile loblolly pine. *TAPPI J.* **1972**, *55*, 1600-1604.
[82] Zobel, B.J. The changing quality of the world wood supply. *Wood Sci. Technol.* **1984**, *18*, 1-17.
[83] Barefoot, A.C.; Hitchings, R.G.; Ellwood, E.L. Wood characteristics and kraft paper properties of four selected loblolly pines. III: effect of fiber morphology on pulp. *TAPPI J.* **1965**, *49*, 137-147.

[84] Barefoot, A.C.; Hitchings, R.G.; Ellwood, E.L. Wood characteristics and kraft paper properties of four selected loblolly pines. I. effect of fiber morphology under identical cooking conditions. *TAPPI J.* **1964**, *47*, 343-356.
[85] Barefoot, A.C.; Hitchings, R.G.; Ellwood, E.L. Wood characteristics and kraft paper properties of four selected loblolly pines. III. effect of fiber morphology in pulps examined at a constant permanganate number. *TAPPI J.* **1966**, *49*, 137-147.
[86] Mancosky, D.G.; Ban, W.; Lucia, L.A. Chemical study of the variation in the bleaching and pulping response of predominantly juvenile and mature northern black spruce fractions. *Ind. Eng. Chem. Res.* **2005**, *44*, 1652-1659.
[87] Kwon, M.; Bedgar, D.L.; Piastuch, W.; Davin, L.B.; Lewis, N.G. Induced compression wood formation in Douglas fir (*Pseudotsuga menziesii*) in microgravity. *Phytochem.* **2001**, *57*, 847-857.
[88] Bamber, R.K. A general theory for the origin of growth stress in reaction wood: how trees stay upright. *IAWA J.* **2001**, *22*, 205-212.
[89] Sjostrom, E. The structure of wood. In *Wood Chemistry, Fundamentals and Applications*; Academic Press: New York, 1993; pp 18-20.
[90] Wardrop, A.B.; Dadswell, H.E. The nature of reaction wood. IV. variations in cell wall organization of tension wood fibers. *Aust. J. Bot.* **1955**, *3*, 177-189.
[91] Bland, D.E. The chemistry of reaction wood. Part I. the lignins of *Eucalyptus goniocalyx* and *Pinus radiata*. *Holzforschung* **1958**, *12*, 36-43.
[92] Shelbourne, C.J.; Ritchie, K.S. Relationships between degree of compression wood development and specific gravity and tracheid characteristics in loblolly pine. *Holzforschung* **1968**, *22*, 185-190.
[93] Wardrop, A.B.; Davies, G.W. The nature of reaction wood. VIII. the structure and differentiation of compression wood. *Aust. J. Bot.* **1964**, *12*, 24-38.
[94] Timell, T.E. Recent progress in the chemistry and topochemistry of compression wood. *Wood Sci. Technol.* **1982**, *16*, 83-122.
[95] Hortling, B.; Tamminen, T.; Pekkala, O. Effects of delignification on residual lignin-carbohydrate complexes in normal pine wood and pine wood enriched in compression wood .1. kraft pulping. *Nordic Pulp Pap. Res. J.* **2001**, *16*, 219-224.
[96] Onnerud, H.; Gellerstedt, G. Inhomogeneities in the chemical structure of spruce lignin. *Holzforschung* **2003**, *57*, 165-170.
[97] Sakakibara, A. A structure model of softwood lignin. *Wood Sci. Technol.* **1980**, *14*, 89-100.
[98] Erickson, M.; Larsson, S.; Miksche, G.E. Gas-chromatographische analyse von ligninoxydationsprodukten. VII. Zur struktur des lignins der Fichte. *Acta Chem. Scand.* **1973**, *27*, 903-904.
[99] Morohoshi, N.; Sakakibara, A. The chemical composition of reaction wood. II. *Mokuzai Gakkaishi* **1971**, *17*, 400-404.
[100] Yasuda, S.; Sakakibara, A. The chemical composition of lignin from compression wood. *Mokuzai Gakkaishi* **1975**, *21*, 363-369.
[101] Nimz, H.H.; Robert, D.; Faix, O.; Nemr, M. Carbon-13 NMR spectra of lignins, 8. Structural differences between lignins of hardwoods, softwoods, grasses and compression wood. *Holzforschung* **1981**, *35*, 16-26.

[102] Lapierre, C.; Monties, B.; Rolando, C. Thioacidolyses of diazomethane-methylated pine compression wood and wheat straw *in situ* lignin. *Holzforschung* **1988**, *42*, 409-411.
[103] Lapierre, C.; Rolando, C. Thioacidolysis of pre-methylated lignin samples from pine compression and poplar woods. *Holzforschung* **1988**, *42*, 1-4.
[104] Suckling, I.D.; Pasco, M.F.; Hortling, B.; Sundquist, J. Assessment of lignin condensation by GPC analysis of lignin thioacidolysis products. *Holzforschung* **1994**, *48*, 501-503.
[105] Fukushima, K.; Taguchi, S.; Matsui, N.; Yasuda, S. Distribution and seasonal changes of monolignol glucosides in *Pinus thunbergii*. *Mokuzai Gakkaishi* **1997**, *43*, 254-259.
[106] Yasuda, S.; Sakakibara, A. Hydrogenolysis of protolignin in compression wood .I. isolation of two dimers with C_{β}–C5 composed of p-hydroxylphenyl and guaiacyl nuclei and two p-hydroxyphenyl nuclei, respectively. *Mokuzai Gakkaishi* **1975**, *21*, 370-375.
[107] Yasuda, S.; Sakakibara, A. Isolation of a new dimeric condensed type compound from hydrogenolysis products of compression wood lignin. *Mokuzai Gakkaishi* **1975**, *21*, 639-640.
[108] Yasuda, S.; Sakakibara, A. Hydrogenolysis of protolignin in compression wood. II. isolation of two dimers with β-aryl ether linkage and phenylisochroman structure. *Mokuzai Gakkaishi* **1976**, *22*, 606-612.
[109] Yasuda, S.; Sakakibara, A. Hydrogenolysis of protolignin in compression wood .III. isolation of four dimeric compounds with carbon to carbon linkage. *Mokuzai Gakkaishi* **1977**, *23*, 114-119.
[110] Yasuda, S.; Sakakibara, A. Hydrogenolysis of protolignin in compression wood. IV. isolation of a diphenyl ether and three dimeric compounds with carbon to carbon linkage. *Mokuzai Gakkaishi* **1977**, *23*, 383-387.
[111] Yasuda, S.; Sakakibara, A. Hydrogenolysis of protolignin in compression wood. V. isolation of two trimeric compounds with γ-lactone ring. *Holzforschung* **1981**, *35*, 183-187.
[112] Lohrasebi, H.; Mabee, W.E.; Roy, D.N. Chemistry and pulping feasibility of compression wood in black spruce. *J. Wood Chem. Technol.* **1999**, *19*, 13-25.
[113] Tanaka, T.; Koshijima, T. Characterization of cellulose in compression and opposite woods of a *Pinus densiflora* tree grown under the influence of strong wind. *Wood Sci. Technol.* **1981**, *15*, 265-273.
[114] Cote, W.A.; Pickard, P.A.; Timell, T.E. Studies in compression wood. IV. Fractional extraction and preliminary characterization of polysaccharides in normal and compression wood of balsam fir. *TAPPI J.* **1967**, *50*, 350-356.
[115] Mukoyoshi, S.; Azuima, J.; Koshijima, T. Lignin-carbohydrate complexes from compression wood of *Pinus densiflora* sieb et. zucc. *Holzforschung* **1981**, *35*, 233-240.
[116] Nanayakkara, B.; Manley-Harris, M.; Suckling, I.D.; Donaldson, L.A. Chemical characterization of compression wood in *Pinus radiata*. *13th International Symposium on Wood, Fibre and Pulping Chemistry (13th ISWFPC), Auckland, New Zealand*; Appita Inc.; Vol. 2, pp 585-592.

[117] Newman, R.H.; Hemmingson, J.A.; Butterfield, B.G. A micro-analytical approach to the carbohydrate chemistry of compression wood. *13th International Symposium on Wood, Fibre and Pulping Chemistry (13th ISWFPC), Auckland, New Zealand*; Appita Inc.; Vol. 2, pp 593-596.
[118] Bouveng, H.O.; Meier, H. Studies on a galactan from norwegian spruce compression wood (*Picea abies* Karst.). *Acta Chem. Scand.* **1959**, *13*, 1884-1889.
[119] Schreuder, H.R.; Cote, W.A.; Timell, T.E. Studies on compression wood. Part 3. Isolation and characterization of a galactan from compression wood of red spruce. *Sven. Papperstidn.* **1966**, *69*, 641-657.
[120] Jiang, K.S.; Timell, T.E. Polysaccharides in compression wood of tamarack (*Larix laricina*). *Sven. Papperstidn.* **1972**, *75*, 592-594.
[121] Minor, J.L. Chemical linkage of pine polysaccharides to lignin. *J. Wood Chem. Technol.* **1982**, *2*, 1-16.
[122] Kutsuki, H.; Higuchi, T. Activities of some enzymes of lignin formation in reaction wood of *Thuja orientalis*, *Metasequoia glyptoboides* and *Robinia pseudoacacia*. *Planta* **1981**, *152*, 365-368.
[123] Zhang, X.H.; Chiang, V.L. Molecular cloning of 4-coumarate:coenzyme A ligase in loblolly pine and the roles of this enzyme in the biosynthesis of lignin in compression wood. *Plant Physiol.* **1997**, *113*, 65-74.
[124] Li, L.G.; Popko, J.L.; Umezawa, T.; Chiang, V.L. 5-Hydroxyconiferyl aldehyde modulates enzymatic methylation for syringyl monolignol formation, a new view of monolignol biosynthesis in angiosperms. *J. Biol. Chem.* **2000**, *275*, 6537-6545.
[125] Popko, J.L. Requlatory enzymes of lignin biosynthesis in normal and compression wood of loblolly pine. M.S. Thesis, Michigan Technology University, 1993.
[126] Anterola, A.M.; van Rensburg, H.; van Heerden, P.S.; Davin, L.B.; Lewis, N.G. Multi-site modulation of flux during monolignol formation in loblolly pine (*Pinus taeda*). *Biochem. Biophys. Res. Comm.* **1999**, *261*, 652-657.
[127] Whetten, R.; Sun, Y.-H.; Zhang, Y.; Sederoff, R.R. Functional genomics and cell wall biosynthesis in loblolly pine. *Plant Mol. Biol.* **2001**, *47*, 275-291.
[128] Takabe, K.; Fujita, M.; Harada, H.; Saiki, H. Autoradiographic investigation of lignification in the cell walls of Cryptomeria (*Cryptomeria japonica* D. Don). *Mokuzai Gakkaishi* **1985**, *31*, 613-619.
[129] Takabe, K.; Fujita, M.; Harada, H.; Saiki, H. Lignification process of japanese black pine (*Pinus Thunbergii* Parl.) tracheids. *Mokuzai Gakkaishi* **1981**, *27*, 813-820.
[130] Terashima, N.; Fukushima, K. Heterogeneity in formation of lignin Part XI: an autoradiographic study of the heteroeneous formation and structure of pine lignin. *Wood Sci. Technol.* **1988**, *22*, 259-270.
[131] Fukushima, K.; Terashima, N. Heterogeneity in formation of lignin Part XV: formation and structure of lignin in compression wood of *Pinus thunbergii* studied by microautoradiography. *Wood Sci. Technol.* **1991**, *25*, 371-381.
[132] Srivastava, L.M. Tropic and nontropic responses to environmental signals. In *Plant Growth and Development: Hormones and Environment*; L.M. Srivastava, Ed.; Academic Press: San Diego, 2001; pp 717-756.

[133] Hellgren, J.M.; Olofsson, K.; Sundberg, B. Patterns of auxin distribution during gravitational induction of reaction wood in poplar and pine. *Plant Physiol.* **2004**, *135*, 212-220.
[134] Little, C.H.A.; Pharis, R.P. Hormonal control of radial and longitudinal growth in the tree stem. In *Plant Stem: Physiological and Function Morphology*; B.L. Gartner, Ed.; Academic Press, Inc.: San Diego, 1995; pp 281-319.
[135] Starbuck, C.J.; Phelps, J.E. Induction of compression wood in rooted cuttings of *Pseudotsuga menziesii* (Mirb.) Franco by indole-3-acetic acid. *IAWA Bull. n.s.* **1986**, *7*, 13-16.
[136] Phelps, J.E.; McGinnes, E.A.; Smolinski, M.; Saniewski, M.; Pieniazek, J. A note on the formation of compression wood induced by morphactin IT3456 in *Thuja* shoots. *Wood Fiber* **1977**, *8*, 223-227.
[137] Yamaguchi, K.; Itoh, T.; Shimaji, K. Compression wood induced by 1-N-naphthylphthalamic acid (NPA), an IAA transport inhibitor. *Wood Sci. Technol.* **1980**, *14*, 181-185.
[138] Funada, R.; Mizukami, E.; Kubo, T.; Fushitani, M.; Sugiyama, T. Distribution of indole-3-acetic acid and compression wood formation in the stems of inclined *Cryptomeria japonica*. *Holzforschung* **1990**, *44*, 331-334.
[139] Wilson, B.F.; Chien, C.T.; Zaerr, J.B. Distribution of endogenous indole-3-acetic acid and compression wood formation in reoriented branches of Douglas-Fir. *Plant Physiol.* **1989**, *91*, 338-344.
[140] Sundberg, B.; Tuominen, H.; Little, C.H.A. Effects of the indole-3-acetic-acid (IAA) transport inhibitors N-1-naphthylphthalamic acid and morphactin on endogenous IAA dynamics in relation to compression wood formation in 1-year-old *Pinus sylvestris* (L) Shoots. *Plant Physiol.* **1994**, *106*, 469-476.
[141] Okuyama, T.; Takeda, H.; Yamamoto, H.; Yoshida, M. Relation between growth stress and lignin concentration in the cell wall: ultraviolet microscopic spectral analysis. *J. Wood Sci.* **1998**, *44*, 83-89.
[142] Huang, Y.S.; Chen, S.S.; Lin, T.P.; Chen, Y.S. Growth stress distribution in leaning trunks of *Cryptomeria japonica*. *Tree Physiol.* **2001**, *21*, 261-266.
[143] Yamamoto, H.; Okuyama, T.; Yoshida, M.; Sugiyama, T. Generation process of growth stresses in cell walls III. Growth stress in compression wood. *Mokuzai Gakkaishi* **1991**, *37*, 94-100.
[144] Nicholls, J.W.P. Wind action, leaning trees and compression wood in *Pinus radiata* D. Don. *Aust. For. Res.* **1982**, *12*, 75-91.
[145] Donaldson, L.A.; Singh, A.P.; Yoshinaga, A.; Takabe, K. Lignin distribution in mild compression wood of *Pinus radiata*. *Can. J. Bot.* **1999**, *77*, 41-50.
[146] Timell, T.E. *Compression Wood in Gymnosperms*,Vol.3; Springer-Verlag: New York, 1986.
[147] Watanabe, H.; Tsutsumi, J.; Kojima, K. Studies on juvenile wood. I. experiments on stems of sugi trees (*Cryptomeria japonica* D.Don). *Mokuzai Gakkaishi* **1963**, *9*, 225-230.
[148] Trethewey, R.N.; Krotzky, A.J.; Willmitzer, L. Metabolic profiling: a Rosetta Stone for genomics? *Curr. Opin. Plant Biol.* **1999**, *2*, 83-85.
[149] Fiehn, O. Metabolomics - the link between genotypes and phenotypes. *Plant Mol. Biol.* **2002**, *48*, 155-171.

[150] Sauter, H.; Lauer, M.; Fritsch, H. Metabolic profiling of plants: a new diagnostic technique. In *American Chemical Society Symposium Series, 443*; D.R. Baker; J.G. Fenyes and W.K. Moberg, Eds.; American Chemical Society: Washington DC, 1991; pp 288-299.
[151] Katona, Z.F.; Sass, P.; Molnar-Perl, I. Simultaneous determination of sugars, sugar alcohols, acids and amino acids in apricots by gas chromatography-mass spectrometry. *J. Chromatogr. A*. **1999**, *847*, 91-102.
[152] Roessner, U.; Wagner, C.; Kopka, J.; Trethewey, R.N.; Willmitzer, L. Simultaneous analysis of metabolites in potato tuber by gas chromatography-mass spectrometry. *Plant J.* **2000**, *23*, 131-142.
[153] Fiehn, O.; Kopka, J.; Dormann, P.; Altmann, T.; Trethewey, R.N.; Willmitzer, L. Metabolite profiling for plant functional genomics. *Nat. Biotechnol.* **2000**, *18*, 1157-1161.
[154] Roessner-Tunali, U.; Hegemann, B.; Lytovchenko, A.; Carrari, F.; Bruedigam, C.; Granot, D.; Fernie, A.R. Metabolic profiling of transgenic tomato plants overexpressing hexokinase reveals that the influence of hexose phosphorylation diminishes during fruit development. *Plant Physiol.* **2003**, *133*, 84-99.
[155] Morris, C.R.; Scott, J.T.; Chang, H.M.; Sederoff, R.R.; O'Malley, D.; Kadla, J.F. Metabolic profiling: a new tool in the study of wood formation. *J. Agric. Food Chem.* **2004**, *52*, 1427-1434.
[156] Fiehn, O. Protocal for Plant Leaf Metabolite Profiling. *http://www.mpimp-golm.mpg.de/fiehn/blatt-protokoll-e.html*. **2000**.
[157] Morris, C.R. Applications of metabolic profiling in the study of wood formation. Ph.D. Thesis, North Carolina State University, 2005.
[158] Fiehn, O. Combining genomics, metabolome analysis, and biochemical modelling to understand metabolic networks. *Comp. Funct. Genom.* **2001**, *2*, 155-168.
[159] Adams, M.A.; Chen, Z.L.; Landman, P.; Colmer, T.D. Simultaneous determination by capillary gas chromatography of organic acids, sugars, and sugar alcohols in plant tissue extracts as their trimethylsilyl derivatives. *Anal. Biochem.* **1999**, *266*, 77-84.
[160] Glassbrook, N.; Beecher, C.; Ryals, J. Metabolic profiling on the right path. *Nat. Biotechnol.* **2000**, *18*, 1142-1143.
[161] Jurs, P.C. Pattern recognition used to investigate multivariate data in analytical chemistry. *Science* **1986**, *232*, 1219-1224.
[162] Roessner, U.; Luedemann, A.; Brust, D.; Fiehn, O.; Linke, T.; Willmitzer, L.; Fernie, A.R. Metabolic profiling allows comprehensive phenotyping of genetically or environmentally modified plant systems. *Plant Cell* **2001**, *13*, 11-29.
[163] Romer, S.; Fraser, P.D.; Kiano, J.W.; Shipton, C.A.; Misawa, N.; Schuch, W.; Bramley, P.M. Elevation of the provitamin A content of transgenic tomato plants. *Nat. Biotechnol.* **2000**, *18*, 666-669.
[164] Fraser, P.D.; Elisabete S. Pinto, M.; Holloway, D.E.; Bramley, P.M. Application of high-performance liquid chromatography with photodiode array detection to the metabolic profiling of plant isoprenoids. *Plant J.* **2000**, *24*, 551-558.
[165] Wilson, I.D.; Nicholson, J.K.; Castro-Perez, J.; Granger, J.H.; Johnson, K.A.; Smith, B.W.; Plumb, R.S. High resolution "Ultra performance" liquid

chromatography coupled to oa-TOF mass spectrometry as a tool for differential metabolic pathway profiling in functional genomic studies. *J. Proteom. Res.* **2005**, *4*, 591-598.

[166] Holland, J.F.; Leary, J.J.; Sweeley, C.C. Advanced instrumentation and strategies for metabolic profiling. *J. Chromatogr.* **1986**, *379*, 3-26.

2. RESEARCH OBJECTIVE

Based on the problems suggested in the review sections, there are two major objectives in this study; one is providing a fast and reliable wood chemical property screening technique, and the other involving a comprehensive within-tree variation study.

The first part of this thesis deals with the development of a rapid and accurate wood chemical property screening tool using transmittance near infrared spectroscopy (Chapter 3 and Chapter 4). This application will be on successfully screening the elite trees for tree-breeding programs.

The second part of this thesis focuses on the within tree variation caused by juvenile and compression wood in loblolly pine. The emphasis will be on whether the morphology and chemistry (Chapter 5) and metabolic phenotypes (Chapter 6) of juvenile wood are identical to compression wood. In addition, whether juvenile wood from the top of the tree is identical to that from the bottom of the tree, and how much chemical structure difference there is between juvenile wood and mature wood (Chapter 7).

3. RAPID PREDICTION OF SOLID WOOD LIGNIN CONTENT USING TRANSMITTANCE NEAR-INFRARED SPECTROSCOPY[ab]

[a]Published in *J. Agric. Food Chem.* (2004) 52:1435-1439.

Ting-Feng Yeh[1], Hou-min Chang[1], and John F. Kadla[1,2]

[1]North Carolina State University, Raleigh, NC 27695

[2]University of British Columbia, Vancouver, B.C. V6T 1Z4

[b]Parts of the content were presented in 12th ISWPC, Madison, Wisconsin USA, June 9-12, 2003

3.1 Summary

A rapid transmittance near infrared (NIR) spectroscopic method has been developed to characterize the lignin content of solid wood. Using simple, multiple regression, and partial least square statistical analysis the lignin content of wood wafers, taken from increment cores, and synthetic wood, prepared by blending milled wood lignin and holocellulose were compared and quantified. Strong correlations were obtained between the predicted NIR results and those obtained from traditional chemical methods. In addition to the experimental protocol and method development, NIR results from wood samples with different particle sizes and varying lignin content are discussed.

3.2 Introduction

Increasing global population is placing substantial pressures on the forest industry. The demand for forest products is increasing. However, environmental concerns and the loss of available land for forestation is making the ability to meet that demand more challenging. In order for the U.S. forest industry to meet future demand and maintain global competitiveness, more wood with targeted characteristics will have to be produced more efficiently on less land. To accomplish this, the majority of the softwood pulpwood supply in this country will have to come from intensively managed fast-growing plantation forests. This will result in a substantial increase in the proportion of juvenile wood entering the pulp mill, significantly impacting both production cost and product quality. Genetic improvement must focus not only on the quantity, but also on the quality of the raw material, and must develop raw materials uniquely suited for a particular processes and products.

The variation in most wood properties within a species is under a relatively high degree of genetic control [1]. Wood properties, which are related to product quality, include density, tracheid diameter and length, cell wall thickness and chemical composition. Paper properties such as burst, tear strength and tensile strength are closely related to fiber morphology [2], while processing costs and resultant profitability are more significantly affected by chemical composition [3]. Despite this, most operational breeding programs have placed limited emphasis on wood quality traits. This is largely due to the high costs of sampling and assessment. As the global market places more emphasis on wood properties, rapid, precise, and cost-effective assessment tools need to be developed.

Near-infrared spectroscopy (NIR) is a rapid, non-destructive technique that has been extensively used both quantitatively and qualitatively in the forest products industry [4-10]. However, this work has been done using reflectance NIR spectroscopy. Reflectance measurements suffer from several limitations, the most serious being the small penetration depth (1-4 mm) into the sample. For nonhomogeneous samples such as wood, this limited penetration leads to a large variation in results and a strong dependence on sample size and preparation technique. Thus, large sample sizes are typically utilized to better represent the sample of interest. By contrast, transmittance techniques, which penetrate fully through the sample [11], are less sensitive to sample preparation and homogeneity and permit analysis of smaller quantity samples. For whatever reason, the utilization of transmittance NIR in the analysis of wood has been limited. Here, we describe the use of transmittance NIR spectroscopy for characterizing the lignin content in wood. Using synthetic wood, produced by mechanically mixing milled wood lignin

and holocellulose and wood increment core microtome sections regression models have been developed and are discussed.

3.3 Experimental

3.3.1 Materials

Wood meal samples were from the mature section (sapwood) of a 33-year old loblolly pine (*Pinus taeda*). The wood was chipped and subsequently ground using a Wiley Mill (standard model #3) into wood meals. The wood meals were further screened into fractions of different particle size using a stack of various mesh screens. Milled wood lignin (MWL) was prepared from the same batch of wood meals according to a previously published method [12].

Wood increment core samples were collected from 12-year-old loblolly pine received from the Tree Breeding Program, Department of Forestry, North Carolina State University. The increment wood cores were extracted by acetone as described previously [13]. The extractives-free wood cores were soaked in deionized. water overnight and the 3rd-year-ring springwood was sectioned into thin wafers using a microtome. The wet-thickness was 200 μm. The wood wafers were dried under vacuum over P_2O_5 overnight prior to NIR measurement. All NIR spectra were recorded prior to lignin content determination (see below).

3.3.2 Holocellulose Preparation

Wood meal, 5 g oven-dried weight, was weighed into a 500 ml Erlenmeyer flask, to which 200 ml of 90 °C deionized water was then added, followed by 10 ml of acetic acid

and 2.5 g of 80% (w/w) $NaClO_2$. The flask was kept at 90 °C for 30 min at which time an additional 10 ml of acetic acid and 2.5 g of 80% (w/w) $NaClO_2$ were added. The 30 min cycle was repeated over the course of 2 hr. At the end of the 2 hr period, the flask was stoppered and the reaction was cooled with cold water to stop the reaction. The reaction mixture was then filtered using a course crucible and dried at 105 °C until the crucible weight was constant, and the holocellulose yield was calculated.

3.3.3 Lignin Content Determination

The lignin content was determined by Klason lignin method. Accordingly, 1 g (oven-dried) of wood meal was placed in a 100 ml beaker to which 15 ml of 72 % H_2SO_4 was added. The mixture was left at room temperature for 2 hr with occasional stirring. The solution was then transferred to a 1 L Erlenmeyer flask, diluted with 560 ml of deionized water to a H_2SO_4 concentration of 3 %, and refluxed for 4 hr. The solution was then filter and the acid insoluble lignin determined gravimetrically. The filtrate was diluted to 1 L with deionized water, and the acid soluble lignin was calculated from the UV absorbance reading at 205 nm. The extinction coefficient used was 110 AU*L/g*cm [14]. For the wood wafers the experimental conditions were reduced accordingly for a 0.1 g (oven-dried) sample weight. The pooled standard error for the Klason lignin content (Lab error) of 7 duplicate samples was 0.30.

3.3.4 NIR Sample Preparation

Wood meal samples for NIR analysis were prepared using a pellet method. The wood meals or holocellulose samples (100 mg OD weight) were put into a stainless steel

capsule and vibrated in an amalgamator (Zenith, model Z-1A) for 1 min to produce a uniform particle size. The powder sample, 75 mg OD weight, was then pressed into a pellet, with a pellet diameter of 1.3 cm.

For the holocellulose and MWL blended samples, the amalgamated samples were separately weighed and mechanically mixed in different ratios using a mortar and pestle prior to being pressed into pellets. The holocellulose/MWL ratio was varied between 100/0 to 60/40.

For the wood wafer samples, the dried wafers were measured directly using a modified sample holder. The wafer diameter was the same as the increment core diameter, 1.2 cm.

3.3.5 Near Infrared Spectroscopy

A Foss NIRSystems Near infrared spectrometer equipped with an InTact Single Tablet Module (NR-1650) and a monochromator (NR-6500-V/H) was used in this study. Absorbance spectra, 32 scans, were collected at 2.0 nm intervals over the range 600-1900 nm.

3.3.6 Calibration Development and Statistics

All statistics, regressions and predictions were performed using VISION software (Version 2.51) from Foss NIRSystems. All spectra were converted to 2^{nd} derivative spectra with a segment of 10 nm and a gap of 0 nm prior to any calibration development. Multiple Correlation Coefficient (R^2) and the Standard Error of Calibration (SEC) were used to evaluate how well a calibration of simple or multiple linear regressions fit the

data. SEC is the standard deviation for the residuals due to the difference between the actual lab values and the fitted values of samples within the calibration set [15,16].

For the Partial Least Squares (PLS) regression, the regression models were developed with four cross validation segments and a maximum of 16 factors. The best number of PLS factors for the model was determined by the PRESS (Prediction Residual Error Sum of Squares) value, which is the sum of all squared differences between the lab and predicted values [5]. The PLS factors that yielded the lowest PRESS value were used to establish each model [5,9]. In addition to R^2 and SEC, Standard Error of Cross Validation (SECV) was also used to evaluate the PLS calibration performance. SECV can be an indication of how well an equation will predict samples which are not used to generate the calibration equation when there are insufficient external validation samples [17]. In cross validation, samples in the original calibration set are grouped into 4 subsets. One subset is withheld to simulate the external validation set while a calibration equation is created using the remaining samples. The resulting equation can then be used to predict the samples in the withheld subset. The standard error between the predicted and the lab values are then calculated. The first subset is then returned to the calibration set and the process is repeated for each group. The standard errors are then combined to produce the SECV [18,19].

The standard error of prediction (SEP) was used in increment core model to evaluate how well the calibration predicts the constituent value of interest for a set of unknown samples that are different from the calibration set [20].

3.4 Results and Discussion

3.4.1 Chemical Components in the NIR Spectra

To utilize the simple regression method, which is based on the Lambert-Beer law, to build the prediction calibration line, it is of great importance to distinguish between each of the component peaks in the NIR spectra. NIR spectra of mature pine wood meal, holocellulose, and mill wood lignin (MWL) pellets were measured. The corresponding 2nd derivative NIR spectra are shown in Figure 3.1.

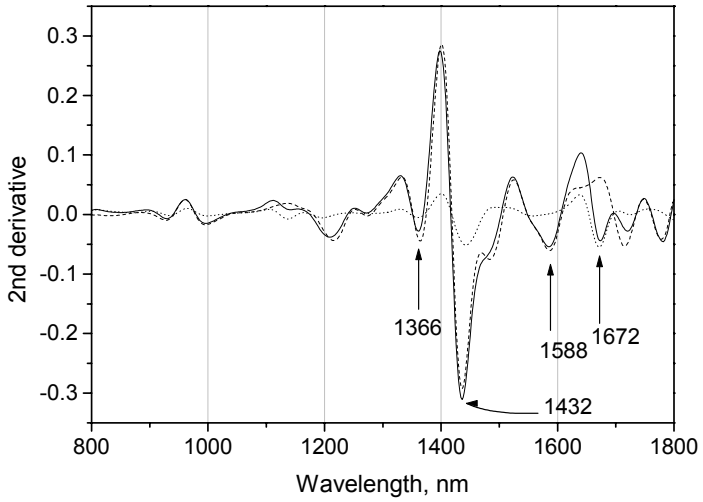

Figure 3.1 Second-derivative NIR spectra of wood and its chemical components: (———) wood meal; (– – – –) holocellulose; (·····) MWL.

The second derivative spectra are the inverse of the original absorbance spectra, in which the peaks are project downward and better resolved than the original spectra. Comparing these three spectra with a pure cellulose spectrum (spectra not shown), the peak at 1672 nm can be assigned to lignin, and the peaks at 1366, 1432, and 1588 nm to

carbohydrates. These peak assignments are similar to the previously reported using diffuse reflectance NIR [21].

3.4.2 Particle Size Effects

Figure 3.2 shows the results obtained for the NIR analysis of fractionated wood meal. Contrary to reports in the literature wherein variations in particle size between 30 to 60 mesh did not have a significant effect on the NIR spectra (diffuse reflectance) [15], it can be seen that as the particle size changes from –10~+20 mesh to –60 mesh, the characteristics peak intensities increase.

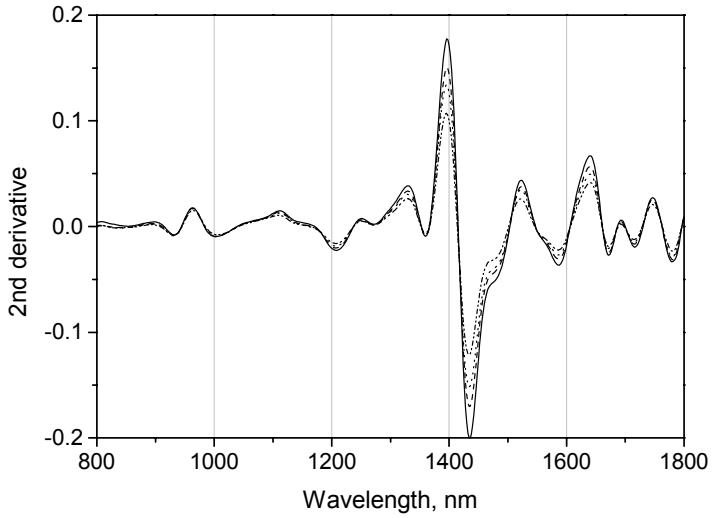

Figure 3.2 Second derivative NIR spectra of the different mesh wood meals; (———) -60 mesh; (– – – –) -35 +60 mesh; (·····) -20 +35 mesh; (–··–··–) -10 +20 mesh.

The peak intensity of the finer particle size wood meal is stronger than that of the larger particle size wood meal. Therefore, Erroneous results regarding lignin concentration or holocellulose content could result if individual peak heights are utilized to determine component concentrations. This can be eliminated by utilizing the ratio of the component peaks, rather than the individual peak data. For the same wood meal, which has the same lignin content, the peak ratio of the lignin peak intensity to the carbohydrate peak intensities is the same and is independent of particle size (Figure 3.3).

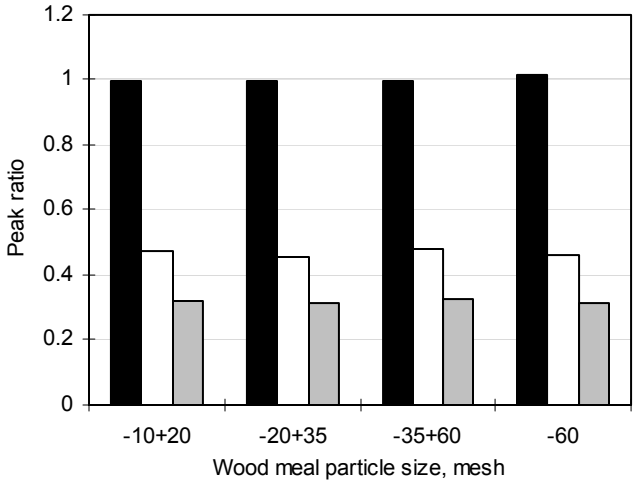

Figure 3.3 Relative peak ratio of different particle size wood meals: (black bar) 1672/1366; (white bar) 1672/1432; (gray bar) 1672/(1366+1432).

3.4.3 Simple and Multiple Regression Methods

Figure 3.4 shows the second-derivative NIR spectra for different lignin content samples prepared by mechanically blending holocellulose with MWL. Distinct differences can be seen been the various bands associated with lignin and carbohydrates as the blend

composition changes. For example, the intensity of the lignin peak at 1672 nm increases with increasing lignin content.

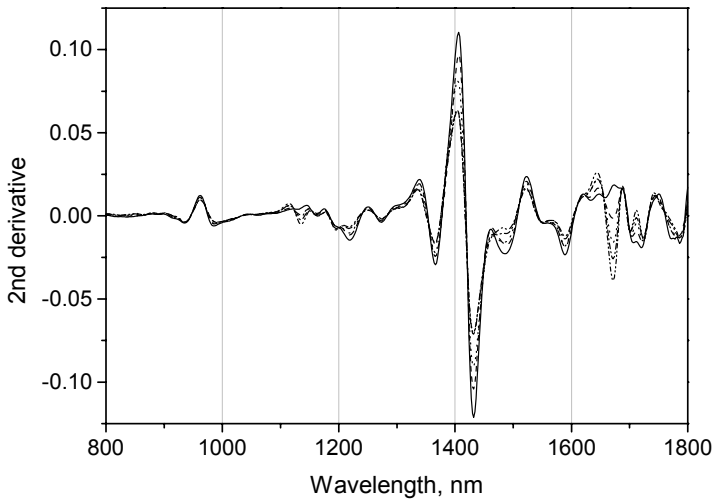

Figure 3.4 Second derivative NIR spectra of different lignin content blending samples: (———) H100L0; (– – – –) H90L10; (·····) H80L20; (–·–·–··) H70L30; (–··–··–) H60L40.

Similarly, changes in other bands and band ratios are observed with the change in lignin and carbohydrate concentration. A linear relationship was found between various other selected peak ratios for lignin and carbohydrates (Figure 3.5). Both the 1672/1366 and 1672/1432 band ratios show a linear relationship with increasing lignin content. The R^2 is 0.9964, and the SEC (Standard Error of Calibration) is 0.80 for the 1672/1366 band ratio.

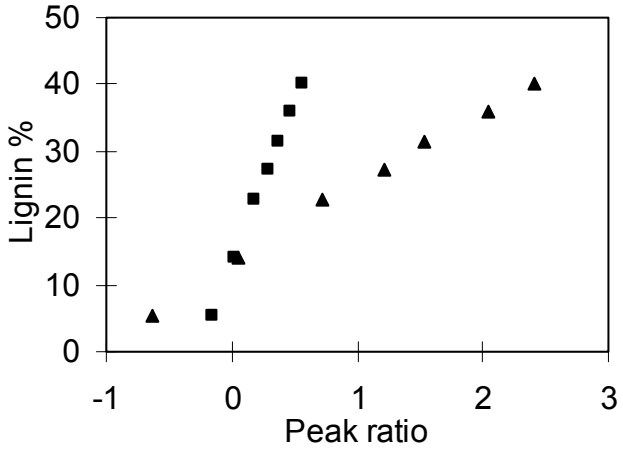

Figure 3.5 Linear relationships of some selected peak ratio; 1672/1366 (▲) y=11.3238x+13.4941 (R^2=0.9964, SEC=0.80); 1672/1432 (■) y=48.738x+13.435 (R^2=0.9986, SEC=0.50).

These band ratios were then used to predict the lignin content of the mature pine wood meals, which are the same wood sources as the holocellulose and MWL used to build the models. The results are shown in Figure 3.6. The total lignin content of the two wood samples as determined by Klason lignin are 27.2% and 27.7% respectively. The predicted values from the 1672/1366 regression line are around 30%, and from the 1672/1432 regression line are around 29%.

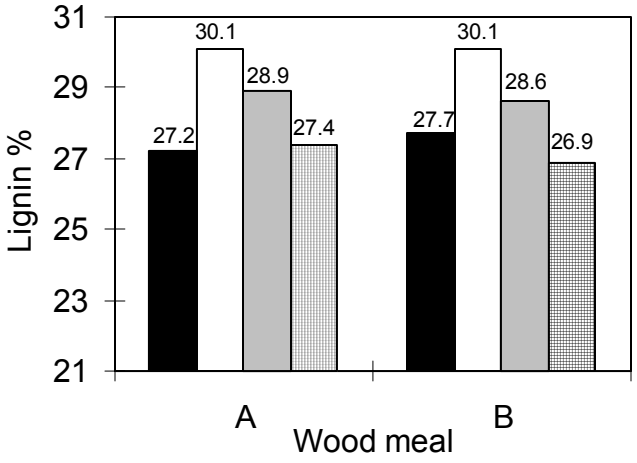

Figure 3.6 NIR predicted lignin content by simple and multiple regression method: (black bar) laboratory data; (white bar) 1672/1366; (gray bar) 1672/1432; (grid bar) (1672/1366)+(1672/1432).

To increase the prediction accuracy, multiple linear regression analysis was applied. This model combines the two simple regression terms used in the previous section. An R^2 = 0.9986 with SEC=0.56 was obtained. The prediction results are also shown in Figure 3.6. The predicted values of 27.4% and 26.9% are much closer to the laboratory values 27.2% and 27.7% respectively, than the values obtained from the simple regression.

3.4.4 PLS Analysis

From the previous analysis, lignin content prediction depends on the peaks chosen and the regression method used. For a complex matrix material such as wood, the NIR spectra are composed of many overtones and combination bands. Therefore, if we can utilize the entire spectra in the regression, in which each individual piece of spectral

information can be taken into consideration, a more powerful regression line can be obtained. Hence, the PLS method was used to obtain a calibration line. An additional 30 standard samples were utilized varying in lignin content from 6.8% to 41.8%. The regression results obtained were explained by 5 PLS factors with an R^2=0.9948, SEC=0.74 and SECV = 1.05. The correlation between the standard lab values and the NIR fitted values of the calibration set is shown in Figure 3.7. The slope of this correlation is very close to 1. The lignin content of the previous wood samples (27.2% and 27.7%) was predicted to be 27.4% and 27.9% respectively by this regression method.

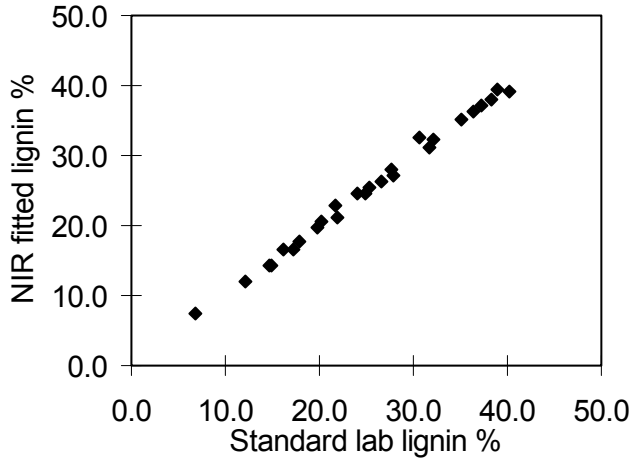

Figure 3.7 PLS correlation between the standard laboratory values and the fitted values of the calibration set from holocellulose and MWL blending samples (y=0.9948x+0.1314, R^2=0.9948, SEC=0.74, SECV=1.05).

Unfortunately, lignin content prediction of wood samples other than those used to build the method, i.e. not the same source as the holocellulose and MWL, is not satisfactory, regardless of the regression model used. The calibration model is very specific, and only good for the prediction of wood sources that are included in the model development. Therefore, the development of a universal calibration line for the prediction of lignin content through the utilization of *synthetic wood* is not feasible. Aside from the poor prediction of wood samples not included in the calibration set, the preparation of blending samples is a tedious process. The samples need to be ground, mixed and pressed into pellets before any NIR analysis.

3.4.5 Increment Core Model

It is apparent that the utilization of NIR for the determination of lignin content depends on the sample set utilized to build the prediction model. Therefore, if a method is to be rapid, as required to screen the enormous number of wood samples produced by breeding programs, minimal sample preparation is critical. To address this we investigated the use of wood wafers produced from increment wood cores traditionally used in wood density analysis. The increment core model was built using 32 different wood cores. Fifteen pieces of thin wood wafers were obtained from the 3rd ring springwood of each increment wood core. The dried wafers were scanned directly by transmittance NIR, and each set of 15 spectra was averaged to represent the 3rd ring springwood NIR spectrum. The total lignin content of each set of 15 wafers was determined by Klason method. The total lignin contents of the 3rd ring springwood of these 32 wood cores ranged from 28.6% to 32.9%. Partial least square analysis was applied to this model, and the correlation

between the lab lignin values and the NIR fitted lignin values of the increment core model is shown in Figure 3.8. The regression results can be explained by 6 PLS factors with R^2=0.8121 and SEC=0.47. The residual values (the difference between the predicted value and lab value) of all of the calibration samples are within one-percent differences. The SECV for this model is 0.73. The prediction results of some external validation samples are shown in Figure 3.9. The SEP (Standard Error of Prediction) is 0.87. These results indicate a good regression model can be obtained using the transmittance mode NIR with wood wafers taken from increment cores. Again, as with all NIR methods the model is dependent on the calibrations set used. However, using NIR transmittance very little sample preparation is required; no grinding, screening, or other tedious preparation procedures required for the wood meal regression models discussed above or the traditional reflectance NIR methods. This new procedure can reduce analysis time and chemical costs, and provide a quick lignin assessment for tree-breeding programs.

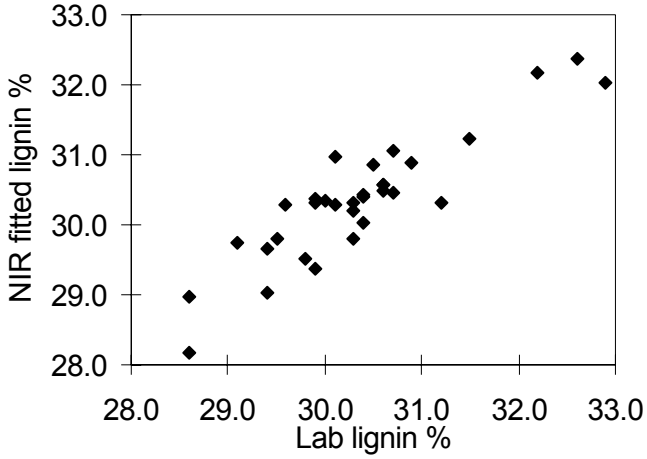

Figure 3.8 PLS correlation between the laboratory lignin values and the NIR fitted lignin values of the increment core model (y=0.8121x+5.701, R^2=0.8121, SEC=0.47, SECV=0.73).

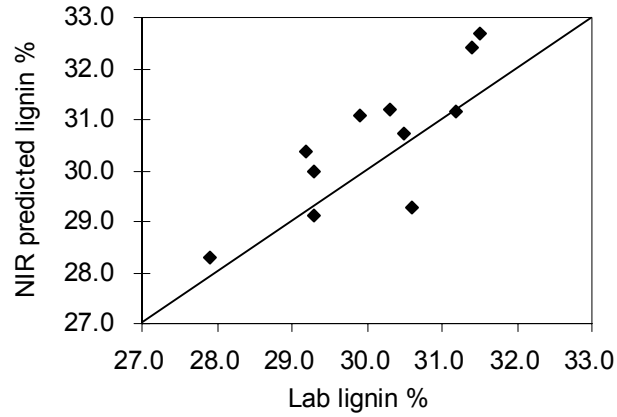

Figure 3.9 Prediction results of the external validation wood wafer samples by using the wood wafer calibration model (R^2=0.7162, SEP=0.87).

3.5 Conclusion

Using transmittance near infrared (NIR) spectroscopic, a rapid characterization method of solid wood lignin content is made. Using simple, multivariate, and partial least square statistical analysis the lignin content of wood wafers, taken from increment cores, and synthetic wood, prepared by blending milled wood lignin and holocellulose were compared and quantified. Strong correlations were obtained between the predicted NIR results and those obtained from traditional chemical methods. Regression model built from wood wafers shows the best prediction result. This new method can significantly reduce processing time and analysis costs, and facilitate a quick lignin assessment for tree-breeding programs.

3.6 References

[1] Zobel, B.J.; Van Buijtenen, J.P. *Wood Variation: Its Causes and Control*; Springer-verlag, Berlin-Heidelberg-New York, 1989.

[2] Kellog, R.M.; Thykeson, E. Influence of wood and fiber properties on kraft converting-paper quality. *TAPPI J.* **1975**, *58*, 131-135.

[3] Michell, A.J.; Schimleck, L.R. Developing a method for the rapid assessment of pulp yield of plantation eucalypt trees beyond the year 2000. *Appita J.* **1998**, *51*, 428-432.

[4] Wessman, C.A.; Aber, J.D.; Peterson, D.L.; Melillo, J.M. Foliar analysis using near-infrared reflectance spectroscopy. *Can. J. For. Res.* **1988**, *18*, 6-11.

[5] Gierlinger, N.; Schwanninger, M.; Hinterstoisser, B.; Wimmer, R. Rapid determination of heartwood extractives in *Larix sp.* by means of Fourier transform near infrared spectroscopy. *J. Near Infrared Spec.* **2002**, *10*, 203-214.

[6] Schimleck, L.R.; Wright, P.J.; Michell, A.J.; Wallis, A.F.A. Near-infrared spectra and chemical compositions of *E. globulus* and *E. nitens* plantation woods. *Appita J.* **1997**, *50*, 40-46.

[7] Schultz, T.P.; Burns, D.A. Rapid secondary analysis of lignocellulose: comparison of near infrared (NIR) and Fourier transform infrared (FTIR). *TAPPI J.* **1990**, *73*, 209-212.

[8] Michell, A.J. Pulpwood quality estimation by near-infrared spectroscopic measurements on eucalypt woods. *Appita J.* **1995**, *48*, 425-428.

[9] Fardim, P.; Ferreira, M.M.C.; Duran, N. Multivariate calibration for quantitative analysis of eucalypt kraft pulp by NIR spectrometry. *J Wood Chem. Technol.* **2002**, *22*, 67-81.
[10] Brunner, M.; Eugster, R.; Trenka, E.; BerganminStrotz, L. FT-NIR spectroscopy and wood identification. *Holzforschung* **1996**, *50*, 130-134.
[11] Workman, J.J. Commercial NIR instrumentation. In *Handbook of Near-Infrared analysis*; D.A. Burns and E.W. Ciurczak, Eds.; Marcel Dekker: New York, 1992; pp 37-51.
[12] Ikeda, T.; Holtman, K.; Kadla, J.F.; Chang, H.M.; Jameel, H. Studies on the effect of ball milling on lignin structure using a modified DFRC method. *J. Agric. Food Chem.* **2002**, *50*, 129-135.
[13] Yokoyama, T.; Kadla, J.F.; Chang, H.M. Microanalytical method for the characterization of fiber components and morphology of woody plants. *J. Agric. Food Chem.* **2002**, *50*, 1040-1044.
[14] Dence, C.W. The determination of lignin. In *Methods in lignin chemistry*; S.Y. Lin and C.W. Dence, Eds.; Springer-Verlag: Berlin/New York, 1992; pp 34-35.
[15] Bailleres, H.; Davrieus, F.; Ham-Pichavant, F. Near infrared analysis as a tool for rapid screening of some major wood characteristics in a eucalyptus breeding program. *Ann. For. Sci.* **2002**, *59*, 479-490.
[16] Mark, H.; Workman, J. *Statistics in Spectroscopy*; Academic Press: San Diego, California, 1991.
[17] FOSS NIRSystems. *Manual for VISION software*: Silver Spring, Maryland, 2001.
[18] Beebe, K.R.; Pell, R.J.; Seasholtz, M.B. *Chemometrics: a practical guide*; John Wiley & Sons: New York, 1998.
[19] Kramer, R. *Chemometric Techniques for Quantitative Analysis*; Marcel Dekker: New York, 1998.
[20] Schimleck, L.R.; Doran, J.C.; Rimbawanto, A. Near infrared spectroscopy for cost effective screening of foliar oil characteristics in a *Melaleuca cajuputi* breeding population. *J. Agric. Food Chem.* **2003**, *51*, 2433-2437.
[21] Michell, A.J.; Schimleck, L.R. NIR spectroscopy of woods from *Eucalyptus globulus*. *Appita J.* **1996**, *49*, 23-26.

4. RAPID SCREENING OF WOOD CHEMICAL COMPONENT VARIATIONS USING TRANSMITTANCE NEAR INFRARED SPECTROSCOPY[a]

[a]Published in *J. Agric. Food Chem.* (2005) 53:3328-3332.

Ting-Feng Yeh[1], Tatsuhiko Yamada[1], Ewellyn Capanema[1], Hou-min Chang[1], Vincent Chiang[1], and John F. Kadla[1,2]

[1]North Carolina State University, Raleigh, NC 27695

[2]University of British Columbia, Vancouver, B.C. V6T 1Z4

4.1 Summary

A rapid transmittance near infrared (NIR) spectroscopy method was developed to predict the variation in chemical composition of solid wood. The effect of sample preparation, sample quantity (single versus stacked multiple wood wafers) and NIR acquisition time on the quantification of α-cellulose and lignin content was investigated. Strong correlations were obtained between laboratory wet chemistry values and the NIR-predicted values. In addition to the experimental protocol and method development, improvements in calibration error associated with utilizing stacked multiple wood wafers as opposed to single wood wafers are also discussed.

4.2 Introduction

To ensure the global competitiveness of the Pulp and Paper Industry in the Southeastern U.S. more wood with targeted characteristics has to be produced more efficiently on less land. One viable solution to meet future industrial wood demands is to greatly increase the productivity of current pine plantations, leaving natural forests to be managed at low intensity, primarily for saw timber, conservation, aesthetics and recreational ends. To achieve efficient utilization of the fast growing plantation wood, tree breeders need to accurately and rapidly screen the large breeding populations for a variety of phenotypic traits.

Wood properties including density, tracheid diameter and length, cell wall thickness and chemical composition have been shown to be related to product quality. For example, paper properties such as burst, tear strength and tensile strength are closely related to fiber morphology [1]. While processing costs and resultant profitability are

more significantly affected by chemical composition [2], specifically α-cellulose and lignin content. Traditional wet chemistry methods for the determination of α-cellulose and lignin content are quite costly and time-consuming [3].

Recently, we reported a rapid transmittance Near-Infrared (NIR) spectroscopic method for the determination of lignin content in solid wood [4]. The lignin content of wood wafers taken from 12mm increment cores were statistically analyzed using multiple regression and partial least square analysis. Strong correlations were obtained between the predicted NIR results and those obtained from traditional chemical methods. This method satisfactorily predicted lignin content for samples not included in the model development. Sykes et al.[5] utilized this model to predict fiber length, coarseness, α-cellulose and lignin content of loblolly pine. However, lignin content could not be adequately predicted using this model due to the large error associated with the lignin measurements.

The single wood wafer NIR method [4] enables good prediction of lignin content, but it requires collecting 15 single-wafer NIR spectra from each ring of an increment wood core. These spectra are then averaged to produce a single NIR spectrum. When considering screening a tree-breeding project where the amount of samples is enormous, the time required to analyze a single sample is crucial. In this paper a new method is proposed wherein a single NIR spectrum is collected utilizing several wafers from the same year ring stacked together. The results obtained from the single stacked wafer NIR spectrum model and the correlation between the wet chemistry and NIR measurements for α-cellulose and lignin content are compared to the averaged multiple single-wafer NIR spectra model.

4.3 Experimental

4.3.1 Materials

Wood increment core samples were collected from thirteen 9-year-old loblolly pine (*Pinus taeda*) received from the Tree Breeding Program, Department of Forestry, North Carolina State University, and from thirty-seven 4-year-old aspen (*Populus trichocarpa*) received from Oak Ridge National Laboratory, Tennessee. The increment wood core extractives were removed by acetone extraction as described previously [6]. The extractives-free increment wood cores were then soaked in deionized water overnight and microtomed into wood wafers (13mm in diameter and 200μm in thickness) [4]. The wood wafers were dried under vacuum over P_2O_5 overnight prior to NIR measurement. All NIR spectra were recorded prior to chemical analysis.

4.3.2 Near Infrared Spectroscopy

A Foss NIRSystems near-infrared spectrometer equipped with an InTact Single Tablet Module (NR-1650) and a monochromator (NR-6500-V/H) was used to analyze the wood wafers. Absorbance spectra totaling 32 scans were collected at 2.0 nm intervals over the range of 600-1900 nm.

4.3.3 NIR Sample Preparation and Measurement

The dried wood wafers were analyzed using a modified sample holder as reported previously [4]. The NIR and wet chemistry measurements were conducted on a ring-by-ring basis. All wood wafers collected from a single growth ring were considered as one

sample. For both the pine and aspen only a limited amount of woody material was available for analysis. Pine α-cellulose content was determined using wood wafers collected from the springwood rings 2, 4, 6 and 8, whereas lignin content was determined from springwood rings 3, 5, and 7. A total of 55 and 59 samples were analyzed for α-cellulose and lignin content, respectively. For the aspen samples the amount of available wood was much lower and only lignin content was determined using the springwood from ring 3. A total of 62 aspen samples were analyzed. In a typical experiment, 10 wood wafers for the pine (corresponding to about 80 mg of wood) or 14 wood wafers for the aspen (corresponding to about 100 mg of wood) were stacked together, placed on the NIR sample holder and scanned. For the averaged *single-wafer model*, the 10 (pine) or 14 (aspen) wood wafers obtained per ring were individually scanned and averaged to represent a single sample spectrum. As a result, the regression models developed for both the *averaged single-wafer* spectrum and the *stacked-wafer* spectrum were obtained from the same wood wafers and therefore correspond to the same reference data obtained from the wet chemistry analyses.

4.3.4 Holocellulose Preparation

The isolation of holocellulose was carried out according to the protocol of Yokoyama et al. [6] utilizing a total of 10 wood wafers per analysis. Specifically, ~100 mg (oven-dried) of wood wafers were suspended in 4 mL of deionized (DI) water at 90 °C, and reacted with 200 mg of 80 % sodium chlorite and 0.8 mL of acetic acid for 1 hour. The reaction mixture was then filtered using a course crucible, washed and dried at 105 °C

until no change in weight was observed. For specimens where 10 wafers were less than 100 mg, the amount of the applied chemicals was reduced proportionally.

4.3.5 α-Cellulose Preparation

α-Cellulose was prepared as per the protocol of Yokoyama et al. [6] wherein 50 mg of the holocellulose (outlined above) was reacted with 4 mL of 17.5 % sodium hydroxide for 30 min, then diluted with 4 mL of DI water and the reaction mixture was left for 30 min. After a total reaction time of 1 hour, the fiber suspension was filtered with a coarse crucible, washed thoroughly with DI water, and soaked in 1.0 M acetic acid for 5 min. The neutralized α-cellulose was then washed with deionized water. The yield was calculated after drying at 105 °C.

4.3.6 Lignin content determination

The lignin content was determined using a modified Klason lignin method. The wood wafers (~ 100 mg oven-dried) were reacted with 1.5 mL of 72 % H_2SO_4 at room temperature with occasional stirring for 2 hr. The solution was then diluted with DI water to a 3 % H_2SO_4 concentration and heated at 121 °C and 2 atm for 1 hr in a commercial pressure cooker. The reaction was filtered and the acid insoluble lignin determined gravimetrically. The filtrate was diluted to 100 mL with DI water and the acid soluble lignin was calculated from the UV absorbance at 205 nm using an extinction coefficient of 110 AU*L/g*cm [7]. The acid insoluble and acid soluble lignin were combined and reported as the total lignin content. No statistically significant difference was observed in

the total lignin content obtained between the classical Klason lignin method and our pressure-cooking method.

4.3.7 Calibration Development and Statistics

The calibration models were developed using Foss NIRSystems Vision software (Version 2.51). First, outliers were identified using the Mahalanobis distance algorithm to measure how far a sample was from the cluster center of the spectra. A sample is considered to be an outlier when its probability level exceeds a threshold value of 0.95 [8]. Once the outliers were removed, the remaining samples are split 75 % for the calibration set and 25 % for the prediction set using an algorithm that measures a Euclidean distance between samples. Redundant samples are moved into the prediction set [8]. A statistical summary of the calibration and prediction sets is given in Table 4.1.

Table 4.1 Summary statistics for α-celluloses and total lignin contents for the calibration and prediction sets.

Chemical compositions (%[a])	Calibration set					Prediction set				
	n	Min	Max	Avg	Std[b]	n	Min	Max	Avg	Std
Pine α-cellulose										
Stacked-wafer model	38	35.6	47.3	42.4	2.4	12	38.2	46.4	42.0	2.5
Single-wafer model	38	35.6	47.3	42.4	2.4	12	38.2	43.8	41.0	2.0
Pine Total lignin	39	28.0	32.0	30.0	0.9	14	28.5	32.0	29.8	0.9
Aspen Total lignin	39	20.9	28.6	25.3	2.3	14	21.4	27.1	24.6	1.9

[a]Based on extractive-free, OD wood weight. [b]Standard deviation.

Prior to any calibration development the original spectra were converted to 2nd derivative spectra with a 10 nm segment and 0 nm gap. Calibration equations were developed using a partial least squares (PLS) regression with four cross validation segments and a maximum of 16 factors. The best number of PLS factors for the model were determined by the PRESS (Prediction Residual Error Sum of Squares) value, which is the sum of all squared differences between the lab and predicted values [9]. The PLS factors that yield the lowest PRESS values were then chosen to establish a model [9,10].

The coefficient of determination (R^2), the standard error of calibration (SEC), and the standard error of cross validation (SECV) were used to evaluate the calibration performance. SEC is the standard deviation for the residuals due to the difference between the actual lab values and the fitted values of samples within the calibration set [11,12]. SECV is an indication of how well an equation will predict samples which were not used to generate the calibration equation in cross validation [8,13,14].

The standard error of prediction (SEP) was used to evaluate how well the calibration predicts the interested constituent value for a set of unknown samples that are different from the calibration set [15]. The predictability of the calibration was evaluated by the ratio of performance to deviation (RPD). The RPD was calculated from the ratio of standard deviation of the reference data of prediction data set to the SEP [16]. The RPD should be as high as possible; values between 5-10 are adequate for quality control, values > 2.5 are satisfactory for screening breeding programs [11,16], and values of ~1.5 can be used as an initial screening tools [15,17,18].

4.4 Results and Discussion

4.4.1 Stacked-wafer Model versus Averaged Single-wafer Model

Our previous model [4] was established by averaging 15 single-wafer NIR spectra from a single growth ring of an increment wood core. The large number of samples (wafers) analyzed ensured the NIR spectra obtained was representative of the entire year of growth and that enough material was available for the subsequent wet chemistry measurements. However, the analysis of 15 spectra per ring was quite laborious and time consuming. In an attempt to minimize data collection time, but analyze a representative amount of wood, 10 wafers from the same year ring were stacked together and one NIR spectrum was taken. Figure 4.1 shows the 2^{nd} derivative NIR spectra obtained from a single NIR spectrum of 10-stacked wafers and the averaged spectrum of 10-single wafer spectra. The intensity of the 2^{nd} derivative NIR spectrum from the 10-stacked wafers was far more intense than that obtained from the averaged spectrum of 10-single wood wafers. In addition to the improved signal-to-noise and reduced calibration error [19], the intense NIR absorption bands of the stacked wafer spectra enhance regression development.

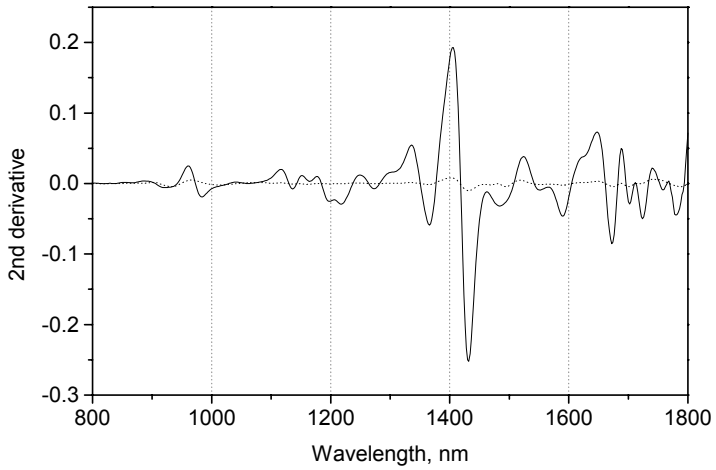

Figure 4.1 Second derivative NIR spectra of (——) 10-stacked wafers, and (·····) averaged 10-single wafer.

The pine wood wafers of the α-cellulose data set were used to develop two calibration models, the *stacked-wafer model* and the *averaged single-wafer model*. Figure 4.2 illustrates the calibration results of α-cellulose content of loblolly pine for the *stacked-wafer model* (Figure 4.2a) and the *averaged single-wafer model* (Figure 4.2b). A stronger correlation was obtained for the *stacked-wafer model* (R^2 = 0.82) than the *averaged single-wafer model* (R^2 = 0.80). The SEC was 1.05 for the *stacked-wafer model* and 1.17 for the *averaged single-wafer model*. Thus, a better fit was obtained for the regression models of the *stacked-wafer model* than the *averaged single-wafer model*. The SECV, which is a better measurement of calibration error [18], exhibited the same trend between both models, i.e. smaller calibration error in the *stacked-wafer model*, SECV = 1.21 versus 1.87 for the *averaged single-wafer model*. The considerably larger SECV than SEC in the *averaged single-wafer model* could possibly be due to over fitting of the data [18]. The lower signal-to-noise in the *averaged single-wafer* spectra (Figure 4.1) could result in some of the noise being modeled during calibration development, thereby reducing the SEC. Therefore, using stacked wafers as opposed to averaging single wafer measurements is not only faster, but results in better signal-to-noise which leads to a reduction in the calibration error. The *stacked-wafer model* will be utilized in all of the proceeding analyses.

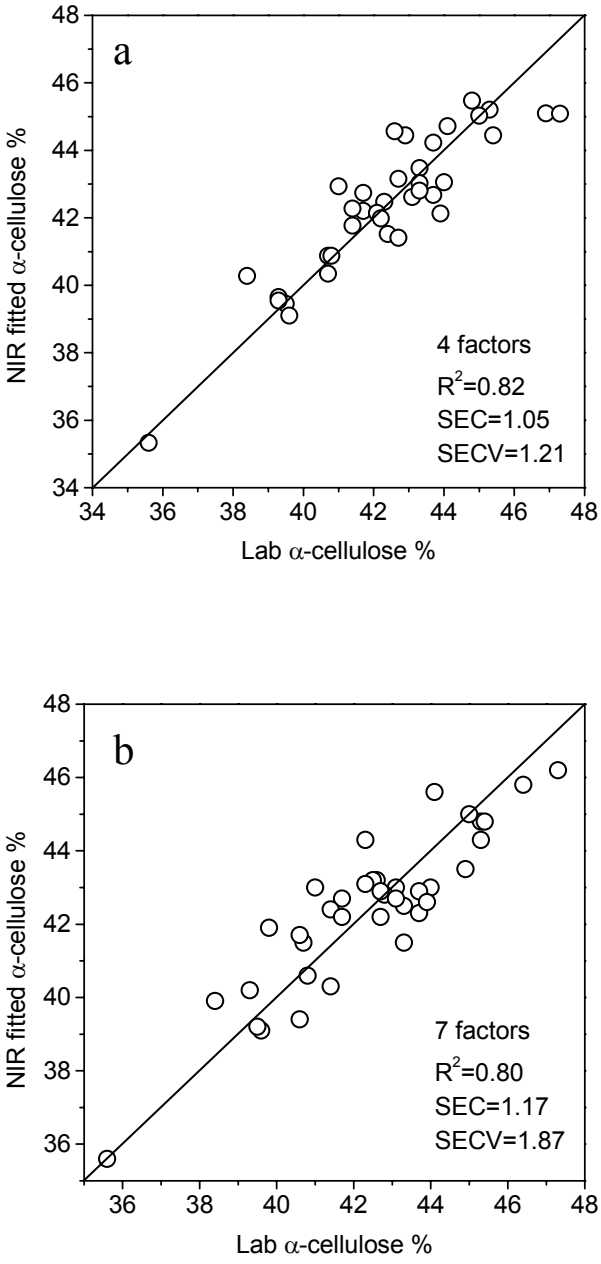

Figure 4.2 Correlation between the lab α-cellulose content and the NIR fitted α-cellulose content of the (a) *stacked-wafer model,* and (b) *averaged single-wafer model*.

4.4.2 Prediction of α-Cellulose Content of Loblolly Pine

The α-cellulose content calibration models were tested using the prediction sample sets (12 loblolly pine wood wafer samples). The relationship between the wet chemistry α-cellulose content measurements and the NIR predicted α-cellulose contents are quite good using the *stacked-wafer model* (R^2 = 0.75). As shown in Figure 4.3a, the SEP is 1.42, which is slightly higher than the SECV (1.21). The RPD is 1.77 indicating that the *stacked-wafer model* could be used as a screening tool for estimating the α-cellulose content of increment core samples. Figure 4.3b illustrates the correlation between the wet chemistry α-cellulose values and the NIR predicted values for the *averaged single-wafer model* (R^2 = 0.65), which is not as good as the *stacked-wafer model*. Furthermore, the SEP is closer to the SEC than SECV, and the RPD (1.54) is lower than that of the *stacked-wafer model*. Thus, the predictability of the *single-wafer model* is weaker than the *stacked-wafer model*. However, they both fulfill the initial screening criterion (RPD = ~1.5).

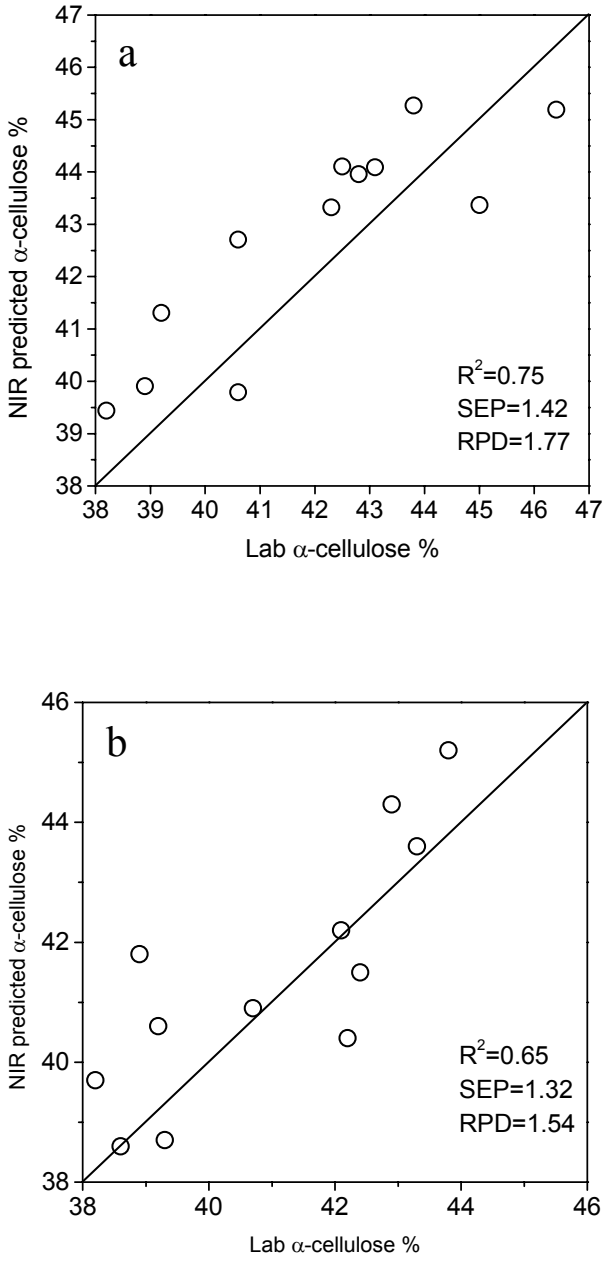

Figure 4.3 Correlation between lab measured α-cellulose content and the NIR predicted α-cellulose content using (a) *stacked-wafer model*, and (b) *averaged single- wafer model*.

4.4.3 PLS Calibrations Based on Lignin Content

The stacked wafer method was also applied to develop two lignin content calibration models based on loblolly pine and aspen. The calibration results are shown in Figure 4.4. The correlation of the pine wet chemistry lignin values and the NIR predicted lignin values was quite good ($R^2 = 0.73$, Figure 4.4a) where the SEC and SECV were 0.47 and 0.58, respectively. These considerably low values as compared to the α-cellulose models (Figure 4.2a), may be due to the lower laboratory error for the reference methods, 0.55 for lignin and 1.05 for α-cellulose. Interestingly, the correlation obtained for the aspen data set was very strong ($R^2 = 0.95$, Figure 4.4b), where the SEC and SECV was 0.56 and 0.66, respectively. The enhanced calibration performance of the aspen data set as compared to the pine data set ($R^2 = 0.73$) may be due to the range of lignin content present [11,19]. The aspen has a broad lignin content range (21-29% lignin) in which the samples are uniformly distributed as compared to the pine samples (28-32% lignin) [20]. Therefore, to improve the calibration performance of loblolly pine more samples with greater differences in lignin content over a wider range of lignin content values are needed.

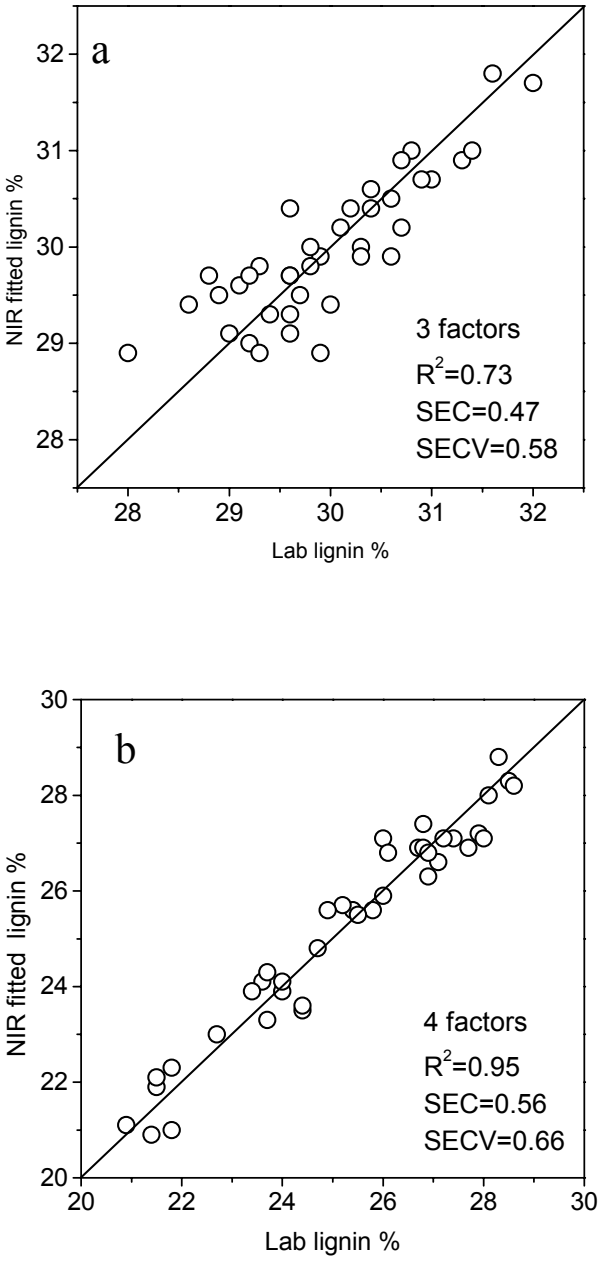

Figure 4.4 Correlation between the wet-chemistry-measured total lignin content and the NIR fitted lignin content for (a) loblolly pine, and (b) aspen.

4.4.4 Prediction of Lignin Content

Both lignin content calibration models were tested on the loblolly pine and aspen prediction sets (14 samples in each). The results are shown in Figure 4.5. The correlation (R^2 = 0.52, Figure 4.5a) for the pine lignin prediction was considerably lower than that of the calibration set (R^2 = 0.73). However, the RPD was 1.49, therefore, the calibration model can still be used for initial screening [15,17,18]. The relationship between the wet chemistry lignin values and the NIR predicted lignin values of the aspen data set is very strong (R^2 = 0.89, Figure 4.5b), and the RPD is 2.58. This high RPD value indicates that this calibration model can be used successfully for screening lignin variation in aspen [11,16].

4.4.5 Improving the Sources of Error

The work presented in this study demonstrates that it is feasible to develop a good calibration model using stacked wood wafers. The calibration error can be reduced by some technical improvements, such as increasing the signal intensities, increasing the accuracy of the reference method, or broadening the variability of the calibration set. Albeit, the greatest source of error in any calibration is generally from the error associated with the reference laboratory data [11,19].

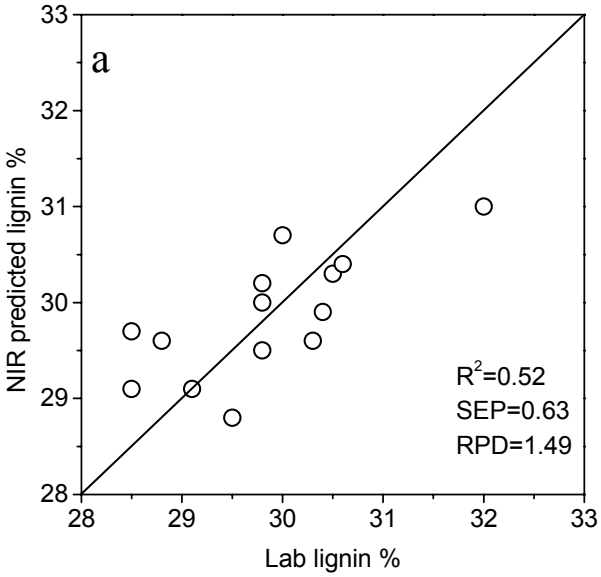

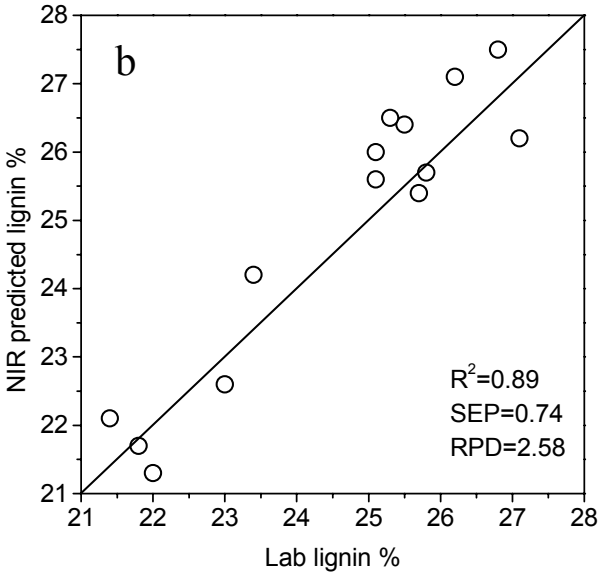

Figure 4.5 Correlation between lab measured total lignin content and the NIR predicted lignin content for (a) loblolly pine, and (b) aspen.

The wet chemistry methods involved in the determination of α-cellulose or lignin content rely on first breaking down the wood into fine wood meals. This provides a more uniform material and increases the chemical accessibility during the respective reactions. However, to facilitate rapid screening, minimal processing of the wood is required. Further, to reduce the introduction of unnecessary variation between the NIR and wet chemistry measurements, our method involves performing the wet chemistry analysis directly on the wafers used in the NIR analyses. Otherwise, these variations would cause a negative influence on the calibration model [18], Therefore, complete dispersion and mixing of chemicals throughout the sample is crucial, particularly for the Klason lignin measurements [21] where care needs to be taken to thoroughly knead and stir the sample mixtures.

In α-cellulose determination the system is more susceptible to error due to the two-step reaction procedure utilized. First, holocellulose must be isolated from the wood wafers by acetic acid and sodium chlorite. As with the lignin analysis care must be taken to ensure sufficient mixing and introduction of reagent chemicals. The resulting holocellulose is then further reacted with $NaOH_{(aq)}$ to produce α-cellulose. These processes involve very frequent weighing, kneading, and stirring. In each step, care must be taken to minimize the possible sources of error.

4.5 Conclusion

A rapid transmittance near infrared (NIR) spectroscopy method was developed to screening the variation in chemical composition of solid wood. The effect of sample preparation, sample quantity (single versus stacked multiple wood wafers) and NIR

acquisition time on the quantification of α-cellulose and lignin content was investigated. Strong correlations were obtained between laboratory wet chemistry values and the NIR predicted values. Stacked multiple wood wafer model showed reduced processing time, better regression results and prediction ability than single wafer model. This stacked wafer model can be used successfully for screening wood chemical variation and choosing the elite trees of tree-breeding programs.

4.6 References

[1] Kellog, R.M.; Thykeson, E. Influence of wood and fiber properties on kraft converting-paper quality. *TAPPI J.* **1975**, *58*, 131-135.

[2] Michell, A.J.; Schimleck, L.R. Developing a method for the rapid assessment of pulp yield of plantation eucalypt trees beyond the year 2000. *Appita J.* **1998**, *51*, 428-432.

[3] Fengel, D.; Wegener, G. Chemical composition and analysis of wood. In *Wood Chemistry, Ultrastructure, Reactions*; Walter de Gruyter: New York, 1989; pp 26-65.

[4] Yeh, T.F.; Chang, H.M.; Kadla, J.F. Rapid prediction of solid wood lignin content using transmittance near-infrared spectroscopy. *J. Agric. Food Chem.* **2004**, *52*, 1435-1439.

[5] Sykes, R.; Li, B.; Hodge, G.; Goldfarb, B.; Kadla, J.; Chang, H.M. Rapid prediction of wood properties of loblloly pine using transmittance near infrared spectroscopy. *Can. J. For. Res.* **2004**, Accepted.

[6] Yokoyama, T.; Kadla, J.F.; Chang, H.M. Microanalytical method for the characterization of fiber components and morphology of woody plants. *J. Agric. Food Chem.* **2002**, *50*, 1040-1044.

[7] Dence, C.W. The determination of lignin. In *Methods in lignin chemistry*; S.Y. Lin and C.W. Dence, Eds.; Springer-Verlag: Berlin/New York, 1992; pp 34-35.

[8] FOSS NIRSystems. *Manual for VISION software*: Silver Spring, Maryland, 2001.

[9] Gierlinger, N.; Schwanninger, M.; Hinterstoisser, B.; Wimmer, R. Rapid determination of heartwood extractives in *Larix sp.* by means of Fourier transform near infrared spectroscopy. *J. Near Infrared Spec.* **2002**, *10*, 203-214.

[10] Fardim, P.; Ferreira, M.M.C.; Duran, N. Multivariate calibration for quantitative analysis of eucalypt kraft pulp by NIR spectrometry. *J. Wood Chem. Technol.* **2002**, *22*, 67-81.

[11] Bailleres, H.; Davrieus, F.; Ham-Pichavant, F. Near infrared analysis as a tool for rapid screening of some major wood characteristics in a eucalyptus breeding program. *Ann. For. Sci.* **2002**, *59*, 479-490.

[12] Mark, H.; Workman, J. *Statistics in Spectroscopy*; Academic Press: San Diego, California, 1991.
[13] Beebe, K.R.; Pell, R.J.; Seasholtz, M.B. *Chemometrics: a pratical guide*; John Wiley & Sons: New York, 1998.
[14] Kramer, R. *Chemometric Techniques for Quantitative Analysis*; Marcel Dekker: New York, 1998.
[15] Schimleck, L.R.; Doran, J.C.; Rimbawanto, A. Near infrared spectroscopy for cost effective screening of foliar oil characteristics in a *Melaleuca cajuputi* breeding population. *J. Agric. Food Chem.* **2003**, *51*, 2433-2437.
[16] Williams, P.C.; Sobering, D.C. Comparison of commercial near infrared transmittance and reflectance instruments for the analysis of whole grains and seeds. *J. Near Infrared Spec.* **1993**, *1*, 25-33.
[17] Schimleck, L.R.; Evans, R. Estimation of *Pinus radiata* D. Don tracheid morphological characteristics by near infrared spectroscopy. *Holzforschung* **2004**, *58*, 66-73.
[18] Schimleck, L.R.; David Jones, P.; Peter, G.F.; Daniels, R.F.; Clarklll, A. Nondestructive estimation of tracheid length from sections of radial wood strips by near infrared spectroscopy. *Holzforschung* **2004**, *58*, 375-381.
[19] Workman, J. NIR spectroscopy calibration basics. In *Handbook of Near-Infrared Analysis*; D.A. Burns and E.W. Ciurczak, Eds.; Marcel Dekker: New York, 1992; pp 247-280.
[20] Sykes, R.; Isik, F.; Li, B.L.; Kadla, J.; Chang, H.M. Genetic variation of juvenile wood properties in a loblolly pine progeny test. *TAPPI J.* **2003**, *2*, 3-8.
[21] Schwanninger, M.; Hinterstoisser, B. Klason lignin: modifications to improve the precision of the standardized determination. *Holzforschung* **2002**, *56*, 161-166.

5. COMPARISON OF MORPHOLOGICAL AND CHEMICAL PROPERTIES BETWEEN JUVENILE WOOD AND COMPRESSION WOOD OF LOBLOLLY PINE[ab]

[a]Published in *Holzforschung* (2005) 59(6): -.

Ting-Feng Yeh[1], Barry Goldfarb[1], Hou-min Chang[1], Ilona Peszlen[1], Jennifer L. Braun[2], and John F. Kadla1[1,2]

[1]North Carolina State University, Raleigh, NC 27695

[2]University of British Columbia, Vancouver, B.C. V6T 1Z4

[b]Parts of the content were presented in 13th ISWPC, Auckland, New Zealand, May 16-19, 2005

5.1 Summary

In conifers, juvenile wood (JW) is always associated with compression wood (CW). Due to their similar properties, there is a common belief that JW is the same as CW. To resolve whether JW is truly identical to CW, twenty-four rooted cuttings of one loblolly pine clone were planted in growth chambers under normal, artificial bending, and windy environments. The results show that the morphology of JW is significantly different from CW. Further, chemical analyses showed that JW and CW are significantly different in chemical composition. Our results indicate that JW is truly different from CW, and the wood formed under a controlled windy environment is a mild type of compression wood.

5.2 Introduction

In the southeast US the demand for timber and pulpwood has increased greatly. However, due to environmental concerns, the land available for wood production has decreased. In order to meet the future wood demand in the US, more wood with target characteristics must be produced from the limited forestland by intensive management practices and genetic improvement [1,2]. Forest product manufacturing is shifting its raw materials from mature trees to short-rotation plantation or juvenile stock.

Juvenile wood, sometimes referred to as core wood, is formed by a young vascular cambium, and is the wood formed near the stem center [3]. Generally, a 15-year-old loblolly pine contains as much as 85% juvenile wood by volume, whereas a 40-year-old tree contains only 20% juvenile wood by volume [4]. Compared to mature wood, juvenile wood has different properties such as lower wood density, shorter fiber length, higher lignin content, and higher compression wood content [5,6].

Due to environmental disturbances, such as prevailing winds or gravitational responses, compression wood is formed under the leaning stems and branches, and manifests its effect by slowly "pushing" the stems or branches back to the original orientation [7]. For juvenile pine, the percentage of compression wood is on average about 18% [1], but can be as high as 44% [8]. Compression wood is generally considered to be inferior for both pulp and solid wood products.

When compared to mature normal wood, both juvenile and compression wood have higher lignin content and lower cellulose content, resulting in higher chemical consumption during pulping and lower pulp yield. Subsequently, it is generally considered that the juvenile wood is the same as compression wood [3,9-11]. As a result, the increased usage of juvenile wood (compression wood) from fast-growing plantation forests can significantly impact industrial production costs and product quality. However, systematic comparisons of the similarity between juvenile wood and compression wood in conifers have been limited. Our objective in this research is to compare whether juvenile wood is identical to compression wood in loblolly pine.

5.3 Experimental

5.3.1 Materials

Twenty-four rooted cuttings of one loblolly pine (*Pinus taeda*) clone were transplanted from Ray Leach Supercells (164 ml) into 9-l pots. After conditioning inside a green house for 4 weeks, they were moved into growth chambers (Phytotron, North Carolina State University) for a 9-month growth period. The chamber photoperiod and temperature were 18 hr at 28°C under incandescent lighting, and 6 hr at 20°C in the dark.

The trees were assigned randomly into three environmental conditions, i.e. control, bent, and augmented wind.

The control and bent trees (8 trees each) were in a reduced wind chamber; the average wind speed was 0.26 m/s. The 8 augmented wind trees were in a growth chamber with two oscillating fans, and an average wind speed of 1.43 m/s (range of 0.5~4.0 m/s). The tree sway frequency was about 5 times/min.

The bent trees were rendered at 45° to the perpendicular stems. When the new growth stem reached about 30 cm, another bend was applied. The trees were bent a total of 3 to 4 times during the 9-month period. The initial average height of the trees was ~20 cm, and became ~150 cm (control and augmented wind trees) and ~100 cm (bent trees) at harvest. All wood samples were collected from the same relative height of each of the stems. By visual inspection, they were separated into 5 groups, juvenile control normal wood (NW), bent opposite wood (BOW), bent compression wood (BCW), wind opposite wood (WOW), and wind compression wood (WCW).

The extractive-free wood sawdust (-35+60 mesh) was milled in a planetary micro mill (Pulverisette 7, Fritsch, Germany) followed by dioxane (96%, v/v) extraction. Milled wood lignin (MWL) was prepared according to the method of Björkman [12]. The yield of purified MWL was about 20% based on the total lignin weight in the OD wood. The MWLs were acetylated according to Adler [13].

5.3.2 Microscopic Analysis

Wood blocks, collected from the same relative height of each stem were softened in water and sliced in the radial direction using a microtome (Spencer Lens Co., Buffalo,

NY). The thickness was 10μm. The microtome slices were stained with 1% aqueous Safranin O, dried, and fixed on microscope slides with Permount (Fisher Science). A Nikon light microscope (model: Eclipse E200) was used to photograph (40X10) the anatomical structures of the wood microtome slices.

5.3.3 Wide-Angle X-Ray Diffraction (WAXD)

Wide-angle X-ray diffraction profiles were recorded at the University of British Columbia on a Bruker D8 Discover X-ray diffractometer with an area detector. Scans were collected from wood samples at 40 kV and 20 mA in the range of $4^o < 2\theta < 40^o$ using $Cu_{K\alpha}$ radiation. The spectra were corrected for incoherent scattering [14] and then the fraction of crystallinity was calculated using the method of Vonk [15].

5.3.4 Basic Chemical Composition and Fiber Analysis

Wood extractives were removed according to TAPPI standard T265 om-88. The total lignin content was determined by the Klason lignin method [16,17], combining both the Klason lignin and acid soluble lignin. Holocellulose content was determined as per Yokoyama et al. [18], and used for fiber quality analysis (FQA) . Fiber length, width, coarseness, kink and curl indexes were recorded using a Fiber Quality Analyzer (FQA, Op Test Equipment, Inc., Hawkesbury, ON) [18].

5.3.5 Monomeric Carbohydrate Determination

The monomeric sugar analysis was carried out according to the procedures of Coimbra et al. [19].

5.3.6 Nitrobenzene Oxidation and Ozonation

Nitrobenzene oxidation was performed according to the method of Chen [20]. The stereochemistry (*erythro* and *threo* forms) of the arylglycerol-β-aryl ether linkages of the lignin were determined by ozonation analysis according to the method of Akiyama et al. [21].

5.3.7 Element and Methoxyl Content Analyses

Element analyses (C, H, and N) were performed by Complete Analysis Laboratories, Inc., Parsippany, NJ. Methoxy content analyses were performed according to the procedure of Goto et al. [22].

5.3.8 Quantitative ^{13}C-NMR Spectroscopy

All NMR spectra were recorded on a Bruker AVANCE 300MHz spectrometer at 300K using DMSO-d_6 as the solvent. The concentration of lignin was about 20%, and chromium(III) acetylacetonate (0.01M) was added to the lignin solution as the relaxation agent [23]. A total of 20,000 scans were collected. A 90º pulse width, 1.2s acquisition time and 1.7s relaxation delay were used [23].

5.4 Results and Discussion

Compression wood has long been noted for its distinct morphological structures [6,7,24-26]. For example, compression wood tracheid lengths are about 10~40% shorter than that of normal wood tracheids [25]. They are more round in shape, with thicker walls and

larger intercellular spaces; and they lack the S_3 layer [7]. The simplest comparison of juvenile wood and compression wood tracheids can be made using light microscopy.

5.4.1 Tracheid Morphology and Fiber Qualities

The tracheid morphology of the five different loblolly pine wood samples is shown in Figure 5.1. The tracheids of the bent compression wood (BCW, Figure 5.1c) are round in shape and have thick cell walls and large intercellular spaces, whereas those of the juvenile control normal wood (NW, Figure 5.1a) are rectangular in shape, without any intercellular space. The bent opposite wood (BOW, Figure 5.1b) and wind opposite wood (WOW, Figure 5.1e) show similar characteristics to those of the normal wood. The tracheids of the wind compression wood (WCW, Figure 5.1d) show a similar pattern to those of the bent compression wood (Figure 5.1c). The compression wood content of each of the trees was estimated microscopically. It was found that the bent trees and wind trees have about 50% and 30% (by volume) compression wood, respectively, whereas the control trees have on the average less than 5% compression wood.

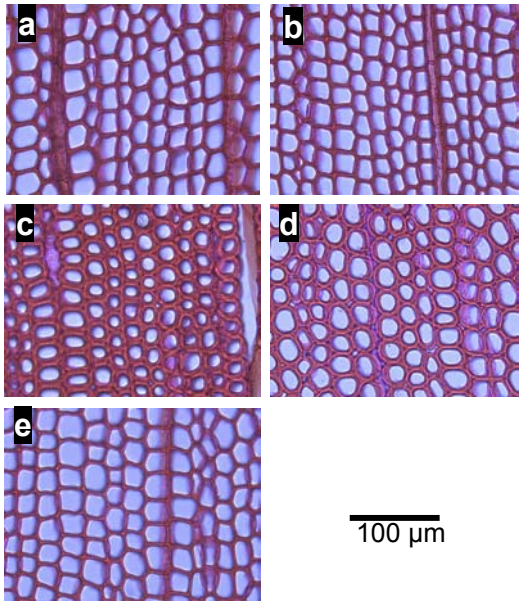

Figure 5.1 Cross-sections of loblolly pine wood from different groups: (a) control normal wood, (b) bent opposite wood, (c) bent compression wood, (d) wind compression wood, (e) wind opposite wood.

Table 5.1 lists the mean values obtained from the fiber quality analyses. The mean tracheid length of the bent compression wood (0.852 mm) is about 40% shorter than that of control, normal wood (1.221 mm). The mean tracheid length of wind compression wood (1.043 mm) is also significant shorter than the normal wood (1.221 mm) or wind opposite wood (1.317mm). Both the bent and wind compression wood have a smaller tracheid width when compared to opposite or normal wood.

Table 5.1 Fiber properties of the various wood specimens[a].

Group[b]	Length, mm[c]	Width, μm	Coarseness, mg/m	Curl index	Kink index	Crystallinity fraction
NW	1.221 A[d]	29.1 A	0.128 A	0.0179 A	0.03 A	0.58 A
WOW	1.317 A	29.8 A	0.142 A	0.0195 B	0.04 A	0.58 A
WCW	1.043 B	24.8 B	0.210 B	0.0283 C	0.28 B	0.59 A
BOW	1.088 B	23.5 B	0.134 A	0.0183 BC	0.03 A	0.57 A
BCW	0.852 C	19.4 C	0.200 B	0.0276 C	0.35 C	0.54 A

[a]Each property of each group is expressed as the mean value.
[b]NW (normal wood), WOW (wind opposite wood), WCW (wind compression wood), BOW (bent opposite wood), BCW (bent compression wood).
[c]Length weighted length.
[d]The letters (A,B,C) indicate significant differences using *Tukey-Kramer* HSD test at α=0.05 level.

The coarseness of the compression wood (~0.2mg/m) is significantly higher than that of the opposite or normal wood (~0.13mg/m). Since the two compression woods have smaller mean tracheid width than the opposite woods and the normal wood, the higher coarseness is obviously due to the thicker cell walls of the compression woods (Figure 5.1). These results are consistent with the higher density and shorter fiber length data reported by others for compression wood [6,25].

Fiber curl and kink are important fiber characteristics, known to that impact paper properties. An increase in fiber curl and kink (all other factors held constant) has a positive impact on out-of-plan tear, bulk, wet web strength, etc., and a negative impact on tensile strength, burst, and bending stiffness [27]. The compression wood samples (BCW and WCW) show higher curl and kink as compared to the opposite and normal wood. Obviously, compression wood is different from juvenile normal wood in tracheid fiber morphology and properties.

The results of wood cellulose crystallinity are also listed in Table 5.1. Although the averaged crystallinity value of bent compression wood is lower than normal wood or bent opposite wood, due to the large lab error associated with separating the crystalline and amorphous contributions, they show no statistical differences. However, Tanaka et al. [28] reported a 45-50% degree of crystallinity in compression wood cellulose, which is lower than that in normal wood (about 50%) and in opposite wood (50-60%).

5.4.2 Basic chemical properties

The lignin and sugar content of the five different groups of wood samples are showed in Table 5.2. The cell wall of compression wood has lower cellulose, mannose, xylose and arabinose content, and higher galactose and lignin than that of normal wood. The lignin content of the normal wood (NW) is 29.4% and is similar in magnitude to that of opposite wood (BOW or WOW), 29.1% and 28.9% respectively. However, the lignin content in the compression wood specimens (BCW and WCW) is rather high, ~ 36%. Further, sugar analysis shows that compression wood has a significant amount of galactose, and relatively low amounts of the other sugar units (Table 5.2). Thus, the juvenile normal wood is quite different from the juvenile compression wood in basic chemical composition, but similar to opposite wood. These results are in agreement with other reports in the literature [6,29,30].

Table 5.2 Lignin contents and carbohydrates compositions of different samples.

	Compositions (mean values)					
Group[a]	Lignin[b]	Arabinose[c]	Xylose[c]	Mannose[c]	Galactose[c]	Glucose[c]
NW	29.4 A[d]	4.0 A	14.4 A	16.2 A	3.3 A	62.1 A
WOW	28.9 A	3.9 A	14.0 A	16.1 A	3.4 A	62.5 A
WCW	36.0 B	3.1 B	11.1 B	12.9 B	16.6 B	56.2 B
BOW	29.1 A	4.0 A	13.8 A	16.4 C	3.5 A	62.3 A
BCW	36.6 B	2.8 B	10.2 B	11.4 D	21.1 C	54.5 C

[a]NW (normal wood), WOW (wind opposite wood), WCW (wind compression wood), BOW (bent opposite wood), BCW (bent compression wood).
[b]% based on OD wood weight.
[c]% based on total carbohydrates.
[d]The letters (A,B,C) indicate significant differences using *Tukey-Kramer* HSD test at α=0.05 level.

5.4.3 Lignin heterogeneity

Compression wood is reported to be rich in *p*-hydroxyphenylpropane (H-type) lignin [6,31-33]. As showed in Figure 5.2, the nitrobenzene oxidation products obtained from the different wood specimens show that the bent and wind compression wood samples have relatively high amounts of *p*-hydroxybenzaldehyde units as compared to the control or opposite wood (BOW and WOW). Nitrobenzene oxidation yields oxidation products from uncondensed lignin structures [20,34], therefore, the yield of nitrobenzene oxidation products can be a relative indicator of how condensed a lignin structure is. The total oxidation product yield of the bent and wind compression wood is lower than the normal or opposite wood. This implies that compression wood lignin is likely more condensed than juvenile normal wood.

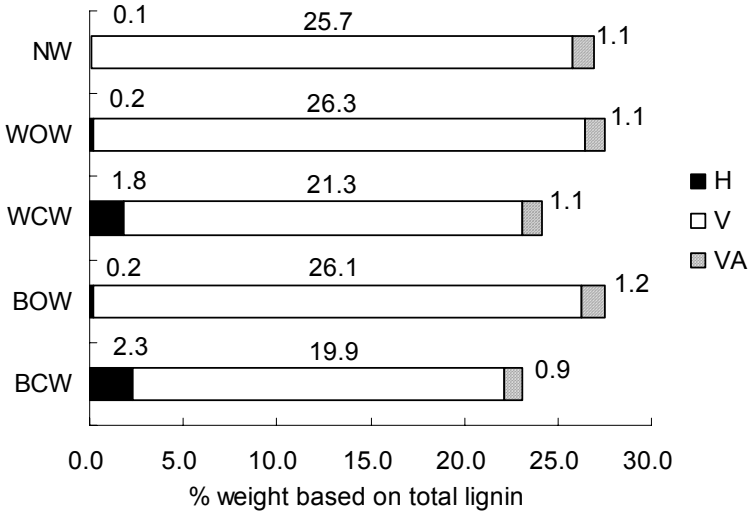

Figure 5.2 Nitrobenzene oxidation products from different groups: (NW) normal wood, (WOW) wind opposite wood, (WCW) wind compression wood, (BOW) bent opposite wood, (BCW) bent compression wood. (H) *p*-hydroxybenzaldehyde, (V) vanillin, (VA) vanillic acid.

Statistically, the yields of nitrobenzene oxidation products for bent compression wood are significantly different from the wind compression wood. Therefore, as compared to bent compression wood the wind compression wood produced with our experimental conditions can be considered as a mild compression wood.

Ozonation is a quantitative tool to analyze the stereochemistry (*erythro* (E) and *threo* (T) isomers) of arylglycerol-β-aryl ether linkages [21]. The ozonation result of the five different wood specimens is shown in Figure 5.3. The total mole % yield of the two isomers (E+T) decreases from an average of 22.0 % for normal, bent opposite and wind opposite wood to an average of 18.5 % for the two compression wood samples (WCW

and BCW). These results suggest an approximate 15% decrease in arylglycerol-β-aryl ether linkages in compression wood lignin. The E/T ratio of juvenile normal wood is 1.08, with no statistically significant difference from the bent opposite (1.07) or wind opposite (1.09) wood. However, the E/T ratios of compression wood, wind (1.15) and bent (1.23), are significantly higher than those of normal wood or opposite wood, suggesting that the decrease in arylglycerol-β-aryl ether linkages in compression wood lignin results more from the decrease in the *threo* isomer (T) than in the *erythro* isomer (E).

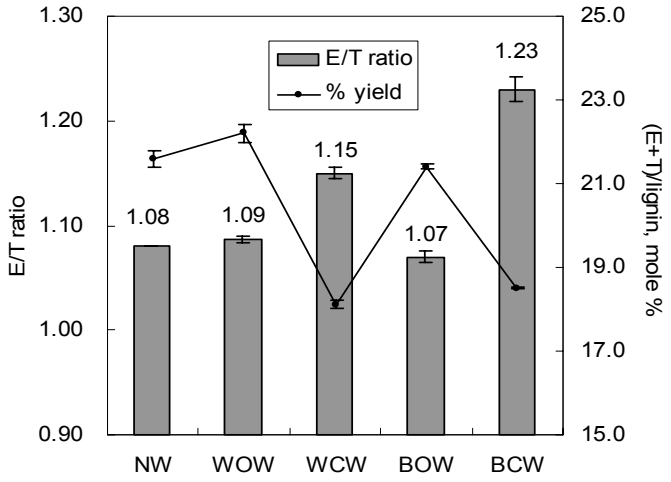

Figure 5.3 *Erythro*/*threo* (E/T) ratios and total yield (E+T) of different wood samples: (NW) normal wood, (WOW) wind opposite wood, (WCW) wind compression wood, (BOW) bent opposite wood, (BCW) bent compression wood.

Normally, the ratio of *erythro* and *threo* forms in gymnosperms is about 1.0 [35-37]. The results here show that in compression wood lignin the *erythro* form is more predominant. This is similar to what has been reported for tension wood of hardwood lignin [37]. Thus, it seems that the *erythro*-isomer is predominant in reaction wood lignin.

The empirical C_9 formulas of the different MWLs obtained from element analysis and methoxyl content analysis are listed in Table 5.3. The methoxyl content of the wind compression wood and bent compression wood are about 0.15 and 0.26 per C_9-unit lower than that of juvenile normal wood, respectively. These data are consistent with the results from nitrobenzene oxidation (Figure 5.2) and the results of Yasuda and Sakakibara [33] who reported a 0.2 per C_9-unit reduction in methoxyl content between compression wood MWL and normal wood MWL from larch (*Larix leptolepis*).

Table 5.3 Empirical formulas of different MWLs.

Group[a]	C_9 empirical formula[b]
NW	$C_9H_{8.32}O_{3.01}(OCH_3)_{0.92}$
WOW	$C_9H_{8.57}O_{3.19}(OCH_3)_{0.88}$
WCW	$C_9H_{8.39}O_{3.18}(OCH_3)_{0.77}$
BOW	$C_9H_{8.28}O_{3.10}(OCH_3)_{0.92}$
BCW	$C_9H_{8.76}O_{3.26}(OCH_3)_{0.66}$

[a]NW (normal wood), WOW (wind opposite wood), WCW (wind compression wood), BOW (bent opposite wood), BCW (bent compression wood).
[b]The C_9 formula did not correct for sugar content.

Quantitative MWL structure characterization was performed by ^{13}C NMR. Table 5.4 lists the major differences in functional groups and inter-unit linkages between the five MWLs. The total H-units (*p*-hydroxyphenyl moieties) are higher in compression wood (WCW and BCW) than the juvenile normal (NW) and opposite wood (WOW and BOW). The major difference in H-units is attributed to the non-conjugated *p*-hydroxyphenyl

moieties. The amount of total hydroxyl groups is slightly higher in the compression wood samples than the juvenile normal wood or opposite wood. Both the phenolic and aliphatic hydroxyl groups are slightly higher in the compression wood samples. These results are similar to that recently reported by Önnerud and Gellerstedt [32], wherein they reported higher phenolic units per 100 phenylpropane units in the compression wood of spruce as compared to normal wood. Similarly, the amount of etherified 5-5' moieties is higher in both compression wood samples as compared to the normal and opposite wood. Based on these results, it is apparent that the lignin structure in MWL isolated from compression wood is different from that obtained from juvenile normal wood.

Table 5.4 Major differences of functional groups and inter-unit linkages between five MWLs [a]

Structures[b]	NW [c]	WNW [c]	WCW [c]	BOW [c]	BCW [c]
Total H units	0.05	0.04	0.11	0.04	0.12
Conjugated	0.01	0.01	0.02	0.01	0.02
Non-conjugated	0.04	0.03	0.09	0.03	0.10
Total OH	1.42	1.43	1.47	1.40	1.48
Phenolic OH	0.28	0.28	0.31	0.28	0.31
Aliphatic OH	1.14	1.15	1.16	1.12	1.17
Etherifed 5-5'	0.10	0.12	0.15	0.09	0.14

[a]The numbers are expressed as per aromatic ring.
[b]The peak assignments and calculations are according to the works of Capanema et al. [23] and Balakshin et al. [38], and the references therein.
[c]NW (normal wood), WOW (wind opposite wood), WCW (wind compression wood), BOW (bent opposite wood), BCW (bent compression wood).

5.5 Conclusion

In order to resolve whether juvenile wood is truly identical to compression wood, loblolly pine ramets were planted in 3 different environments, the unaltered control, constrained bending and excess wind, yielding 5 different wood specimens. Our results show that

juvenile wood is different from compression wood in morphology and chemical characteristics, including tracheid shape and length, sugar composition, and lignin structure. Compared to the compression wood produced by artificial bending the wood produced in the windy environment can be classified as a mild type compression wood.

5.6 References

[1] Bendtsen, B.A. Production of wood from improved and intensively managed trees. *Forest Prod. J.* **1978**, *28*, 61-72.

[2] Zobel, B.J.; van Buijtenen, J.P. *Wood Variation: Its Causes and Control*; Springer-Verlag: Berlin, 1989.

[3] Zobel, B.J.; Sprague, J.R. *Juvenile Wood in Forest Trees*; Springer-Verlag: Berlin, 1998.

[4] Zobel, B.J. Using the juvenile wood concept in the southern pines. *South. Pulp Paper Mfg.* **1975**, 14-16.

[5] Zobel, B.J. Wood quality from fast-grown plantation. *TAPPI J.* **1981**, *64*, 71-74.

[6] Timell, T.E. *Compression Wood in Gymnosperms*,Vol.I; Springer-Verlag: Berlin, 1986.

[7] Scurfield, G. Reaction wood: its structure and function. *Science* **1973**, *179*, 647-655.

[8] Zobel, B.J.; McElwee, R.L. Variation of cellulose in loblolly pine. *TAPPI J.* **1958**, *41*, 167-170.

[9] Lee, C.L. Crystallinity of wood cellulose fiber. *Forest Prod. J.* **1961**, *11*, 108-112.

[10] Watanabe, H.; Tsutsumi, J.; Kojima, K. Studies on juvenile wood. I. Experiments on stems of Sugi trees (*Cryptomeria japonica* D. Don). *Mokuzai Gakkaishi* **1963**, *9*, 225-230.

[11] Zobel, B.J. The changing quality of the world wood supply. *Wood Sci. Technol.* **1984**, *18*, 1-17.

[12] Bjorkman, A. Studies on finely divided wood. Part I. Extraction of lignin with neutral solvents. *Svensk Papperstidn.* **1956**, *59*, 477-485.

[13] Adler, E.; Brunow, G.; Lundquist, K. Investigation of the acid-catalysed alkylation of lignins by means of NMR spectroscopic methods. *Holzforschung* **1987**, *41*, 199-207.

[14] Krassig, H.A. Cellulose: Structure, Accessibility, and Reactivity. Gordon and Breach Science: Switzerland, 1993; pp 91-92.

[15] Vonk, C.G. Computerization of Ruland's X-ray method for determination of the crystallinity in polymers. *J. Appl. Cryst.* **1973**, *6*, 148-152.

[16] Dence, C.W. The determination of lignin. In *Methods in Lignin Chemistry*; S.Y. Lin and C.W. Dence, Eds.; Springer-Verlag: Berlin/New York, 1992; pp 34-35.

[17] Yeh, T.F.; Yamada, T.; Capanema, E.; Chang, H.M.; Chiang, V.; Kadla, J.F. Rapid screening of wood chemical component variations using transmittance near infrared spectroscopy. *J. Agric. Food Chem.* **2005**, 3328-3332.

[18] Yokoyama, T.; Kadla, J.F.; Chang, H.M. Microanalytical method for the characterization of fiber components and morphology of woody plants. *J. Agric. Food Chem.* **2002**, *50*, 1040-1044.
[19] Coimbra, M.A.; Delgadillo, I.; Waldron, K.W.; Selvendran, R. Isolation and analysis of cell wall polymers from olive pulp. In *Modern Methods of Plant Analysis*; H.F. Linskens and J.F. Jackson, Eds.; Springer-Verlag: Berlin, 1996; pp 33-44.
[20] Chen, C.L. Nitrobenzene and cupric oxide oxidation. In *Methods in Lignin Chemistry*; S.Y. Lin and C.W. Dence, Eds.; Springer-Verlag: Berlin, 1992; pp 301-321.
[21] Akiyama, T.; Sugimoto, T.; Matsumoto, Y.; Meshitsuka, G. Erythro/threo ratio of β-O-4 structures as an important structural characteristic of lignin. I: Improvement of ozonation method for the quantitative analysis of lignin side-chain structure. *J. Wood Sci.* **2002**, *48*, 210-215.
[22] Goto, H.; Koda, K.; Matsumoto, Y.; Meshitsuka, G. Precise determination of methoxyl content as an important indication of the extent of lignin oxidation remaining in bleached pulp. *11th International Symposium on Wood and Pulping Chemistry, Nice, France*; Vol. III, pp 417-420.
[23] Capanema, E.A.; Balakshin, M.Y.; Kadla, J.F. A comprehensive approach for quantitative lignin characterization by NMR spectroscopy. *J. Agric. Food Chem.* **2004**, *52*, 1850-1860.
[24] Wardrop, A.B.; Davies, G.W. The nature of reaction wood. VIII. The structure and differentiation of compression wood. *Aust. J. Bot.* **1964**, *12*, 24-38.
[25] Shelbourne, C.J.A.; Ritchie, K.S. Relationships between degree of compression wood development and specific gravity and tracheid characteristics in loblolly pine. *Holzforschung* **1968**, *22*, 185-190.
[26] Kwon, M.; Bedgar, D.L.; Piastuch, W.; Davin, L.B.; Lewis, N.G. Induced compression wood formation in Douglas fir (*Pseudotuga menziesii*) in microgravity. *Phytochem.* **2001**, *57*, 847-857.
[27] OpTestEquipment, I. *Fiber quality analyzer operation manual*; OpTest Equipment Inc.: Ontario, Canada, 1999.
[28] Tanaka, F.; Koshijima, T.; Okuyama, T. Characterization of cellulose in compression wood and opposite woods of a *Pinus densiflora* tree grown under the influence of strong wind. *Wood Sci. Technol.* **1981**, *15*, 265-273.
[29] Bland, D.E. The chemistry of reaction wood. Part I. the lignin of *Eucalyptus goniocalyx* and *Pinus radiata*. *Holzsforschung* **1958**, *12*, 36-43.
[30] Lohrasebi, H.; Mabee, W.E.; Roy, D.N. Chemistry and pulping feasibility of compression wood in black spruce. *J. Wood Chem. Technol.* **1999**, *19*, 13-25.
[31] Fukushima, K.; Taguchi, S.; Matsui, N.; Yasuda, S. Distribution and seasonal changes of monolignol glucosides in *Pinus thunbergii*. *Mokuzai Gakkaishi* **1997**, *43*, 254-259.
[32] Önnerud, H.; Gellerstedt, G. Inhomogeneities in the chemical structure of spruce lignin. *Holzsforschung* **2003**, *57*, 165-170.
[33] Yasuda, S.; Sakakibara, A. The chemical composition of lignin from compression wood. *Mokuzai Gakkaishi* **1975**, *21*, 363-369.

[34] Chang, H.M.; Allan, G.G. Oxidation. In *Lignin: Occurrence, Formation, Structure and Reactions*; K.V. Sarkanen and C.H. Ludwig, Eds.; Wiley-Interscience: New York, 1971; pp 433-485.
[35] Lundquist, K. NMR studies of lignins. 4. Investigation of spruce lignin by 1H NMR spectroscopy. *Acta Chem. Scand. Ser. B.* **1980**, *34*, 21-26.
[36] Matsumoto, Y.; Ishizu, A.; Nakano, J. Studies of chemical structure of lignin by ozonation. *Holzforschung* **1986**, *40*, 81-85.
[37] Akiyama, T.; Matsumoto, Y.; Okuyama, T.; Meshitsuka, G. Ratio of *erythro* and *threo* form of β-O-4 structures in tension wood lignin. *Phytochem.* **2003**, *64*, 1157-1162.
[38] Balakshin, M.Y.; Capanema, E.; Goldfarb, B.; Frampton, J.; Kadla, J.F. NMR studies on Fraser fir *Abies fraseri* (Pursh) Poir. lignins. *Holzforschung* **2005**, *59*, 488-496.

6. THE UTILIZATION OF METABOLIC PROFILING IN THE STUDY OF THE DIFFERENCES BETWEEN JUVENILE WOOD AND COMPRESSION WOOD IN LOBLOLLY PINE (*Pinus taeda*)[a]

[a]Submitted to *Tree Physiology* (July 7, 2005)

Ting-Feng Yeh[1], Cameron R. Morris[1], Barry Goldfarb[1], Hou-min Chang[1], and John F. Kadla[1,2]

[1]North Carolina State University, Raleigh, NC 27695

[2]University of British Columbia, Vancouver, B.C. V6T 1Z4

6.1 Summary

In conifers, juvenile wood (JW) is typically associated with compression wood (CW). Due to their similar properties, there is a common belief that JW is the same as CW. To resolve whether JW can be metabolically separated from CW, twenty-four rooted cuttings of one loblolly pine clone were planted in growth chambers under normal, artificial bending, and windy environments. With metabolic profiling using gas chromatography and principal component analysis, we were able to assign clusters into the treatment groups representing different environmental disturbances. Substantial increases in abundances of coniferin and *p*-glucocoumaryl alcohol are responsible for the separation of the clustering between compression wood and juvenile normal wood xylem tissue. These findings demonstrate that metabolic profiling can be a useful tool for biochemical phenotyping of trees, providing valuable information for physiological responses to environmental conditions study.

6.2 Introduction

Increasing utilization of rapidly growing trees in plantations in the southeast US is sifting the raw materials for solid wood and pulp from predominately mature wood to a greater proportion of short-rotation juvenile wood [1,2]. Juvenile wood is the wood formed near the stem center and is formed by a young vascular cambium [3]. A typical 15-year-old loblolly pine contains as much as 85% juvenile wood by volume, as compared to only 20% in a 40-year-old tree [4]. Compared to mature wood, juvenile wood has lower wood density, shorter fiber length, higher lignin content, and higher compression wood content [5,6].

The percentage of compression wood in juvenile pine is on average about 18% [7], but can be as high as 44% [8]. Compression wood, the tissue formed under leaning stems and branches arises from environmental disturbances, such as gravitropic responses or prevailing winds [5,9]. Its formation causes "pushing" the stems or branches toward a vertical orientation [10]. Compression wood is generally considered to be inferior for both pulp and solid wood products. In chemical pulping, the utilization of juvenile and compression wood increase chemical consumption and decrease pulp yield, due to the higher lignin and lower cellulose content. As a result, increased usage of juvenile wood (and compression wood) from fast-growing plantation forests can significantly impact industrial production costs and product quality.

It has been generally considered that juvenile wood is similar to compression wood [3,11-13]. However, we have recently shown that the morphology and chemical structure of juvenile wood is different from that of compression wood [14]. To further investigate compression wood formation, metabolic profiling of loblolly pine xylem tissue [15] was performed. Metabolic profiling is a chromatographic technique that can examine changes in metabolite pools during development or in response to environmental or chemical stresses [16-23]. In this paper we report the metabolic profiling of juvenile loblolly pine trees grown under different mechanical stress conditions. Using principal component analysis (PCA), changes in the metabolites produced in response to compression wood formation are presented and comparisons between compression wood and normal juvenile wood xylem tissue are made.

6.3 Experimental

6.3.1 Materials

Twenty-four rooted cuttings of one loblolly pine (*Pinus taeda*) clone were transplanted from Ray Leach Supercells (164 ml) into 9-l pots. After conditioning inside a greenhouse for 4 weeks, they were moved into growth chambers (Southeastern Plant Environment Laboratory, North Carolina State University) for a 9-month growth period. The chamber photoperiod and temperature were 18 h at 28 °C under incandescent light, and 6 h at 20 °C in the dark. Trees were assigned randomly into three environmental conditions; i.e. control, bent, and augmented wind. The control and bent trees (8 trees each) were placed in a reduced wind chamber in which normal air circulation was reduced to produce an average wind speed of 0.26 m s^{-1}. The 8 augmented wind trees were placed in a growth chamber with two additional oscillating fans, producing an average wind speed of 1.43 m s^{-1} (range of 0.5~4.0 m s^{-1}). The tree sway frequency was approximately 5 times min^{-1}.

The bent trees were rendered at 45° to the perpendicular stems. When the new growth stem reached about 30 cm, another bend was applied. The trees were bent a total of 3 to 4 times during the 9-month period. The strings, which fastened the bent trees, were released two days immediately before tissue harvest to manifest gravitropic response. The initial average height of the trees was ~20 cm, and became ~150 cm (control and augmented wind trees) and ~100 cm (bent trees) at harvest.

6.3.2 Chemicals

Methanol (CH_3OH), chloroform ($CHCl_3$), pyridine, ribitol, methoxyamine hydrochloride, and, *N*-methyl-*N*-(trimethylsilyl) trifluoroacetamide (MSTFA) were of analytical reagent grade (Aldrich Chemical Co.) and used as received.

6.3.3 Sampling Procedure

The trees were separated into 4 groups, juvenile control normal wood (NW), windy wood (WW), bent opposite wood (BOW) and bent compression wood (BCW). All xylem samples were collected from the same relative height of each of the stems. Xylem tissue was collected immediately after removal of the phloem of the tree stems by rapid scraping of the xylem tissue into a pre-frozen sterile centrifuge tubes, according to the procedure of Morris et al. [15]. The tissue was then immediately immersed in liquid nitrogen and transferred to a dry ice chest for transport to the laboratory. At the laboratory, the samples were placed in a -80 °C freezer for storage prior to analysis.

6.3.4 Metabolite Extraction and Analysis

Metabolite analysis of xylem tissue by GC-MS was carried out by the protocol of Morris et al. [15]. Specifically, the frozen (-80 °C) xylem tissue was ground into a fine powder in liquid nitrogen with a mortar and pestle. The ground tissue (300 ± 10 mg) was extracted with 1.4 ml of CH_3OH, and 100µl of internal standard (ribitol, 10 mg ml^{-1} in H_2O). The tissue was extracted by shaking the mixture for 30 min at 70°C. The sample was then centrifuged for 3 min at 2600*g*. The supernatant was removed and diluted with 1.4 ml of H_2O in a second centrifuge tube, vortexed, and set aside. The remaining

centrifugate was further extracted for 10 min at 37 °C with 2 ml of $CHCl_3$. The mixture was centrifuged at 2600*g* for 3 min, and the supernatant was transferred to the CH_3OH-water extract. The combined extracts were vortexed and centrifuged at 2600*g* for 15 min.

Because most of the metabolites we were interested in are found in the polar extraction phase, after the centrifugation, the upper, polar CH_3OH/water phase was taken and reduced to dryness in a vacuum. The dried polar phase was dissolved in 100 µl of methoxyamine hydrochloride (20 mg ml^{-1} in pyridine) and shaken for 90 min at 30 °C. Two hundred microliters of MSTFA was then added for derivatization, and the solution was shaken for 30 min at 37 °C and then left standing for 2 h at 25 °C. The mixture was then diluted with 200 µl of pyridine, vortexed, and directly injected (2 µl) onto the GC and/or GC-MS. Two full technical replicates, including extraction, derivatization, and GC injection were conducted for each individual xylem tissue sample.

The GC system consisted of a Hewlett-Packard 6890 GC-FID, which was controlled by ChemStation software (Rev. A7.01). GC was performed on a 30-m DB-1 column with 0.25 µm film thickness and 0.32mm I.D. (J&W Scientific Inc.). The injection temperature was set to 250 °C, and the FID detector was set to 300 °C. Helium flow was 2 ml min^{-1}. After a 5-min isothermal heating at 70 °C, the oven temperature was increased at 5 °C min^{-1} to 300 °C. The oven was then held isocratic for 5 min and cooled to 70 °C. A threshold cutoff for metabolite analysis was set at 2% of the peak area of the internal standard.

A ThermoFinnigan TraceGC equipped with a PolarisQ ion trap mass spectrometer (GC-MS) and Xcalibur software (version 1.3) was used for metabolite identification. The column and method used for analyzing metabolites on the GC-MS system were the same

as used in the GC analysis, except the ion source was adjusted to 200°C. Mass spectra were recorded from *m*/*z* 50 to 650 at 0.58 s scan^{-1} with an electron ionization of 70 eV. Identification of most of the signals was made on the search results from NIST Mass Spectral Search Program (National Institute of Standard and Technology, USA) and/or comparison to authentic compounds (both retention time and mass spectra). A total of 25 metabolites where identified in the polar metabolites obtained from the xylem tissue of NW (Figure 6.1).

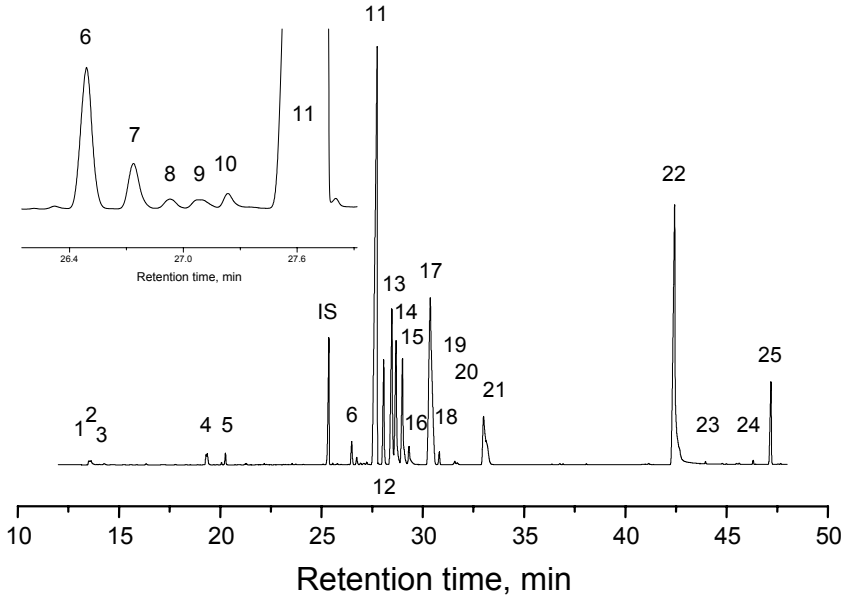

Figure 6.1 GC chromatogram of the polar phase metabolites identified from normal wood xylem. Peak identification: (**1**) Glycine TMS; (**2**) Phosphoric acid TMS; (**3**) Succinic acid TMS; (**4**) Malic acid TMS; (**5**) 4-aminobutyric acid TMS; (**6**) Shikimic acid TMS; (**7**) Citric acid TMS; (**8**) Unknown 1; (**9**) Unknown 2; (**10**) Unknown 3; (**11**) Pinitol TMS; (**12**) Quinic acid TMS; (**13**) Fructose MEOX1 TMS; (**14**) Fructose MEOX2 TMS; (**15**) Glucose MEOX1 TMS; (**16**) Glucose MEOX2 TMS; (**17**) Ononitol TMS; (**18**) Glucose TMS; (**19**) Galactonic acid TMS; (**20**) Gluconic acid TMS; (**21**) Inositol TMS; (**22**) Sucrose TMS; (**23**) Maltose TMS; (**24**) *p*-Glucocoumaryl alcohol TMS; (**25**) Coniferin TMS.

6.3.5 Mass Spectra of Significant Metabolites

Glycine TMS (**1**) MS m/z (rel. int.) 262(4) 188(3), 174(98), 158(3), 147(23), 133(14), 117(4), 100(39), 86(39), 73(100)

Phosphoric acid TMS (**2**) MS m/z (rel. int.) 314(5), 299(40), 283(4), 225(6), 211(10), 207(4), 191(5), 181(4), 151(6), 147(5), 133(10), 115(5), 103(4), 73(100)

Succinic acid TMS (**3**) MS m/z (rel. int.) 247(6), 172(4), 149(27), 148(12), 147(100), 131(3), 129(7), 85(2), 75(20), 73(40)

Malic acid TMS (**4**) MS m/z (rel. int.) 335(2), 307(3), 265(4), 245(4), 233(5), 217(4), 189(5), 175(5), 149(13), 147(45), 133(14), 117(3), 101(6), 73(100)

4-aminobutyric acid TMS (**5**) MS m/z (rel. int.) 304(14), 216(8), 174(64), 149(14), 147(57), 142(9), 131(8), 100(18), 86(33), 73(100)

Shikimic aicd TMS (**6**) MS m/z (rel. int.) 372(4), 357(3), 282(10), 255(8), 204(74), 189(12), 147(35), 133(9), 73(100)

Citric acid TMS (**7**) MS m/z (rel. int.) 375(7), 363(4), 347(12), 303(2), 273(42), 257(14), 221(6), 211(14), 183(15), 147(64), 129(10), 73(100)

Unknown 1 (**8**) MS m/z (rel. int.) 347(3), 319(4), 257(9), 217(12), 204(29), 189(9), 157(4), 147(30), 133(6), 129(8), 73(100)

Unknown 2 (**9**) MS m/z (rel. int.) 347(2), 319(2), 257(2), 217(13), 204(8), 189(5), 157(3), 147(35), 133(16), 129(10), 73(100)

Unknown 3 (**10**) MS m/z (rel. int.) 362(2), 319(2), 257(3), 217(10), 204(6), 191(7), 189(5), 149(15), 147(32), 133(12), 129(7), 95(5), 73(100)

Pinitol TMS (**11**) MS m/z (rel. int.) 627(15), 555(4), 507(11), 449(26), 433(33), 405(2), 375(29), 359(5), 343(24), 318(6), 305(3), 285(3), 265(25), 260(15), 247(6), 217(16), 207(24), 191(30), 163(6), 159(8), 147(19), 133(21), 129(20), 103(6), 89(7), 73(100)

Quinic acid TMS (**12**) MS m/z (rel. int.) 419(2), 372(3), 345(34), 334(2), 255(35), 239(5), 204(5), 191(8), 147(35), 133(8), 73(100)

Fructose MEOX1 TMS (**13**) MS m/z (rel. int.) 364(3), 307(6), 277(2), 217(33), 189(3), 173(3) 147(20), 133(7), 129(8), 117(5), 103(19), 89(5), 73(100)

Fructose MEOX2 TMS (**14**) MS m/z (rel. int.) 364(2), 307(5), 277(2), 217(33), 189(3), 173(3) 147(23), 133(5), 129(8), 117(5), 103(22), 89(6), 73(100)

Glucose MEOX1 TMS (**15**) MS m/z (rel. int.) 570(2), 554(2), 319(6), 217(8), 205(4), 189(2), 160(7), 157(13), 147(30), 129(28), 117(7), 103(5), 89(6), 73(100)

Glucose MEOX2 TMS (**16**) MS m/z (rel. int.) 570(2), 554(2), 319(7), 217(8), 205(6), 189(3), 160(4), 157(17), 147(37), 129(27), 117(7), 103(9), 89(7), 73(100)

Ononitol TMS (**17**) MS m/z (rel. int.) 343(2), 318(10), 305(9), 260(12), 217(23), 204(4), 191(12), 163(5), 159(6), 149(11), 147(35), 133(15), 129(15), 103(10), 89(6), 73(100)

Glucose TMS (**18**) MS m/z (rel. int.) 539 (2), 433(2), 345(2), 291(2), 217(8), 204(36), 191(18), 147(23), 133(6), 129(9), 103(3), 73(100)

Galactonic acid TMS (**19**) MS m/z (rel. int.) 433(2), 359(2), 333(8), 319(3), 305(5), 292(6), 217(11), 205(4), 189(5), 157(7), 147(41), 143(8), 129(14), 117(5), 103(6), 89(2), 73(100)

Gluconic acid TMS (**20**) MS m/z (rel. int.) 319(5), 220(5), 217(9), 204(36), 189(8), 157(9), 147(20), 129(9), 117(3), 103(4), 89(5), 73(100)

Inositol TMS (**21**) MS m/z (rel. int.) 507(2), 433(2), 393(2), 318(5), 305(10), 291(3), 265(6), 217(16), 204(4), 191(11), 147(38), 129(16), 103(12), 73(100)

Sucrose TMS (**22**) MS m/z (rel. int.) 437(5), 361(44), 319(3), 271(11), 257(6), 243(11), 217(28), 191(7), 169(40), 147(23), 129(21), 103(10), 81(4), 73(100)

Maltose TMS (**23**) MS m/z (rel. int.) 361(30), 331(2), 271(12), 243(17), 217(17), 207(7), 195(20), 191(7) 169(39), 147(25), 129(20), 103(8), 73(100)

p-Glucocoumaryl alcohol TMS (**24**) MS m/z (rel. int.) 450(6), 361(33), 294(100), 271(20), 243(14), 217(31), 204(13), 191(10), 169(25), 147(31), 129(28), 103(13), 73(72)

Coniferin TMS (**25**) MS m/z (rel. int.) 450(12), 361(39), 324(100), 293(7), 271(20), 243(28), 217(47), 204(9), 169(46), 147(36), 129(23), 103(12), 73(90)

6.3.6 Statistical Analysis

For most applications of profiling technology, the relative values of metabolites is more important than absolute values [19]. Due to the side reaction of derivatization, fructose peaks (**13** and **14**) and glucose peaks (**15**, **16**, and **18**) were combined individually to give only one fructose (**13'**) and one glucose (**15'**) peaks, assuming that the response factors of these related derivatized compounds are all the same. All metabolite peaks were expressed as the area ratio based on the internal standard. The mean values of two technical replicates are used in the following analyses.

To enable a comprehensive analysis of the GC data and extract information relative to the different wood samples, two statistical methods were applied: principal component analysis (PCA) and hierarchical cluster analysis (HCA). Both methods use all the

metabolic data from a xylem sample to compute an individual metabolic profile and simultaneously compare this profile with all other tree metabolic profiles. Once the samples accumulate in the same cluster, this cluster can be viewed as a specific "metabolic phenotype" [19].

PCA is a pattern recognition technique which applies an *n*-dimensional vector approach to separate samples on the basis of cumulative correlation of all metabolite data and identifies the basic vector (eigenvector) that yields the best separation between samples [21,24]. HCA presents the cluster results in a dendrogram, where the similarity of two samples can be determined from the distance at which they connect in a single cluster (the smaller the distance, the more similar the sample) [21].

In order to reduce the type I error rate, all treatments were compared all together by multiple means comparisons (*Tukey* HSD test, α=0.05) to test for significant metabolite differences among treatments (SAS JMP, Version 5.1, SAS Institute Inc, USA).

6.4 Results and Discussion

6.4.1 PCA and HCA Clustering of the Tree Metabolic Change in Different Environments

The metabolic phenotypic clustering results for the xylem tissues were expressed using the first three principal components, which contain 73.3% of the total information content derived from the metabolite variance (Figure 6.2). The individual tree samples separate well according to the treatment groups. The BCW is separated by principal component 3 (PC3) from the NW. The BCW samples and WW samples are below the principal component 1 (PC1) and principal component 2 (PC2) plane, whereas the NW and BOW

are above the PC1 and PC2 plane. PC1 further separates the BCW (right side) and WW (left side). However, the NW group and BOW group are close to each other, with a slight overlap.

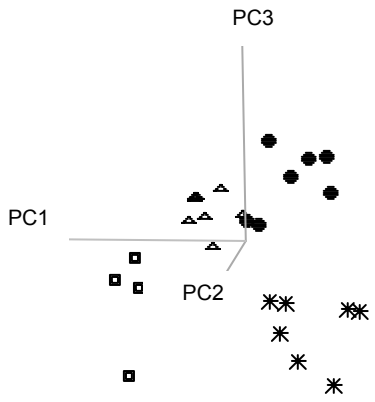

Figure 6.2 Metabolic phenotypic clustering results for different xylem tissues: △, normal wood (NW); ✳, bent compression wood (BCW); ●, bent opposite wood (BOW); □, windy wood (WW).

The metabolite data were further analyzed by HCA. The dendrogram shows that the windy wood samples (WW#) clustered in one group and the bent compression wood (BCW#) samples clustered in another (Figure 6.3). Two of the opposite wood samples (BOW1 and BOW2) overlapped with the normal wood samples (Figure 6.3). This phenomenon is reasonable as the chemical properties of opposite wood and normal wood are quite similar [5,25,26]. In fact, chemical analysis of the two wood samples from the same trees that were analyzed for metabolites in developing xylem in this study shows

they are similar in wood properties [14]. Our metabolite results support this similarity and extend it to metabolite pools during wood formation.

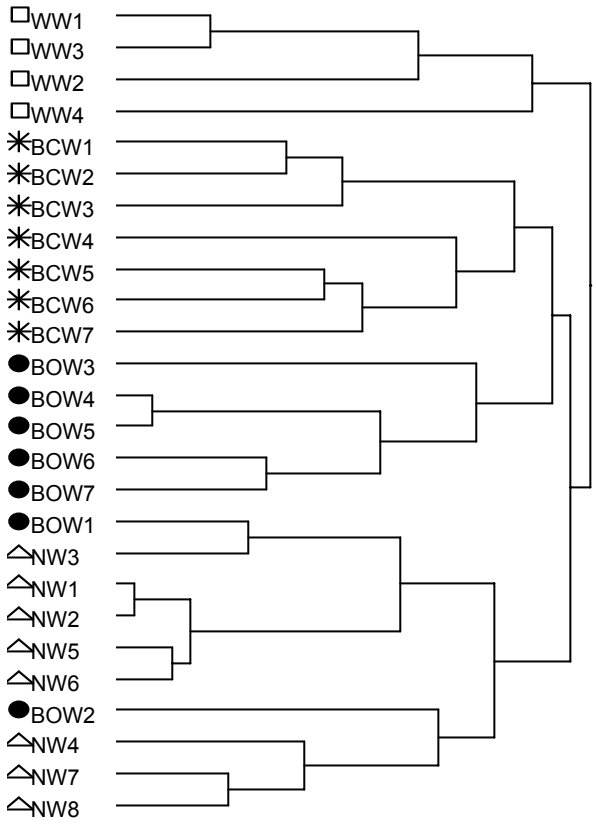

Figure 6.3 Dendrogram obtained after hierarchical cluster analysis (HCA) of the metabolic profiles from different xylem tissues: △, normal wood (NW); ✳, bent compression wood (BCW); ●, bent opposite wood (BOW); □, windy wood (WW).

6.4.2 Metabolite Impacts on Clustering Results

PCA data can further be used to evaluate which metabolites have impact on the clustering calculation. As PC3 separates the BCW from the NW (Figure 6.2), PC1 and PC3, which represent about 60% of the total variance of the data, were plotted to show how each individual metabolite is utilized in the calculation of the principal component (Figure

6.4). The metabolites farthest away from zero have the greatest impact on the linear combination that is used to calculate the principal component vector [15,19,23]. The results from Figure 6.4 show that the most important metabolites responsible for separating the BCW group from the NW group (vector 3) are mainly coniferin (**25**), p-glucocoumaryl alcohol (**24**), pinitol (**11**), and shikimic acid (**6**). Due to compression wood is known for higher lignin and different lignin composition than normal wood [5,27], it is expected that there are different levels of abundance of these metabolites between BCW xylem and NW xylem in juvenile wood.

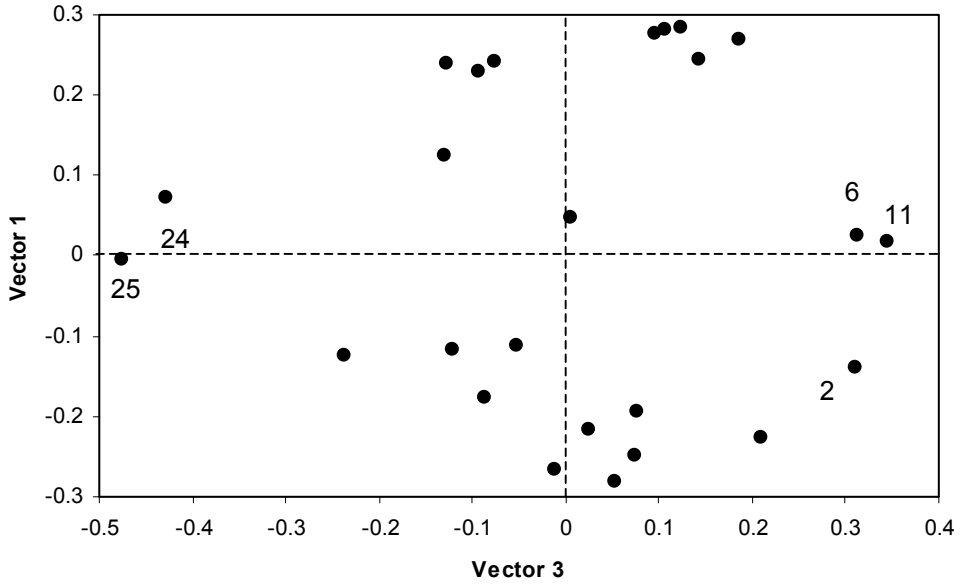

Figure 6.4 Impact of individual metabolites on metabolic clustering. Number identification: (**2**) Phosphoric acid TMS; (**6**) Shikimic acid TMS; (**11**) Pinitol TMS; (**24**) *p*-Glucocoumaryl alcohol TMS; (**25**) Coniferin TMS.

6.4.3 Comparison of the Relative Metabolite Levels in Xylem Tissue

In Tukey HSD test comparison, the BCW xylem tissue had relatively higher abundances of six compounds: glycine (**1**), malic acid (**4**), shikimic acid (**6**), maltose (**23**), p-glucocoumaryl alcohol (**24**), and coniferin (**25**), and a relatively lower abundances of pinitol (**11**), fructose (**13'**), glucose (**15'**), gluconic acid (**20**), and inositol (**21**), compared to NW (Figure 6.5). Significant increases in the pools of shikimic acid (**6**), p-glucocoumaryl alcohol (**24**) and coniferin (**25**), are consistent with an increase in lignin production, both quantitatively (higher lignin content), and qualitatively (more H-lignin), in response to compression wood formation.

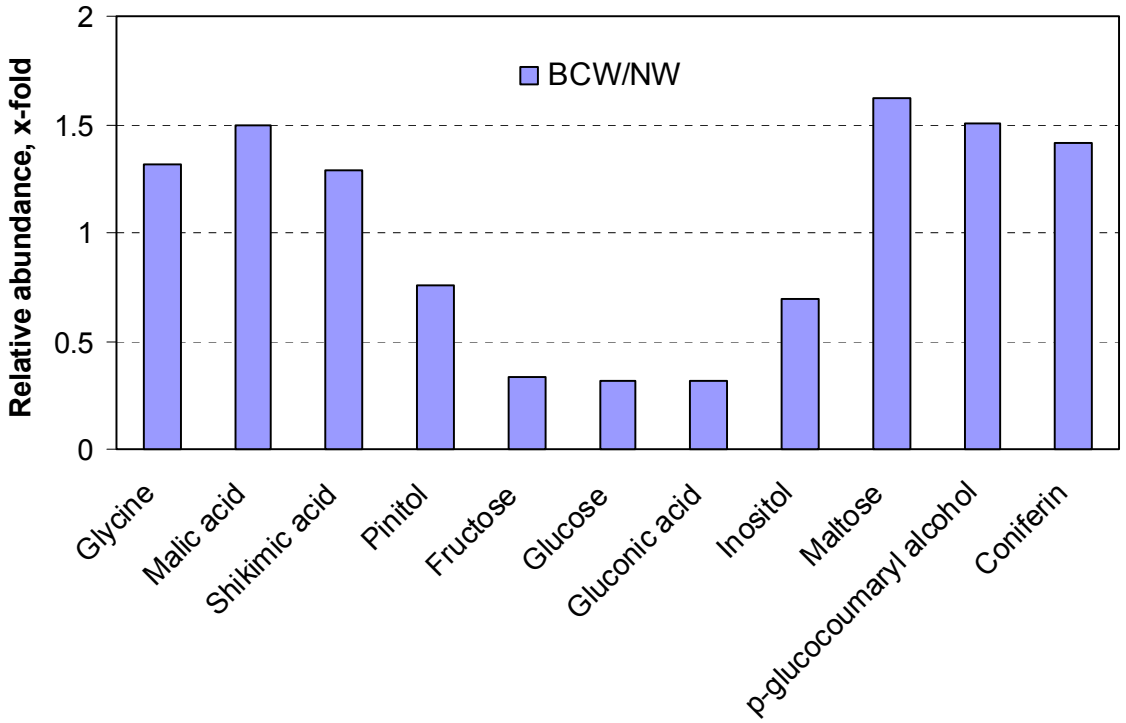

Figure 6.5 Significant metabolite differences between bent compression wood (BCW) and normal wood (NW), *Tukey* HSD test at α=0.05.

It has been reported [28,29] that the monolignol glucosides, both coniferin and p-glucocoumaryl alcohol, accumulate in the early stage of differentiating xylem, immediately before lignification, and are deposited into the S_2 layer of the cell wall in compression wood [27]. Chemical analysis of the wood sample from these same trees showed that the lignin content in the BCW was 36.6% as compared to 29.4% in the NW [14]. Furthermore, there was 2.3% of H-type lignin in the BCW versus only 0.1% in the NW [14].

The accumulation of fructose and glucose in NW might be related to the higher cellulose content in NW (44%) compared to BCW (34%) [14]. UDP-glucose is believed to be the immediate substrate for cellulose biosynthesis [30-32]. However, UDP-glucose can be formed in either of two pathways. The first pathway is from glucose to glucose-6-phosphate, glucose-1-phosphate, and followed by the conversion to UDP-glucose by pyrophosphorylase, and the second pathway is the conversion of sucrose to UDP-glucose via sucrose synthase and produces fructose as the byproduct [30-32]. The accumulation of glucose in NW could promote a higher production of UDP-glucose, and the accumulation of fructose could be a result of the conversion of sucrose to UDP-glucose. Both pathways result the higher cellulose content in NW compared to BCW.

Fewer metabolites differed significantly between WW and NW (Figure 6.6) than between BCW and NW. The WW xylem tissue had relatively higher abundances of glucose (**15'**), ononitol (**17**), inositol (**21**), and sucrose (**22**), and lower abundances of 4-aminobutyric acid (**5**), pinitol (**11**), and quinic acid (**12**). The accumulation of inositol (**21**) and ononitol (**17**) may be a response to drought stress in the windy trees, due to the

constant wind during the treatment period. Inositol (**21**) and the methylated derivatives, ononitol (**17**) and pinitol (**11**), are believed to be correlated with drought tolerance [33,34], providing an osmotic adjustment and/or osmoprotection function [35]. However, the reduction in the relative amount of pinitol in WW xylem tissues in comparison to NW can not be explained by drought stress. Further investigation of this phenomenon is required.

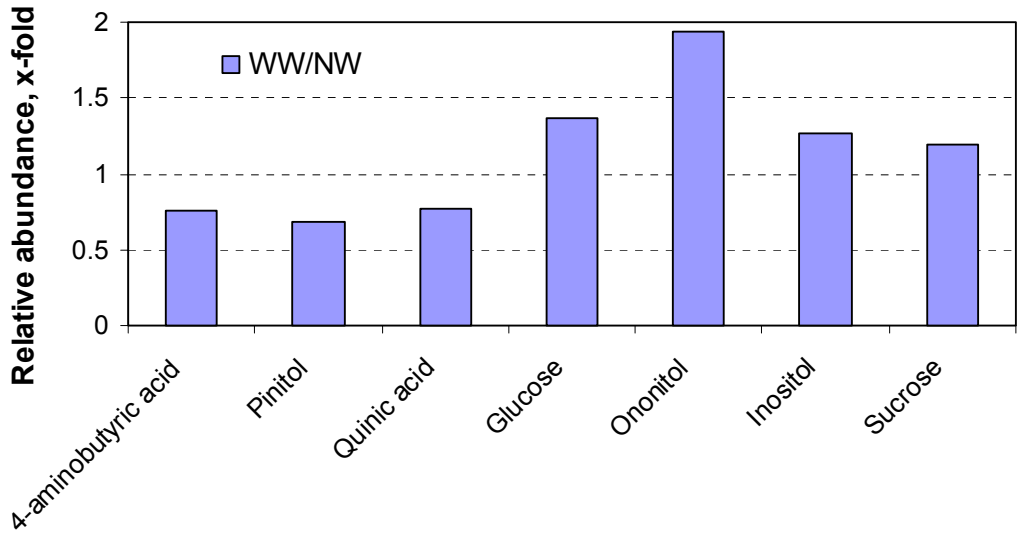

Figure 6.6 Significant metabolite differences between windy wood (WW) and normal wood (NW), *Tukey* HSD test at α=0.05.

Microscopic analysis of the wood produced in the windy wood trees showed the presence of approximately 30% compression wood by volume [14]. However, no significant difference in the relative abundance of coniferin and *p*-glucocoumaryl alcohol was detected between WW and NW (Figure 6.6). Due to the small size of the woody material analyzed, after only 9 months growth in the treatment, xylem tissue was

collected from the entire stem. Compression wood is expected to be found only in the "crooked" or "stressed" parts of the stem. As a result, the absence of any significant differences between the WW and NW xylem may be the result of dilution effects.

An about 10% increase in diameter was observed in WW trees compared to NW trees. Many researchers [36,37] have reported the increased radial growth and density of trees under flexure stress. Since cellulose accounts for 40~50% of the wood weight, the accumulation of glucose and sucrose in WW (Figure 6.6) could be related to the increased diameter growth in windy trees compared to normal juvenile wood. This helps transform into a greater mass and volume of xylem per cambial surface area in response to wind flexure [9].

The pattern of metabolite differences between BCW and WW (Figure 6.7) are more similar to that between BCW and NW. The higher abundance of coniferin in BCW compared to WW again is related to the higher lignin content in BCW than in the whole trees of WW. Windy trees have higher abundances of ononitol and inositol, which are possibly related to drought stress resulted from constant wind treatment, and the higher abundances of fructose, glucose and sucrose are closely associated to the increased radial growth compared to BCW.

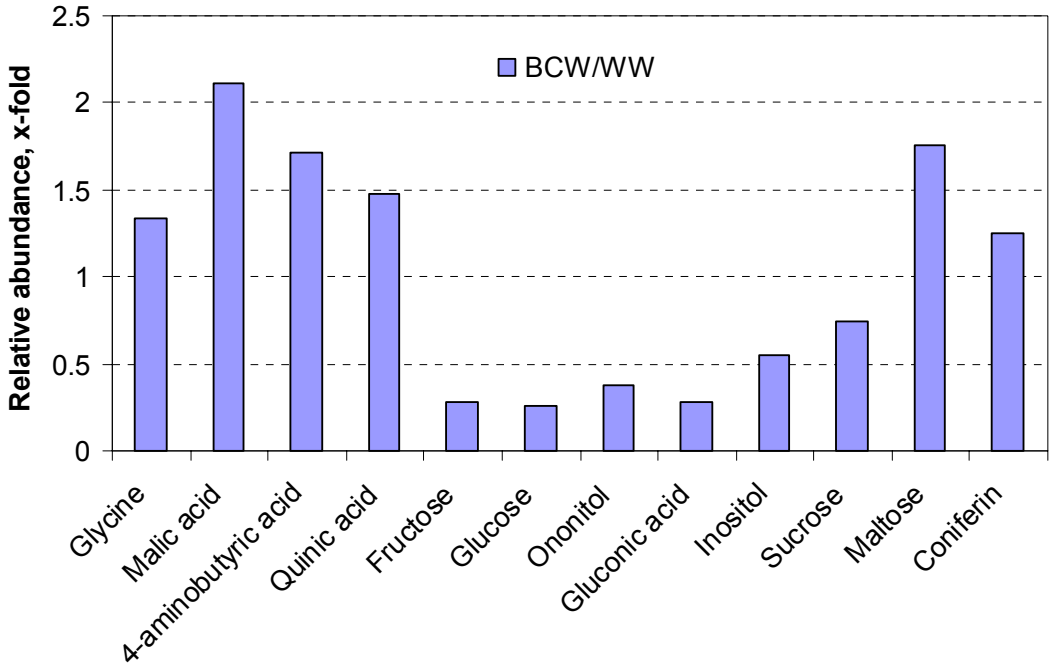

Figure 6.7 Significant metabolite differences between bent compression wood (BCW) and windy wood (WW), *Tukey* HSD test at α=0.05.

6.5 Conclusion

Results presented in this paper show that metabolic profiling, coupled with principal component analysis, can be a useful tool for understanding wood formation under different stress conditions. Distinct differences in metabolite profiles were detected between physically bent and normal juvenile wood xylem. Substantial differences in the abundance of metabolites associated with lignin production, coniferin and *p*-glucocoumaryl alcohol, were detected and determined responsible for the separation of the clustering between compression wood and juvenile normal wood xylem tissue. These results, combined with chemical analysis of the formed wood [14], demonstrate that,

although compression wood and juvenile wood share some properties, they are distinct in their chemistry during development and in final wood chemistry and anatomy.

6.6 References

[1] Prestemon, J.P.; Abt, R.C. Timber products supply and demand. In *Southern Forest Resource Assessment. Gen. Tech. Rep. SRS-53*; D.N. Wear and J.G. Greis, Eds.; Department of Agriculture, Forest Service, Southern Research Station: Asheville, 2002; pp 299-325.

[2] Siry, J.P. Intensive timber management practices. In *Southern Forest Resource Assessment. Gen. Tech. Rep. SRS-53*; D.N. Wear and J.G. Greis, Eds.; Department of Agriculture, Forest Service, Southern Research Station: Asheville, 2002; pp 327-340.

[3] Zobel, B.J.; Sprague, J.R. *Juvenile Wood in Forest Trees*; Springer-Verlag: Berlin, 1998.

[4] Zobel, B.J. Using the juvenile wood concept in the southern pines. *South. Pulp Paper Mfg.* **1975**, 14-16.

[5] Timell, T.E. *Compression Wood in Gymnosperms*,Vol.I; Springer-Verlag: Berlin, 1986.

[6] Zobel, B.J. Wood quality from fast-grown plantation. *TAPPI J.* **1981**, *64*, 71-74.

[7] Bendtsen, B.A. Production of wood from improved and intensively managed trees. *Forest Prod. J.* **1978**, *28*, 61-72.

[8] Zobel, B.J.; McElwee, R.L. Variation of cellulose in loblolly pine. *TAPPI J.* **1958**, *41*, 167-170.

[9] Telewski, F.W. Wind-induced physiological and developmental responses in trees. In *Wind and Trees*; M.P. Coutts and J. Grace, Eds.; Cambridge University Press: New York, 1995; pp 237-263.

[10] Scurfield, G. Reaction wood: its structure and function. *Science* **1973**, *179*, 647-655.

[11] Zobel, B.J. The changing quality of the world wood supply. *Wood Sci. Technol.* **1984**, *18*, 1-17.

[12] Watanabe, H.; Tsutsumi, J.; Kojima, K. Studies on juvenile wood. I. Experiments on stems of Sugi trees (*Cryptomeria japonica* D. Don). *Mokuzai Gakkaishi* **1963**, *9*, 225-230.

[13] Lee, C.L. Crystallinity of wood cellulose fiber. *Forest Prod. J.* **1961**, *11*, 108-112.

[14] Yeh, T.F.; Braun, J.L.; Goldfarb, B.; Chang, H.M.; Peszlen, I.; Kadla, J.F. Comparison of morphological and chemical properties between juvenile wood and compression wood of loblolly pine. *Holzforschung* **2005**, *59*.

[15] Morris, C.R.; Scott, J.T.; Chang, H.M.; Sederoff, R.R.; O'Malley, D.; Kadla, J.F. Metabolic profiling: a new tool in the study of wood formation. *J. Agric. Food Chem.* **2004**, *52*, 1427-1434.

[16] Trethewey, R.N.; Krotzky, A.J.; Willmitzer, L. Metabolic profiling: a Rosetta Stone for genomics? *Curr. Opin. Plant Biol.* **1999**, *2*, 83-85.

[17] Fiehn, O. Metabolomics - the link between genotypes and phenotypes. *Plant Mol. Biol.* **2002**, *48*, 155-171.
[18] Charlton, A.; Allnutt, T.; Holmes, S.; Chisholm, J.; Bean, S.; Ellis, N.; Mullineaux, P.; Oehlschlager, S. NMR profiling of transgenic peas. *Plant Biotechnol. J.* **2004**, *2*, 27-35.
[19] Fiehn, O.; Kopka, J.; Dormann, P.; Altmann, T.; Trethewey, R.N.; Willmitzer, L. Metabolite profiling for plant functional genomics. *Nat. Biotechnol.* **2000**, *18*, 1157-1161.
[20] Overy, S.A.; Walker, H.J.; Malone, S.; Howard, T.P.; Baxter, C.J.; Sweetlove, L.J.; Hill, S.A.; Quick, W.P. Application of metabolite profiling to the identification of traits in a population of tomato introgression lines. *J. Exp. Bot.* **2005**, *56*, 287-296.
[21] Roessner, U.; Luedemann, A.; Brust, D.; Fiehn, O.; Linke, T.; Willmitzer, L.; Fernie, A.R. Metabolic profiling allows comprehensive phenotyping of genetically or environmentally modified plant systems. *Plant Cell* **2001**, *13*, 11-29.
[22] Roessner, U.; Willmitzer, L.; Fernie, A.R. Metabolic profiling and biochemical phenotyping of plant system. *Plant Cell Rep.* **2002**, *21*, 189-196.
[23] Morris, C.R. Applications of metabolic profiling in the study of wood formation. Ph.D. Thesis, North Carolina State University, 2005.
[24] Jurs, P.C. Pattern recognition used to investigate multivariate data in analytical chemistry. *Science* **1986**, *232*, 1219-1224.
[25] Bland, D.E. The chemistry of reaction wood. Part I. the lignin of *Eucalyptus goniocalyx* and *Pinus radiata*. *Holzforschung* **1958**, *12*, 36-43.
[26] Lohrasebi, H.; Mabee, W.E.; Roy, D.N. Chemistry and pulping feasibility of compression wood in black spruce. *J. Wood Chem. Technol.* **1999**, *19*, 13-25.
[27] Fukushima, K.; Terashima, N. Heterogeneity in formation of lignin Part XV: formation and structure of lignin in compression wood of *Pinus thunbergii* studied by microautoradiography. *Wood Sci. Technol.* **1991**, *25*, 371-381.
[28] Fukushima, K.; Hato, C.; Mori, H.; Tsuji, Y. Localizations and roles of monolignol glucosides in the tree xylem. *13th International Symposium on Wood, Fibre and Pulping Chemistry (13th ISWFPC), Auckland, New Zealand*; Appita, Inc.; Vol. 2, pp 461-463.
[29] Fukushima, K.; Taguchi, S.; Matsui, N.; Yasuda, S. Distribution and seasonal changes of monolignol glucosides in *Pinus thunbergii*. *Mokuzai Gakkaishi* **1997**, *43*, 254-259.
[30] Babb, V.M.; Haigler, C.H. Sucrose phosphate synthase activity rises in correlation with high-rate cellulose synthesis in three heterotrophic systems. *Plant Physiol.* **2001**, *127*, 1234-1242.
[31] Delmer, D.P.; Haigler, C.H. The regulation of metabolic flux to cellulose, a major sink for carbon in plants. *Meta. Eng.* **2002**, *4*, 22-28.
[32] Srivastava, L.M. Cell wall, cell division, and cell growth. In *Plant Growth and Development: Hormones and Environment*; L.M. Srivastava, Ed.; Academic Press: San Diego, 2001; pp 23-74.
[33] Loewus, F.A.; Loewus, M.W. *myo*-Inositol: its biosynthesis and metabolism. *Ann. Rev. Plant Physiol.* **1983**, *34*, 137-161.
[34] McCue, K.F.; Hanson, A.D. Drought and salt tolerance: towards understanding and application. *Trends Biotechnol.* **1990**, *8*, 358-362.

[35] Bohnert, H.J.; Nelson, D.E.; Jensen, R.G. Adaptations to environmental stresses. *Plant Cell* **1995**, *7*, 1099-1111.
[36] Telewski, F.W. Growth, wood density, and ethylene production in response to mechanical perturbation in *Pinus taeda*. *Can. J. Forest Res.* **1990**, *20*, 1277-1282.
[37] Holbrook, N.M.; Putz, F.E. Influence of neighbors on tree form: effects of lateral shade and prevention of sway on the allometry of *Liquidambar styraciflua* (Sweet gum). *Am. J. Bot.* **1989**, *76*, 1740-1749.

7. MORPHOLOGICAL AND CHEMICAL VARIATIONS BETWEEN JUVENILE WOOD, MATURE WOOD, AND COMPRESSION WOOD OF LOBLOLLY PINE (*Pinus taeda*)[a]

[a]Accepted in *Holzforschung* (October 24, 2005)

Ting-Feng Yeh[1], Jennifer L. Braun[2], Barry Goldfarb[1], Hou-min Chang[1], and John F. Kadla[1,2]

[1]North Carolina State University, Raleigh, NC 27695

[2]University of British Columbia, Vancouver, B.C. V6T 1Z4

7.1 Summary

In order to better understand the within-tree variation between juvenile wood, mature wood, and compression wood, a 35-year-old mature bent loblolly pine wood was separated into seven groups by different positions in the tree. Both morphological and chemical structures analyses, such as fiber qualities, X-ray diffraction, sugar and lignin contents, nitrobenzene oxidation, ozonation, and NMR spectroscopy, were applied to all seven groups. Fiber properties are significantly different concerning tree top juvenile normal wood and tree bottom juvenile normal wood, juvenile normal and mature normal wood, juvenile compression and mature compression wood. However, differences in the chemical structure and composition are less significant within the specific tissues indicated above.

7.2 Introduction

It is well known that wood varies from tree to tree depending on genetic and environmental controls [1,2]. There is also considerable variation within the tree; from the center outward and from the top to bottom [2-4]. In conifers, the within tree variation pattern is highly associated with the characteristic and location of the juvenile wood, and its relative portion to mature wood [2]. Compared to mature wood, juvenile wood has different properties such as lower wood density, shorter fiber length, higher lignin content, and higher compression wood content [5,6].

In our previous publication is clearly demonstrated that juvenile normal wood is different from juvenile compression wood in morphological and chemical characteristics [7]. It is crucial for tree-breeding programs to select the elite trees based on objective

criteria. Currently, wood property assessments of tree-breeding projects mostly rely on sampling of increment cores and on non-destructive assessment techniques of the cores. Erroneous results may arise if the presence of reaction wood not detected in the samples. A comprehensive study of within-tree wood property variation could help to evaluate the material more adequately for breeding purposes.

An extensive research has been invested into within-tree variation, such as fiber properties, wood chemical and physical properties, and pulping evaluation [2,3,6,8-12]. These publications provided valuable information about specific aspects of the within-tree variation but a comprehensive evaluation of this issue is lacking. In this paper, we provide a comprehensive study of the within-tree variation of a loblolly pine focusing on morphological and chemical structure analysis. Our main objectives are to resolve whether the juvenile wood at the top of the tree is the same as the juvenile wood at the bottom of the tree, whether juvenile compression wood is identical to mature compression wood, and how much difference in chemical composition exists between mature normal wood and juvenile normal wood.

7.3 Experimental

7.3.1 Materials

A thirty-five-year-old loblolly pine (*Pinus taeda*), harvested in May 2004 from Orange County, North Carolina, USA, was used in this study. The loblolly pine was about 20 m in height, with a significant bend in the stem at about 6 m from the ground. Three wood sections were sampled from the tree, at 0.5 m (bottom), 6 m (middle), and above 18 m (top). They were further separated into 7 groups according to the position and year ring

in the tree; Bottom Juvenile Normal wood (BJN), Bottom Mature Normal wood (BMN), Middle Juvenile Compression wood (MJC), Middle Mature Compression wood (MMC), Middle Juvenile Opposite wood (MJO), Middle Mature Opposite wood (MMO), and Top Juvenile Normal wood (TJN).

To avoid the possible contamination of colored-heartwood into the bottom juvenile normal wood (BJN), all juvenile wood was sampled from rings 5-8, while the mature wood was sampled from rings 19-27. The compression wood content within the three wood sections was determined visually from the distinctively red appearance (Figure 7.1) and estimated to be about 5% by volume in the bottom, 50% by volume in the middle, and 20% by volume in the top section. The wood blocks were chipped and subsequently ground using a Wiley Mill (standard model #3) into wood meals to pass a 40-mesh screen (250-425 μm). Wood extractives were removed according to TAPPI standard T264 om-88 by ethanol/benzene (1/2, v/v) for 24 hours followed by ethanol for 24 hours.

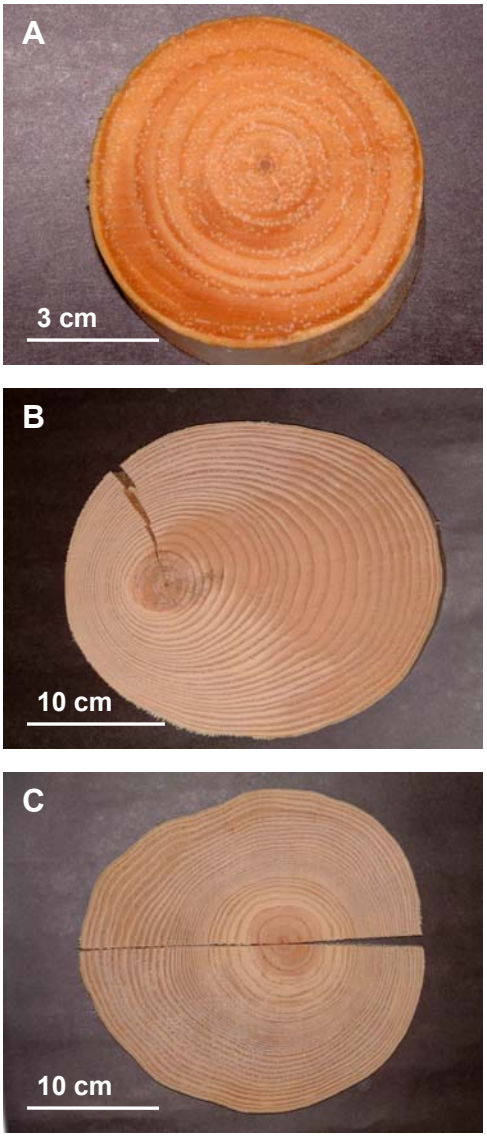

Figure 7.1 Compression wood distribution within three different sections: (A) top; (B) middle; (C) bottom.

Cellulolytic enzyme lignin (CEL) was prepared according to the method of Chang et al. [13]. The extractive-free wood meal was milled in a planetary micro mill (Pulverisette 7, Fritsch, Germany). The finely ground wood meals were enzyme-treated (FibreZyme ACL, Dyadic International, Inc., Florida, USA) at 45 ºC, pH = 4.5 (acetate buffer), for 3 days, freeze-dried and subsequently extracted for 5-days with dioxane/water (96%, v/v). The crude CELs were purified as per Björkman [14]. The yields of purified CEL were approximately 30% based on the total lignin, and the carbohydrate contents are about 6% with pooled standard deviation of 0.28%. Acetylation of the CELs was performed according to Adler [15].

7.3.2 Lignin Content Determination and Fiber Quality Analysis

The total lignin content was determined by the modified Klason lignin method [16,17], combining both the Klason lignin and acid soluble lignin (extinction coefficient used was 110 L g^{-1} cm^{-1}). Holocellulose was isolated from microtome (Reichert-Jung, Austria) sectioned (200 μm) wood wafers as per Yokoyama et al. [18]. The holocellulose was used to determine fiber length, width, coarseness, kink, and curl indexes using a Fiber Quality Analyzer (FQA, Op Test Equipment, Inc., Hawkesbury, ON).

7.3.3 Wide-Angle X-Ray Diffraction (WAXD)

Wide-angle X-ray diffraction profiles were recorded on a Bruker D8 Discover X-ray diffractometer equipped with an area-array detector. All scans were collected at 40 kV and 20 mA in the range of $4^o < 2\theta < 40^o$ using $Cu_{K\alpha}$ radiation. For each sample, 1mm

wood sections were stacked together, such that an average value was obtained for early and late wood. Plots of intensity vs. 2θ were corrected for incoherent scattering [19] and then the fraction of crystallinity was calculated using the method of Vonk [20]. The 002 and 040 peaks from the corrected 2θ plots were used to calculate the transverse and longitudinal crystallite dimensions from the Scherrer equation [19,21]. Microfibril angle was calculated from plots of intensity vs. azimuthal angle for the 040 peak using a method published by Lotfy et al. [22].

7.3.4 Monomeric Carbohydrate Determination

The monomeric sugar analysis was carried out using alditol acetate method according to the procedures of Coimbra et al. [23].

7.3.5 Nitrobenzene Oxidation and Ozonation

Nitrobenzene oxidation was performed as previously reported [24]. The stereochemistry (*erythro* and *threo* forms) of the arylglycerol-β-aryl ether linkages of the lignin was determined by ozonation analysis according to the method of Akiyama et al. [25].

7.3.6 Quantitative ^{13}C-NMR Spectroscopy

All NMR spectra were recorded on a Bruker AVANCE 300MHz spectrometer at 300K using DMSO-d_6 as the solvent. The concentration of lignin was about 20%, and chromium(III) acetylacetonate (0.01M) was added to the lignin solution as the relaxation agent. A total of 20,000 scans were collected. A 90º pulse width, 1.2s acquisition time and 1.7s relaxation delay were used [26]. Both acetylated and non-acetylated CELs were

examined as per Capanema et al [26]. The peak assignments and calculations were according to the works of Capanema et al. [26] and Balakshin et al. [27], and the references therein.

7.3.7 Statistical Analysis

The multiple comparisons of different properties between different groups were tested by *Tukey* HSD test at α=0.05 using SAS JMP (Version 5.1, SAS Institute Inc, USA).

7.4 Results and Discussion

7.4.1 Differences in Fiber Properties

The fiber quality analyses (Figure 7.2) reveal that the fiber lengths of the juvenile wood samples are significantly shorter than those of mature wood samples, while there is no difference between the juvenile compression wood and mature compression wood (Figure 7.2A). Mature wood tends to have a smaller fiber width than juvenile wood; however juvenile compression wood is thinner than mature compression wood. The fiber length of juvenile normal wood from the top of the tree is shorter than that from the bottom of the tree, with the fiber width showing a similar tendency. These results are in contrast those previously reported [11,28] wherein longer fiber lengths were reported for the top of the tree; however, this might be due to variations in sampling.

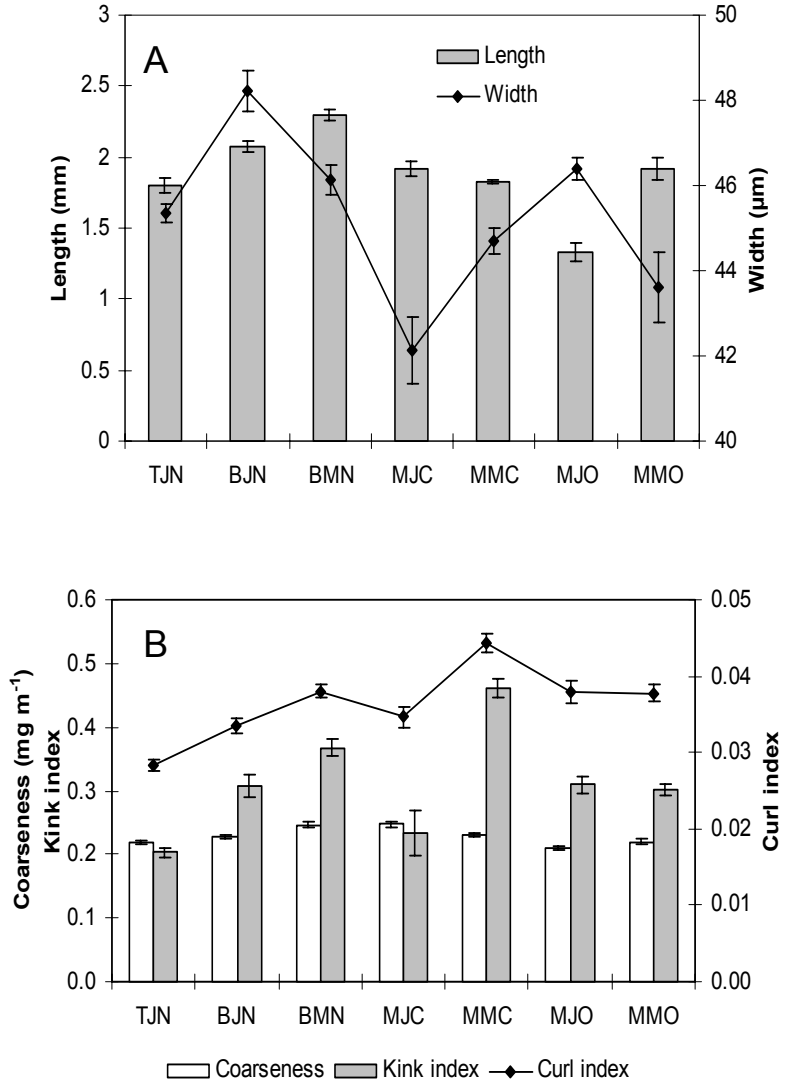

Figure 7.2 Fiber quality analysis of different groups: (A) length weighted fiber length and fiber width; (B) coarseness, kink and curl index; (TJN) top juvenile normal wood; (BJN) bottom juvenile normal wood; (BMN) bottom mature normal wood; (MJC) middle juvenile compression wood; (MMC) middle mature compression wood; (MJO) middle juvenile opposite wood; (MMO) middle mature opposite wood.

It has been suggested that fiber length increases from the base of the tree upward, maximizing at a certain height, then reducing towards the top of the tree [12,28].

Therefore, the fiber length of the samples collected from the top of the tree could be either longer or shorter than that at the base of the tree depending on where the top sample is collected. As our samples were collected within 2 meters from the top of the tree, it is reasonable to observe shorter fiber lengths than those sampled from the base of the tree.

By contrast, the differences in fiber coarseness (Figure 7.2B) are not as significant between groups. However, juvenile compression wood has higher coarseness than juvenile normal wood from either the top or base of the tree; this is consistent with our previous findings [7]. The higher coarseness values accompanied by the smaller cell width clearly indicate that the juvenile compression wood has a much thicker cell wall than the corresponding juvenile normal wood [7]. Bottom mature normal wood has a slightly higher coarseness than the bottom juvenile normal wood, apparently due to the thinner cell wall of juvenile wood as compared to that of mature wood [29].

Juvenile normal wood from the top of the tree has lower curl and kink indices than that from the bottom of the tree (Figure 7.2B); i. e. juvenile normal wood fibers from the bottom of the tree tend to curl more than those from the top of the tree. The average curl and kink index values of mature normal wood from the bottom of the tree are apparently higher than those of the corresponding juvenile normal wood, however, there is no statistical difference due to the large standard error associated with the samples. The most significant difference can be seen for the compression wood samples. The mature compression wood fibers from the middle of the tree have substantially higher curl and kink indices than the corresponding juvenile compression wood.

Microfibril angle (MFA) analysis of the different wood sections (Figure 7.3A) revealed that the MFA of the juvenile normal wood from the bottom of the tree is higher than that from the top of the tree. Compression wood samples have substantially higher MFA values than any of the juvenile wood samples. However, the juvenile wood samples have a larger MFA than the corresponding mature wood samples. These results are consistent with those of other researchers obtained from different conifer species [8-10,12,28,30].

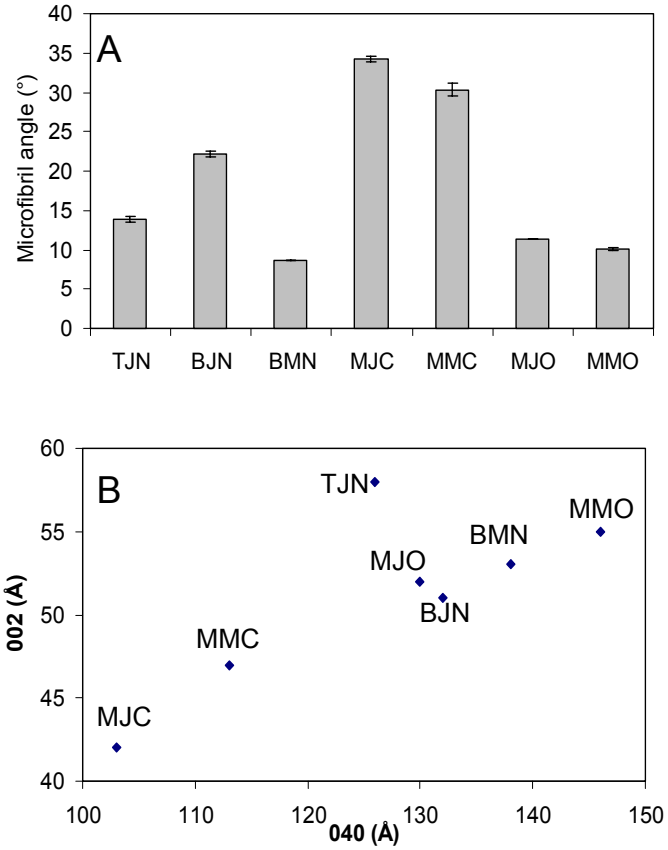

Figure 7.3 Microfibril angles (A) and cellulose crystallite dimensions (B) of different groups by X-ray diffraction: (TJN) top juvenile normal wood; (BJN) bottom juvenile normal wood; (BMN) bottom mature normal wood; (MJC) middle juvenile compression wood; (MMC) middle mature compression wood; (MJO) middle juvenile opposite wood; (MMO) middle mature opposite wood.

Figure 7.3B shows the variation of cellulose crystallite dimension between the different groups. Accordingly, juvenile normal wood from the top of the tree has slightly thicker (larger dimension in 002 plane) but shorter (smaller dimension in 040 plane) crystallite size as compared to juvenile normal wood from the bottom of the tree. As expected, compression wood samples show smaller crystallite dimensions than juvenile or mature wood samples [10,21], and mature wood samples show larger dimensions than the corresponding juvenile wood samples.

7.4.2 Basic Chemical Properties

The basic chemical properties of the various wood samples are listed in Table 7.1. The amount of benzene alcohol extractives in the juvenile wood from the top of the tree (5.1%) is higher than that from the bottom (3.3%) of the tree. This may be due to the fact that the living moiety (the cambial part) on the top of a tree is higher. Thus, the amount of primary extractives (containing compounds relevant to the metabolism) is also higher. Comparison of juvenile normal wood from the bottom of the tree with the corresponding mature normal wood reveals higher extractives content in the inner juvenile normal wood, 3.3% vs 2.5% respectively, and this is likely due to heartwood formation. Heartwood formation is associated with the accumulation of polyphenolic compounds [31]. Mature compression wood contains slightly more extractives than juvenile compression wood, 3.3% vs 2.7%, whereas no difference in extractives content was determined between the respective opposite wood (3.1% and 3.4%). Comparison of the extractives contents in Table 7.1, reveals that the dark color of the compression wood tissues cannot be explained by the extractive yield.

Table 7.1 Basic chemical constituents between different wood samples.

%	TJN	BJN	BMN	MJC	MMC	MJO	MMO	Pooled Std
Extractives[*]	5.1	3.3	2.5	2.7	3.3	3.4	3.1	0.05
Lignin[#]	29.6	28.5	27.4	37.5	37.4	28.6	28.4	0.17
Arabinose[$]	2.4	1.9	1.7	1.8	1.9	1.9	1.7	0.05
Xylose[$]	11.7	10.0	9.3	12.5	12.0	10.7	8.5	0.07
Mannose[$]	17.2	19.5	20.6	10.6	11.6	17.4	19.2	0.24
Galactose[$]	2.7	2.3	2.1	15.3	12.8	2.9	2.2	0.07
Glucose[$]	66.0	66.3	66.3	59.7	61.6	67.0	68.4	0.32

[*]: % based on OD wood weight.
[#]: % based on extractive-free, OD wood weight.
[$]: % based on total carbohydrates.
Abbreviations: (TJN) top juvenile normal wood; (BJN) bottom juvenile normal wood; (BMN) bottom mature normal wood; (MJC) middle juvenile compression wood; (MMC) middle mature compression wood; (MJO) middle juvenile opposite wood; (MMO) middle mature opposite wood.

Juvenile and mature compression wood contains significantly higher amounts of lignin (about 37.5%, Table 7.1). The lignin content of juvenile wood from the top of the tree (29.6%) is higher than that of from the bottom of the tree (28.5%), and in turn higher than that of the corresponding mature wood (27.4%). However, the maximum lignin content difference between mature wood and juvenile wood is only about 2%. No difference in lignin content was found between the juvenile opposite wood and middle mature opposite wood samples, all about 28.5%.

In a previous study on genetic variations of fourteen full-sib families, very little genetic variation was found among families, whereas large within familiy variations were found for all families [1]. Since all juvenile wood contains various amounts of compression wood, it is likely that the large within-family variations in lignin content

may be caused by variations in compression wood content within each increment core sample. This also points to the need for a rapid quantification of compression wood content in each increment core sample in micro-analytical protocols. This topic is being investigated in our laboratory.

The major difference in sugar content is between compression wood and normal wood (Table 7.1), that is compression wood contains more galactose and less glucose and mannose as compared to both juvenile and mature normal wood. The abundance of galactose in compression wood is representative of galactan [32-34]. The ratio of galactose/glucose has been used as an indicator for compression wood detection [35,36]. Both juvenile compression wood and mature compression wood show high galactose/glucose ratios in the range of 0.21~0.26, whereas these ratios of other normal wood or opposite wood (both juvenile and mature) are only about 0.03~0.04. However, the galactose/mannose ratios in normal and opposite wood are in the range of 0.10~0.17, whereas the ratios in compression wood are 1.11~1.14. Accordingly, this index is more sensitive as galactose/glucose ratio. Hence, galactose/mannose ratio is a better indicator for detecting the existence of compression wood.

Slightly lower glucose and mannose and higher galactose, xylose and arabinose are detected in juvenile normal wood from the top than from the bottom (Table 7.1). Comparison of juvenile normal wood from the bottom with the corresponding mature normal wood reveals only subtle differences. The former has approximately the same glucose content as the mature wood (Table 7.1), slightly lower mannose contents, and slightly higher galactose, arabinose and xylose contents. Although some of these

differences are small, a general trend is evident, and seems to indicate that the juvenile character is more pronounced of a normal wood from the top than that from the bottom.

7.4.3 Lignin structure differences

Nitrobenzene oxidation yields oxidation products from uncondensed lignin structures [24,37], and as a result, the yields of nitrobenzene oxidation products not only indicate the compositions of lignin types (H-, G-, and S-type), but can also be a relative indicator of the condensation degree. The corresponding results are presented in Figure 7.4. Both juvenile compression wood and mature compression wood have lower total yields of oxidation products and higher amounts of *p*-hydroxybenzaldehyde (H-type lignin) in total oxidation products when compared to the other wood, however the difference between them is small. The degree of condensation in compression wood is apparently higher than normal and opposite wood. There are no significant differences between the juvenile normal wood from the top (TJN) and the bottom (BJN). The mature wood from the bottom (BMN) has about 1% higher yield in nitrobenzene oxidation products than the corresponding juvenile wood (BJN), however the difference is statistically not significant. The vanillin yield from the mature opposite wood (MMO) is about 1.7% lower than that from the juvenile opposite wood (MJO). This may support the hypothesis that the lignin of mature opposite wood (MMO) is slightly more condensed than that of juvenile opposite wood (MJO).

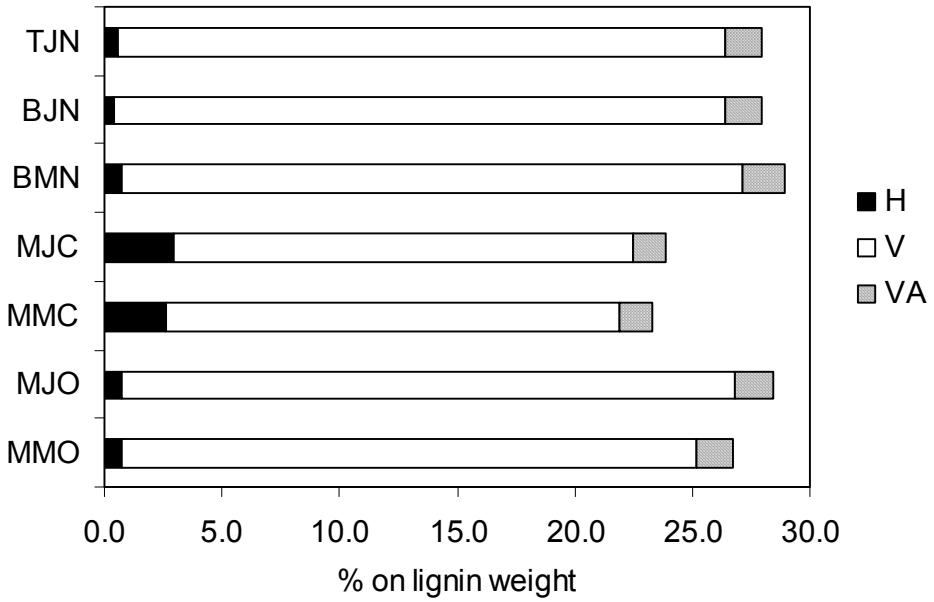

Figure 7.4 Nitrobenzene oxidation products between different groups: (H) *p*-hydroxybenzaldehyde; (V) vanillin; (VA) vanillic acid; (TJN) top juvenile normal wood; (BJN) bottom juvenile normal wood; (BMN) bottom mature normal wood; (MJC) middle juvenile compression wood; (MMC) middle mature compression wood; (MJO) middle juvenile opposite wood; (MMO) middle mature opposite wood.

Ozonation is a quantitative tool used to analyze the stereochemistry, *erythro* (E) and *threo* (T) isomers, and yields of β-O-4 linkages [25]. Generally, the ratio of *erythro* and *threo* forms in gymnosperms is about 1.0 [38-41]. Our previous work [7] has demonstrated that juvenile compression wood has a higher E/T ratio (~1.23) and less β-O-4 linkages (E+T) compared to juvenile normal wood. The results of ozonation are illustrated in Figure 7.5. As expected, the compression wood samples, both juvenile (MJC) and mature (MMC) compression wood, show higher E/T ratios and lower β-O-4 yields compared to the other wood specimens. The decrease in β-O-4 linkages in

compression wood lignin actually results more from the decrease in the *threo* isomer (T) than in the *erythro* isomer (E), which is consistent with our previous results [7].

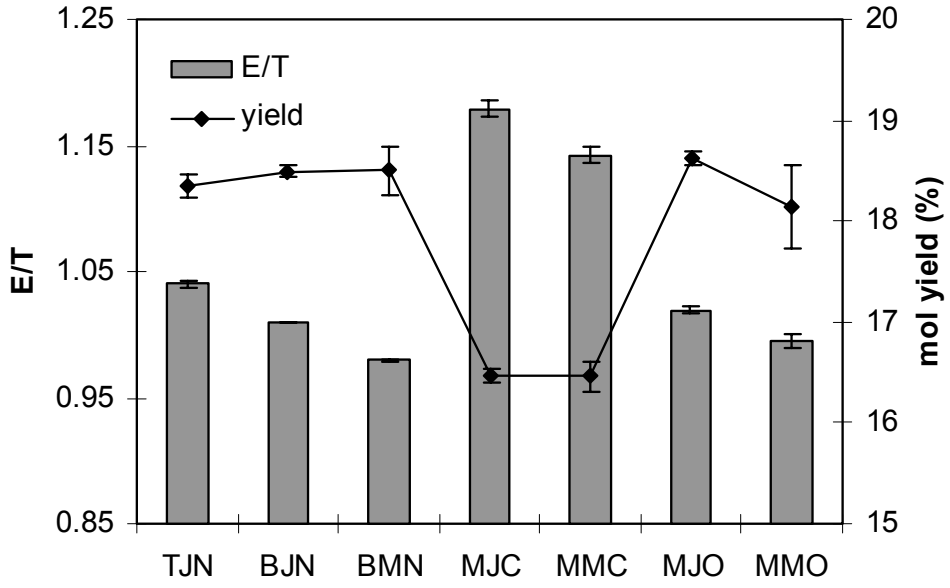

Figure 7.5 E/T ratios and total yield (E+T) of different wood samples, assuming that the molecular weight of a phenylpropanoid unit is 180: (TJN) top juvenile normal wood; (BJN) bottom juvenile normal wood; (BMN) bottom mature normal wood; (MJC) middle juvenile compression wood; (MMC) middle mature compression wood; (MJO) middle juvenile opposite wood; (MMO) middle mature opposite wood.

Slightly more E isomer is found in the juvenile normal (TJN) wood from the top than in that from the bottom (BJN). These values are slightly higher than that from the corresponding mature normal wood (BMN). The E/T ratios of these samples (TJN, BJN, BMN) as well as the opposite wood (MJO, MMO) samples are all around one. However, a general trend of slightly more E isomer in juvenile wood are perceptible as compared to mature wood. However, no significant differences in β-O-4 yields were detected between juvenile normal and mature normal wood.

To further characterize differences between the various wood specimens cellulolytic enzyme lignin (CEL) was isolated, purified and studied by ^{13}C NMR. The ^{13}C NMR spectra of different CELs (exclude opposite wood CELs) are shown in Figure 7.6, the major differences being between normal wood and compression wood CELs (Figure 7.6A, 160-155ppm). The structure differences of these CELs were further estimated by the equations according to Capanema et al. (2004) and Balakshin et al. (2005). Table 7.2 summarizes the major differences in functional groups and inter-unit linkages of CELs. The difference between juvenile normal wood from the top and juvenile normal wood from the bottom was very little, as was the difference between the corresponding mature normal wood. As expected, the compression wood samples had higher amount of H-units (*p*-coumaryl units) and etherified 5-5' moieties, and lower methoxyl groups than the normal or opposite wood samples. The main contribution to the high H-unit in compression wood CEL is from non-conjugated H-units (159-156 ppm), which is in agreement with our previous findings (Yeh et al. 2005). However, the amounts of H units and methoxyl contents for the compression wood CELs do not well match as compared to that of normal wood or opposite wood. This might be due to that not all H-units in compression wood CEL were shown in the NMR region estimated (162-156 ppm), and therefore further model compound experiment will be needed to confirm this. The juvenile compression wood CEL and the mature compression wood CEL are quite similar in structure, and the main difference being a slightly higher amount of total OH content in the mature compression wood.

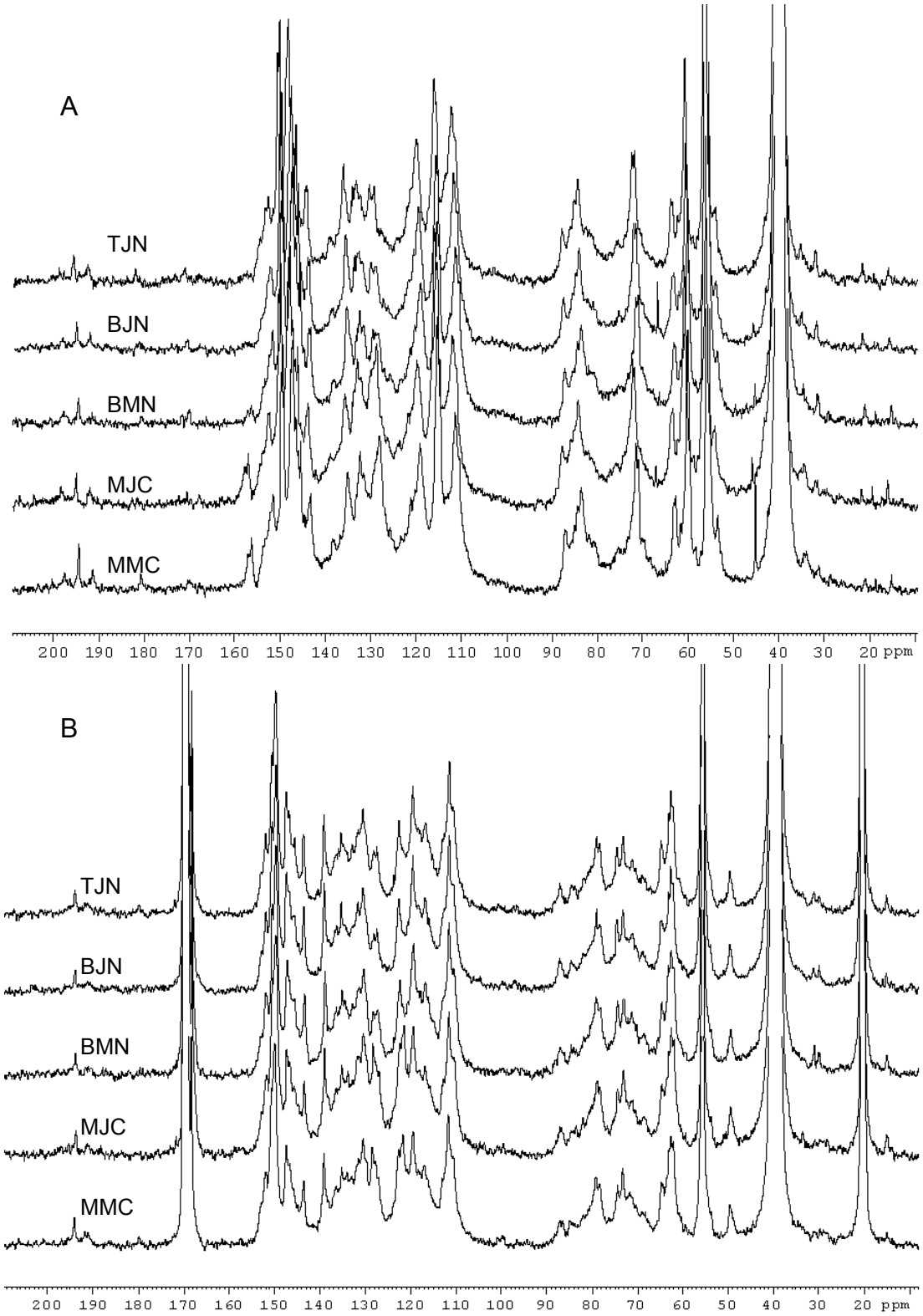

Figure 7.6 Quantitative ^{13}C NMR spectra of different CELs: (A) non-acetylated CELs; (B) Acetylated CELs; (TJN) top juvenile normal wood; (BJN) bottom juvenile normal wood; (BMN) bottom mature normal wood; (MJC) middle juvenile compression wood; (MMC) middle mature compression wood.

Table 7.2 Major differences of functional groups and inter-unit linkages between different CELs[#].

Structures	TJN	BJN	BMN	MJC	MMC	MJO	MMO
Total H units	0.04	0.04	0.05	0.14	0.14	0.05	0.05
Conjugated	0.01	0.01	0.01	0.02	0.02	0.01	0.01
Non-conjugated	0.03	0.03	0.04	0.12	0.12	0.04	0.04
Methoxyl	0.95	0.95	0.93	0.78	0.75	0.91	0.92
Total OH	1.46	1.48	1.46	1.44	1.54	1.40	1.48
Phenolic OH	0.28	0.30	0.28	0.27	0.29	0.26	0.28
Aliphatic OH	1.18	1.18	1.18	1.17	1.25	1.14	1.20
Etherifed 5-5’	0.10	0.11	0.09	0.15	0.14	0.11	0.12

[#]: The numbers are expressed as per aromatic ring.
Abbreviations: (TJN) top juvenile normal wood; (BJN) bottom juvenile normal wood; (BMN) bottom mature normal wood; (MJC) middle juvenile compression wood; (MMC) middle mature compression wood; (MJO) middle juvenile opposite wood; (MMO) middle mature opposite wood.

Since the purified CELs contain about 6% carbohydrates, sugar analyses were performed on the CELs to study the sugar composition in the lignin-carbohydrate complexes (LCC). As some of the LCC are lost during the purification processes, the LCC in the purified CEL is better defined as “CEL LCC”. The sugar compositions of the purified CELs are listed in Table 7.3. No significant differences were observed between the corresponding pairs in our targeted comparisons. However, the CEL LCC in the compression wood CELs shows higher galactose content and lower mannose content than the normal or opposite wood CELs. This is consistent with previously published work [42-44] wherein higher galactose contents were reported in compression wood LCC, in

which the 1→4 linked galactan bind to lignin almost exclusively at the C-6 position [43,44].

Table 7.3 Carbohydrate composition of purified cellulolytic enzyme lignin from different groups.

% in carbohydrates	TJN	BJN	BMN	MJC	MMC	MJO	MMO
Arabinose	3.8	3.3	3.5	3.9	3.5	3.5	5.2
Xylose	14.4	11.3	12.6	16.5	15.5	17.2	14.8
Mannose	30.2	33.1	35.6	24.5	25.5	32.2	35.9
Galactose	4.2	3.1	3.5	7.4	9.8	4.9	1.4
Glucose	47.4	49.2	44.9	47.6	45.6	42.1	42.7

Abbreviations: (TJN) top juvenile normal wood; (BJN) bottom juvenile normal wood; (BMN) bottom mature normal wood; (MJC) middle juvenile compression wood; (MMC) middle mature compression wood; (MJO) middle juvenile opposite wood; (MMO) middle mature opposite wood.

7.5 Conclusion

In an effort to comprehensively understand the within-tree variation between juvenile wood, compression wood, and mature wood, a mature bent loblolly pine was sampled and separated into seven groups. The morphological analyses demonstrate that juvenile normal wood from the top of the tree shows different fiber properties compared to the juvenile normal wood from the bottom of the tree. Similarly, juvenile compression wood was distinctly different from mature compression wood. Fiber property differences were also found between juvenile normal wood and mature normal wood. Differences in chemical structure between the various wood specimens are less significant. The majority of the differences in the final wood related products are due to the fiber quality.

7.6 References

[1] Sykes, R.F.; Isik, F.; Li, B.; Kadla, J.F.; Chang, H.M. Genetic variation of juvenile wood properties in a loblolly pine progeny test. *TAPPI J.* **2003**, *2*, 3-8.

[2] Zobel, B.J.; van Buijtenen, J.P. *Wood Variation: Its Causes and Control*; Springer-Verlag: Berlin, 1989.

[3] Hatton, J.V.; Hunt, K. Wood density and chemical properties of second-growth lodgepole pine. *Pulp Pap. Canada* **1993**, *94*, 140-141.

[4] Wilkes, J. Review of the significance of variations in wood structure in the utilization of *Pinus radiata*. *Aust. For. Res.* **1987**, *17*, 215-232.

[5] Timell, T.E. *Compression Wood in Gymnosperms*,Vol.I; Springer-Verlag: Berlin, 1986.

[6] Zobel, B.J. Wood quality from fast-grown plantation. *TAPPI J.* **1981**, *64*, 71-74.

[7] Yeh, T.F.; Braun, J.L.; Goldfarb, B.; Chang, H.M.; Peszlen, I.; Kadla, J.F. Comparison of morphological and chemical properties between juvenile wood and compression wood of loblolly pine. *Holzforschung* **2005**, *59*.

[8] Kretschmann, D.F.; Alden, H.A.; Verrill, S. Variations of microfibril angle in loblolly pine: comparison of iodine crystallization and X-ray diffraction techniques. In *Microfibril angle in wood*; B.G. Butterfield, Ed.; International Association of Wood Anatomists, International Union of Forestry Research Organizations: Christchurch, 1998; pp 157-176.

[9] Donaldson, L.A. Within-and between-tree variation in microfibril angle in *Pinus radiata*. *New Zeal. J. For. Sci.* **1992**, *22*, 77-86.

[10] Marton, R.; Rushton, P.; Sacco, J.S.; Sumiya, K. Dimensions and ultrastructure in growing fibers. *TAPPI J.* **1972**, *55*, 1499-1504.

[11] Zobel, B.J. Using the juvenile wood concept in the southern pines. *South. Pulp Paper Mfg.* **1975**, 14-16.

[12] Zhu, J.; Tadooka, N.; Takata, K. Growth and wood quality of sugi (*Cryptomeria japonica*) planted in Akita prefecture (II). juvenile/mature wood determination of aged trees. *J. Wood Sci.* **2005**, *51*, 95-101.

[13] Chang, H.M.; Cowling, E.B.; Brown, W. Comparative studies on cellulolytic enzyme lignin and milled wood lignin of sweetgum and spruce. *Holzforschung* **1975**, *29*, 153-159.

[14] Bjorkman, A. Studies on finely divided wood. Part I. extractions of lignin with neutral solvents. *Svensk Papperstid.* **1956**, *59*, 477-485.

[15] Adler, E.; Brunow, G.; Lundquist, K. Investigation of the acid-catalysed alkylation of lignins by means of NMR spectroscopic methods. *Holzforschung* **1987**, *41*, 199-207.

[16] Dence, C.W. The determination of lignin. In *Methods in Lignin Chemistry*; S.Y. Lin and C.W. Dence, Eds.; Springer-Verlag: Berlin/New York, 1992; pp 34-35.

[17] Yeh, T.F.; Yamada, T.; Capanema, E.; Chang, H.M.; Chiang, V.; Kadla, J.F. Rapid screening of wood chemical component variations using transmittance near infrared spectroscopy. *J. Agric. Food Chem.* **2005**, 3328-3332.

[18] Yokoyama, T.; Kadla, J.F.; Chang, H.M. Microanalytical method for the characterization of fiber components and morphology of woody plants. *J. Agric. Food Chem.* **2002**, *50*, 1040-1044.
[19] Krassig, H.A. Cellulose: Structure, Accessibility, and Reactivity. Gordon and Breach Science: Switzerland, 1993; pp 91-92.
[20] Vonk, C.G. Computerization of Ruland's X-ray method for determination of the crystallinity in polymers. *J. Appl. Cryst.* **1973**, *6*, 148-152.
[21] Tanaka, F.; Koshijima, T.; Okuyama, T. Characterization of cellulose in compression wood and opposite woods of a *Pinus densiflora* tree grown under the influence of strong wind. *Wood Sci. Technol.* **1981**, *15*, 265-273.
[22] Lotfy, M.; El-Osta, M.; Kellogg, R.M.; Foschi, R.O.; Butters, R.G. A direct x-ray technique for measuring microfibril angle. *Wood Fiber Sci.* **1973**, *5*, 118-128.
[23] Coimbra, M.A.; Delgadillo, I.; Waldron, K.W.; Selvendran, R. Isolation and analysis of cell wall polymers from olive pulp. In *Modern Methods of Plant Analysis*; H.F. Linskens and J.F. Jackson, Eds.; Springer-Verlag: Berlin, 1996; pp 33-44.
[24] Chen, C.L. Nitrobenzene and cupric oxide oxidation. In *Methods in Lignin Chemistry*; S.Y. Lin and C.W. Dence, Eds.; Springer-Verlag: Berlin, 1992; pp 301-321.
[25] Akiyama, T.; Sugimoto, T.; Matsumoto, Y.; Meshitsuka, G. Erythro/threo ratio of β-O-4 structures as an important structural characteristic of lignin. I: Improvement of ozonation method for the quantitative analysis of lignin side-chain structure. *J. Wood Sci.* **2002**, *48*, 210-215.
[26] Capanema, E.A.; Balakshin, M.Y.; Kadla, J.F. A comprehensive approach for quantitative lignin characterization by NMR spectroscopy. *J. Agric. Food Chem.* **2004**, *52*, 1850-1860.
[27] Balakshin, M.Y.; Capanema, E.; Goldfarb, B.; Frampton, J.; Kadla, J.F. NMR studies on Fraser fir *Abies fraseri* (Pursh) Poir. lignins. *Holzforschung* **2005**, *59*, 488-496.
[28] Megraw, R.A. *Wood Qualitiy Factors in Loblolly Pine*; TAPPI Press: Atlanta, GA, USA, 1985.
[29] Zobel, B.J. The changing quality of the world wood supply. *Wood Sci. Technol.* **1984**, *18*, 1-17.
[30] Sahlberg, U.; Salmen, L.; Oscarsson, A. The fibrillar orientation in the S2-layer of wood fibres as determined by X-ray diffraction analysis. *Wood Sci. Technol.* **1997**, *31*, 77-86.
[31] Plomion, C.; Leprovost, G.; Stokes, A. Wood formation in trees. *Plant Physiol.* **2001**, *127*, 1513-1523.
[32] Jiang, K.-S.; Timell, T.E. Polysaccharides in compression wood of tamarack (*Larix laricina*). *Svensk Papperstid.* **1972**, *75*, 592-594.
[33] Schreuder, H.R.; Cote, W.A.; Timell, T.E. Studies on compression wood. Part 3. Isolation and characterization of a galactan from compression wood of red spruce. *Svensk Papperstid.* **1966**, *69*, 641-657.
[34] Bouveng, H.; Meier, H. Studies on a galactan from norwegian spruce compression wood (*Picea abies* Karst.). *Acta Chem. Scand.* **1959**, *13*, 1884-1889.
[35] Nanayakkara, B.; Manley-Harris, M.; Suckling, I.D.; Donaldson, L.A. Chemical characterization of compression wood in *Pinus radiata*. *13th International*

Symposium on Wood, Fibre and Pulping Chemistry (13th ISWFPC), Auckland, New Zealand; Appita Inc.; Vol. 2, pp 585-592.

[36] Newman, R.H.; Hemmingson, J.A.; Butterfield, B.G. A micro-analytical approach to the carbohydrate chemistry of compression wood. *13th International Symposium on Wood, Fibre and Pulping Chemistry (13th ISWFPC), Auckland, New Zealand*; Appita Inc.; Vol. 2, pp 593-596.

[37] Chang, H.M.; Allan, G.G. Oxidation. In *Lignin: Occurrence, Formation, Structure and Reactions*; K.V. Sarkanen and C.H. Ludwig, Eds.; Wiley-Interscience: New York, 1971; pp 433-485.

[38] Akiyama, T.; Goto, H.; Nawawi, D.S.; Syafii, W.; Matsumoto, Y.; Meshitsuka, G. *Erythro/threo* ratio of β-O-4-structures as an important structural characteristic of lignin. Part 4: variation in the *erythro/threo* ratio in softwood and hardwood lignins and its relation to syringyl/guaiacyl ratio. *Holzforschung* **2005**, *59*, 276-281.

[39] Akiyama, T.; Matsumoto, Y.; Okuyama, T.; Meshitsuka, G. Ratio of *erythro* and *threo* form of β-O-4 structures in tension wood lignin. *Phytochem.* **2003**, *64*, 1157-1162.

[40] Matsumoto, Y.; Ishizu, A.; Nakano, J. Studies of chemical structure of lignin by ozonation. *Holzforschung* **1986**, *40*, 81-85.

[41] Lundquist, K. NMR studies of lignins. 4. Investigation of spruce lignin by ^{1}H NMR spectroscopy. *Acta Chem. Scand. Ser. B* **1980**, *34*, 21-26.

[42] Obst, J.R. Frequency and alkali resistance of lignin-carbohydrate bonds in wood. *TAPPI J.* **1982**, *65*, 109-112.

[43] Minor, J.L. Chemical linkage of pine polysaccharides to lignin. *J. Wood Chem. Technol.* **1982**, *2*, 1-16.

[44] Mukoyoshi, S.; Azuma, J.; Koshijima, T. Lignin-carbohydrate complexes from compression wood of *Pinus densiflora* Sieb et. Zucc. *Holzforschung* **1981**, *35*, 233-240.

8. FUTURE WORK

Method developments of transmittance NIR (Chapter 3 and Chapter 4) showed that successful wood chemical property screening could be made with minimum amounts of samples. However, the distribution of juvenile wood within a tree is not uniform with tree height (see Figure 1.7), and the property of juvenile wood within any cross-section is not consistent with year ring, either (see Figure 1.8). Evaluating a tree's property by using only one increment core will fail to objectively reflect the true property of that tree. A better sampling procedure within a tree should be developed. Questions, such as where to sample, how many cores to take, and from which year ring to measure, should be carefully addressed before applying the transmittance NIR technique to select the elite tree for future breeding.

Future development of the transmittance NIR model should also include important fiber qualities, such as microfibril angle and crystallinity. An intact measurement using wood blocks, both in transmittance NIR analysis and X-ray diffraction, would provide a rapid and accurate assessment of fiber quality. Transmittance NIR should also be applied to evaluate intact wood properties, such as wood density, module of elasticity (MOE), and module of rupture (MOR), which are critical for solid wood product utilization.

Wood variation studies showed that the results obtained from trees grown in growth chambers (Chapter 5 and Chapter 6) are consistent with that from nature stand (Chapter 7). They both showed that juvenile wood is significantly different from compression wood, and hence, trees grown in growth chamber can be used as a experimental model for future research in wood chemistry. Results from juvenile and mature wood comparison (Chapter 7) further showed that juvenile wood differ more from compression

wood than from mature wood. However, in our juvenile wood analysis, in order to avoid the possible contamination from heartwood (ring 1-4), our juvenile wood samples were actually taken from ring 5-8, which was approximately in the boundary between juvenile and mature wood (see Figure 1.8). To gain a more precise estimation of the difference between juvenile and mature wood, further research should include the ring-by-ring analysis using a mature tree devoid of heartwood, and analyze the wood sample from the year ring close to pith.

Any loblolly pine tree, either produced from growth chamber (Chapter 5) or from natural stand (Chapter 7), all juvenile wood contains various amounts of compression wood. These embedded compression wood tissues will affect the analysis of juvenile wood. Currently, wood property assessments of tree-breeding project heavily rely on analyses of increment core samples. Erroneous results from the compression wood contamination within cores might fail to select the elite trees successfully. Hence future research should also develop a methodology to assess the percentages of compression wood within increment cores.

Metabolic profiling coupled with PCA analysis could separate juvenile normal wood and juvenile compression wood into different phenotypic clusters based on the differences of metabolite level identified from GC and GC/MS (Chapter 6). However, as stated in Section 1.5.4, HPLC/MS based profiling can identify higher molecular weight and thermallabile compounds that cannot be detected by using current GC/MS protocol. Therefore, future work of metabolic profiling should also include the development of HPLC/MS based metabolic profiling technique to identify and quantify more metabolites. Combining both GC/MS and HPLC/MS profiling results would provide thoroughly

biochemical information of tree metabolism in response to any biological event or environmental stimulation.

9. APPENDIX

9.1 Ozonation

The procedures for ozonation are according to Akiyama et al. [1,2]. 50 mg (OD) of extractive-free wood meals with particle size smaller than 80 mesh are suspended in 30 ml of ozonation solvent, acetic acid/water/methanol (80/15/5, v/v/v). Oxygen containing ca. 3% ozone (ozone generator, model T-816, Polymetrics, Inc., San Jose, CA) was bubbled into the solution with stirring at the rate of 0.5 l min^{-1} for 2 h at 0°C. After 2-h, the residual ozone was removed by continuous oxygen bubbling for about 15 min. The reaction mixture was further reduced with 300µl of 0.1M sodium thiosulfate (reductive posttreatment) [2].

The reaction solvent of the mixtures was evaporated using a rotavapor (R-114, Buchi) at 40°C. The residual acetic acid was removed by rotavaporation with water. The ozonation products were saponified with 0.1 M NaOH (20 ml) at room temperature and left over night. One milliliter of 5mM erythritol was added as an internal standard. The solution was then passed through a column filled with ca. 10 ml of cation-exchange resin (Dowex-50W-X8, NH_4^+ form), and the column was washed with water until the pH of eluent was 7-8, resulting a total volume of 100 ml. 2 ml from this eluent was dried by rotavapor at 40°C.

The dried product was silylated in 300 µl of dimethylsulfoxide (DMSO, Aldrich), with 200 µl of hexamethyldisilazane (HMDS, Aldrich), and 100 µl of trimethylchlorosilane (TMCS, Aldrich) at 60°C for 30 min. The reaction phase separates and the upper phase was used for GC analysis.

Quantitative gas chromatography (GC) analysis was carried out on a HP 6890 GC equipped with a flame ionization detector and HP-1 column (30m × 0.32mm × 0.25μm). The injection temperature was 250°C, the detector temperature was 280°C, and the column flow was 2 ml helium/min. The column was held for 5 min at 120°C, increased to 170°C at 4°C/min, then at 10°C/min to 280°C, and kept isothermal at 280°C for 5 min. A typical GC chromatogram is showed in Figure 9.1, and the GC calibration lines of the erythronic acid and threonic acid are showed in Figure 9.2.

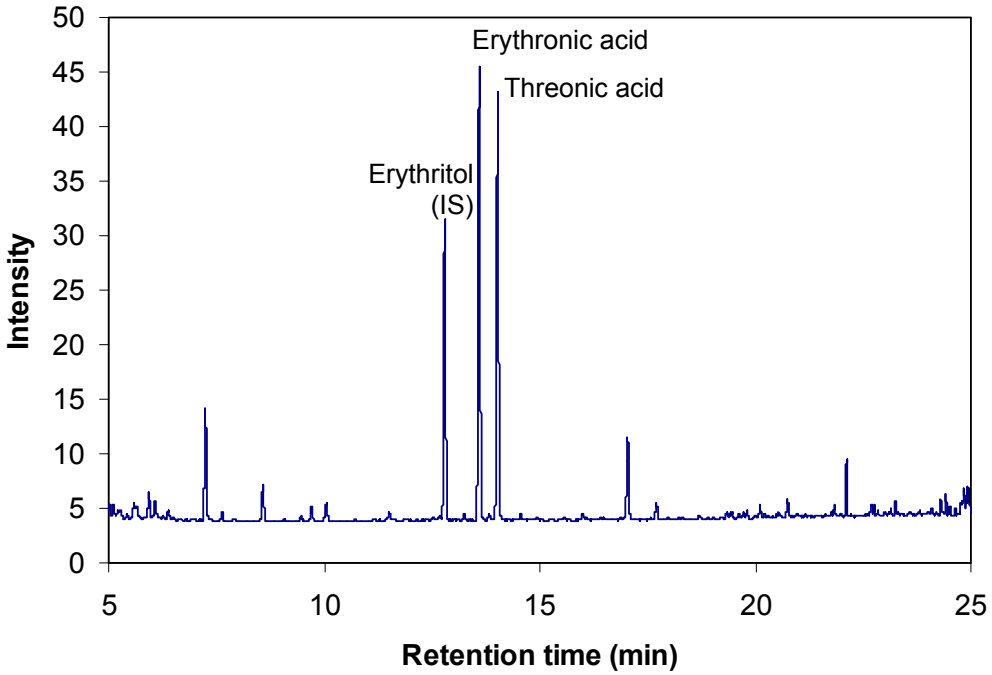

Figure 9.1 Ozonation product GC chromatogram of juvenile normal wood in loblolly pine.

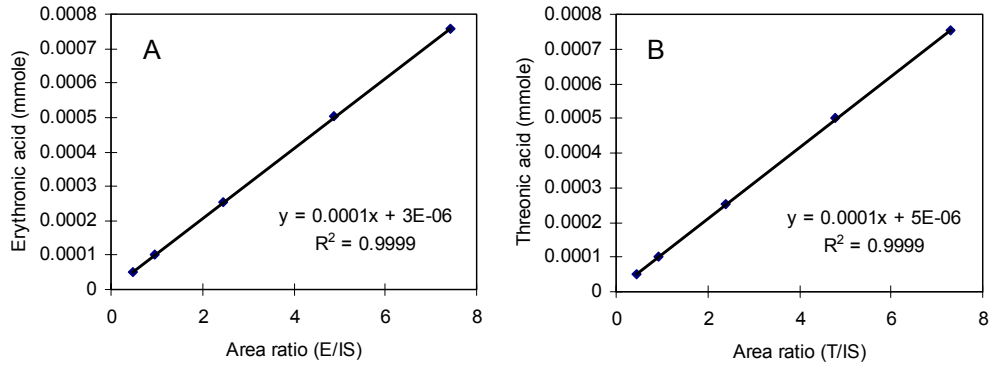

Figure 9.2 Calibration lines of (A) erythronic acid, and (B) threonic aicd. Area ratio is expressed as area of acids divided by that of internal standard (IS), erythritol.

9.2 Nitrobenzene Oxidation

Nitrobenzene oxidation was performed according to Chen [3] and modified as per Katahira and Nakatsubo [4]. 100 mg of OD wood meals (-40+60 mesh) were reacted with 5 ml 2N $NaOH_{(aq)}$ and 0.4 ml nitrobenzene in a stainless bomb at 165˚C for 2.75 h. After 2.75 h, the hot stainless bomb was cooled down immediately by ice water, and 1 ml of 5-iodovanillin (80 mg in 5 ml dioxane) was added as internal standard. The reaction mixture was extracted with CH_2Cl_2 3 times and the organic phase (CH_2Cl_2 phase) was discarded. The remaining water phase (alkali solution) was then acidified with 2N HCl to pH 2-3. The acidified solution was further extracted again with CH_2Cl_2 for 3 times, and this organic phase (CH_2Cl_2 phase) was collected for analysis. The CH_2Cl_2 phase was dried over $Na_2SO_{4(S)}$ and the volume was adjusted to 100 ml. 1 ml of this solution was dried by rotavapor at 30°C. The dried product was dissolved in 50 µl of pyridine, and 60 µl of *N*-methyl-*N*-(trimethylsilyl) trifluoroacetamide (MSTFA) was added, and the

solution was shaken for 15 min at 50 °C. The derivatized mixture was then directly injected (2 µl) onto the GC.

Quantitative GC analysis was carried out on a HP 6890 GC equipped with a flame ionization detector and HP-1 column (30m × 0.32mm × 0.25µm). The injection temperature was 200°C, the detector temperature was 270°C, and the column flow rate was 2 ml helium/min. The column was held for 3 min at 120°C, raised at 5°C/min to 200°C, followed by 10°C/min to 260°C, and kept isothermal at 260°C for 5 min. The GC chromatogram and calibration lines of the *p*-hydroxybenzoaldehyde, *p*-hydroxybenzoic acid, vanillin, vanillic acid, and syringaldehyde are showed in Figure 9.3 and Figure 9.4. A typical GC chromatogram from nitrobenzene oxidation of compression wood is shown in Figure 9.5.

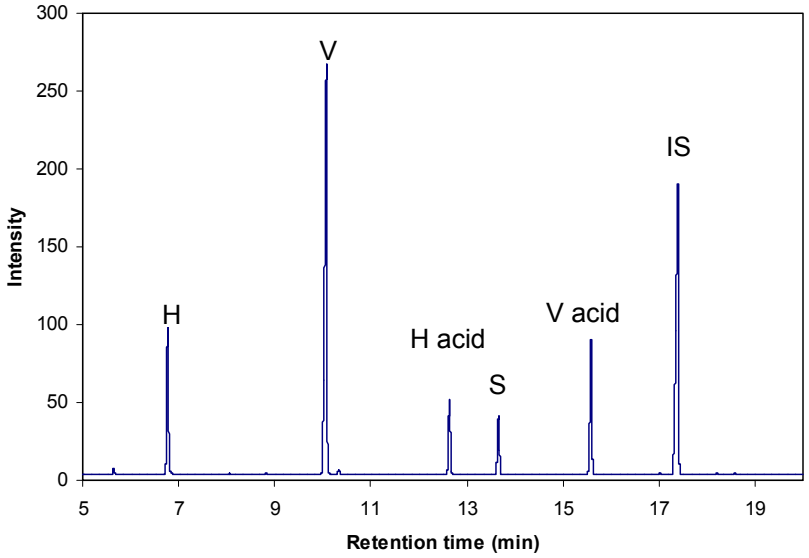

Figure 9.3 GC chromatogram of 5 nitrobenzene oxidation products: (H) *p*-hydroxybenzoaldehyde, (H acid) *p*-hydroxybenzoic acid, (V) vanillin, (V acid) vanillic acid, (S) syringaldehyde, and (IS) 5-iodovanillin.

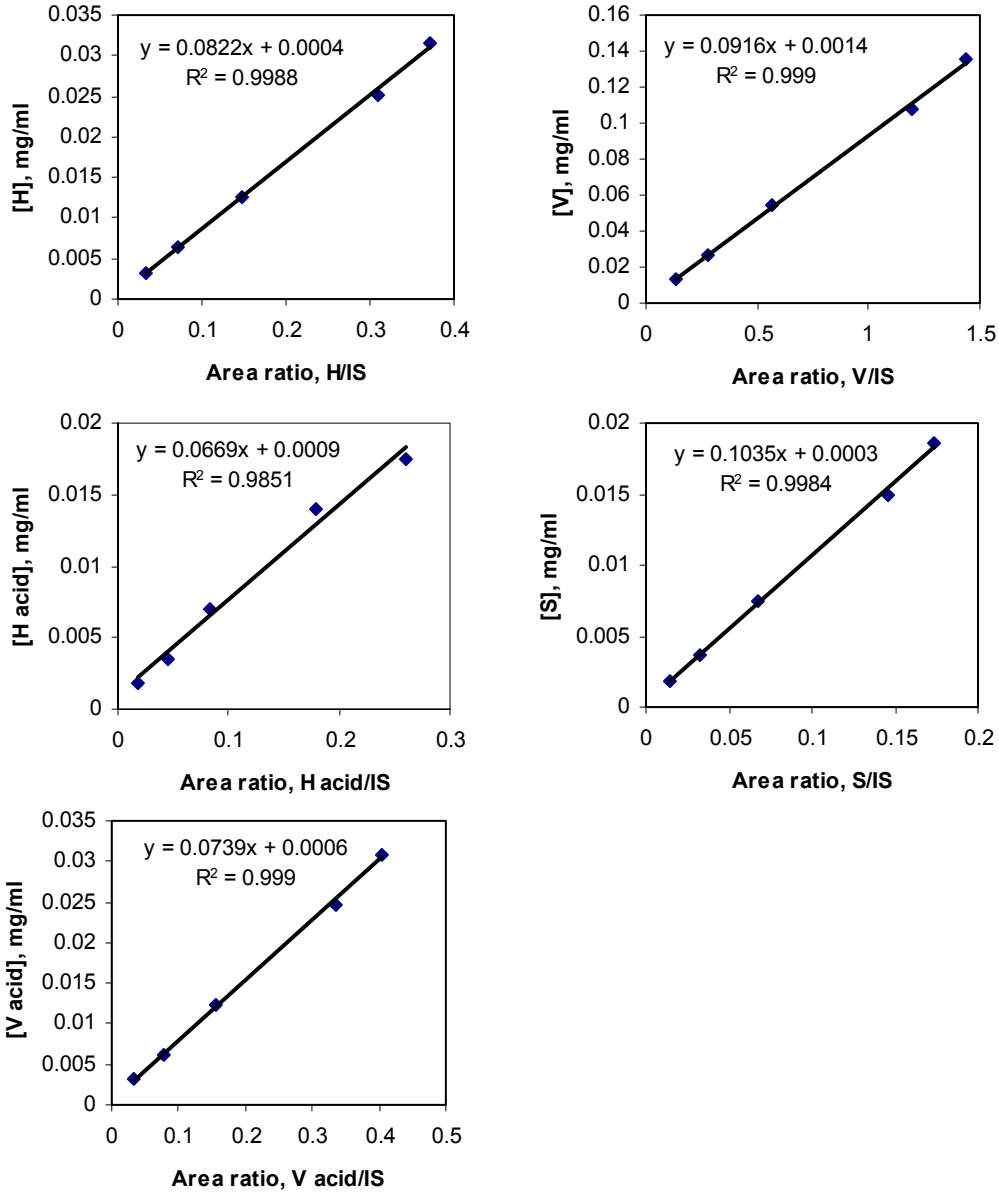

Figure 9.4 GC calibration lines of 5 nitrobenzene oxidation products: (H) *p*-hydroxybenzoaldehyde, (H acid) *p*-hydroxybenzoic acid, (V) vanillin, (V acid) vanillic acid, and (S) syringaldehyde.

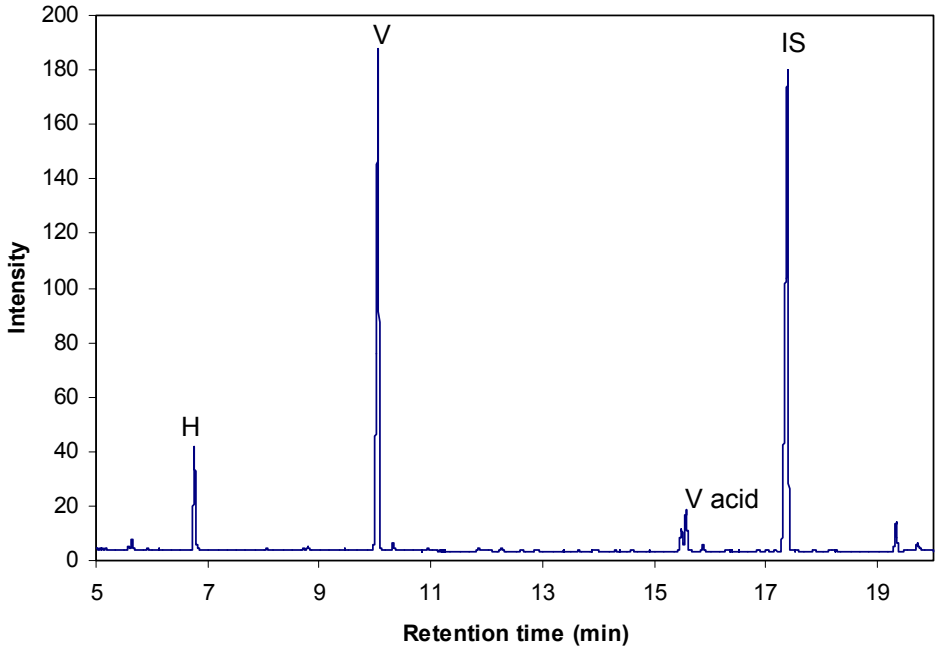

Figure 9.5 GC chromatogram of nitrobenzene oxidation product of juvenile compression wood in loblolly pine: (H) *p*-hydroxybenzoaldehyde, (H acid) *p*-hydroxybenzoic acid, (V) vanillin, and (IS) 5-iodovanillin.

9.3 Sugar Analysis

Monosaccharide composition of the wood cell wall was done using a modified klason lignin method [5] followed by the alditol-acetate method according to Blakeney et al. [6] and Coimbra et al. [7]. 100 mg (OD) of wood meal (-40+60 mesh) was treated with 1.5ml of 72% $H_2SO_{4(aq)}$ for 2 h at room temperature. After 2 h, this solution was diluted to 3% $H_2SO_{4(aq)}$, and heated for 1 h at 121˚C at 2 atm [5]. The solution was then cooled down, and filtered to remove the klason lignin. 50 µl of inositol (20 mg in 10 ml H_2O) was added to 200 µl of the filtrate as an internal standard, and 70 µl of 3M $NH_4OH_{(aq)}$ and 1ml of $NaBH_{4(aq)}$ (2 g $NaBH_4$ in 100ml DMSO) were subsequently added. The mixture

was then reacted for 90 min at 40˚C. After 90 min, 100 µl of acetic acid was added to stop the reaction.

Acetylation was done by adding 200 µl 1-methylimidazole and 2 ml of acetic anhydride to the reaction mixture and kept in room temperature for 10 min. After 10 min, the reaction was stopped by adding 5 ml water, and 1 ml of CH_2Cl_2 was added to extract the alditol acetate compounds. The CH_2Cl_2 phase was dried over $Na_2SO_{4(S)}$ and 2 µl of this solution was injected on to the GC.

Quantitative gas chromatography (GC) analysis was carried out on a HP 6890 GC equipped with a flame ionization detector and Rtx-225 column (15m × 0.32mm × 0.25µm). The injection temperature was 220°C, the detector temperature was 240°C, and the column flow rate was 2 ml helium/min. The initial column temperature was 210°C, and was raised to 230°C at 2°C/min. A typical alditol acetate GC chromatogram of juvenile wood is showed in Figure 9.6. The GC calibration lines of the sugars are showed in Figure 9.7. The sugar content of the all hexoses, glucose, mannose, galactose, and pentoses, arabinose, xylose, were corrected by multiplying the sugar contents by 0.9 and 0.88, respectively.

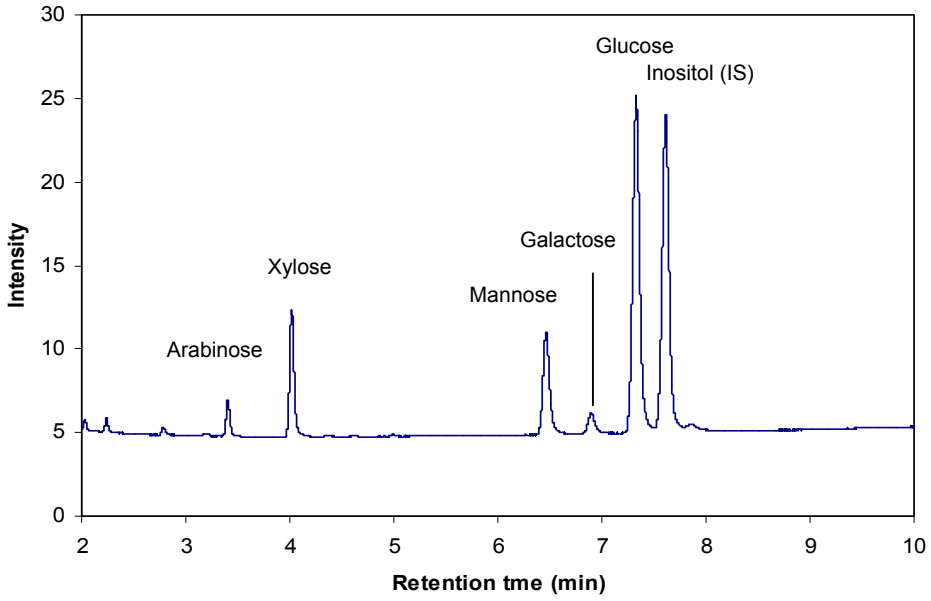

Figure 9.6 A typical alditol acetate GC chromatogram of juvenile wood.

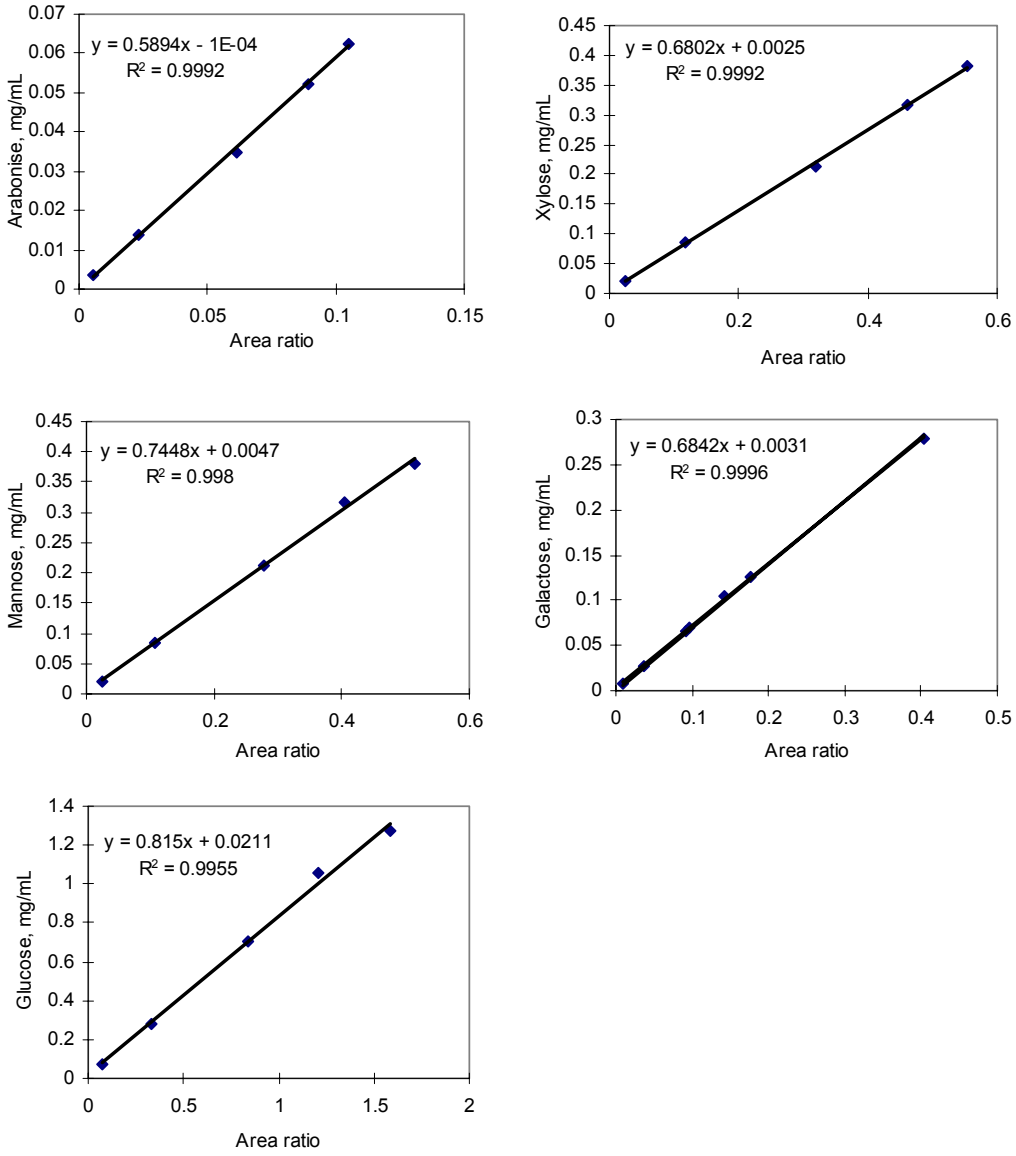

Figure 9.7 GC calibration lines of 5 sugars. Area ratio is expressed by the area of each individual sugar divided by that of internal standard.

9.4 Methoxyl Content Analysis

Methoxyl content analysis was done according to Baker [8] and Goto et al. [9]. Accordingly, 10 mg (OD) of milled wood lignin (MWL) was placed in a reaction vial.

Ten ml of 57% hydriodic acid (Aldrich) was added, and the reaction vial was sealed and reacted for 25 min at 130˚C. After 25 min, the sample was cooled with ice and water for 15 min, and 1 ml of ethyl iodide (EtI, Aldrich) (500 mg in 100 ml CCl_4) was added into the vial as an internal standard. The reaction mixture was further extracted with 10 ml of CCl_4. The CCl_4 extract was dried over $Na_2SO_{4(s)}$, and 2 µl was injected on the GC for methoxyl content quantitation.

Quantitative gas chromatography (GC) analysis was carried out on a HP 6890 GC equipped with a flame ionization detector and HP-1 column (15m × 0.32mm × 0.25µm). The injection temperature was 200°C, the detector temperature was 250°C, and the column flow rate was 1 ml helium/min. The column was held for 8 min at 40°C, then raised to 200°C at 20°C/min. A typical GC chromatogram of methoxyl content analysis is showed in Figure 9.8, and the GC calibration line of iodomethane (MeI) is showed in Figure 9.9.

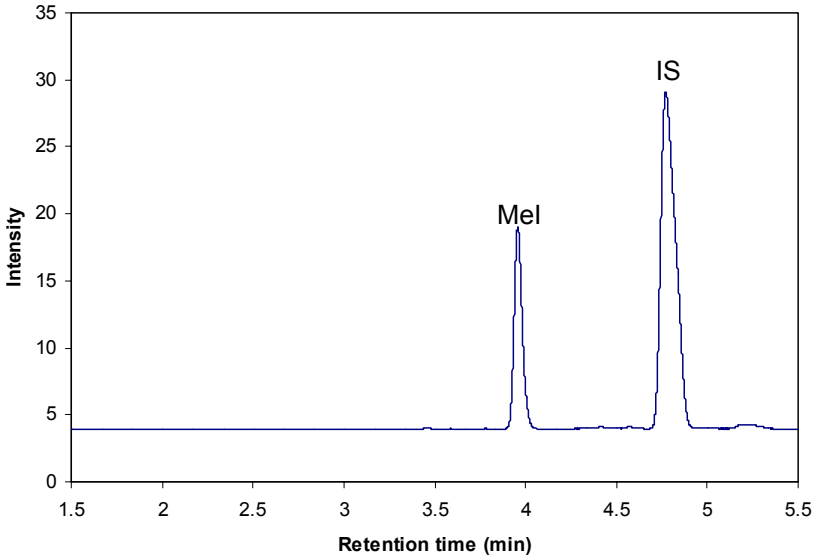

Figure 9.8 GC chromatogram of methoxyl content analysis from juvenile normal wood MWL: (IS) internal standard, EtI.

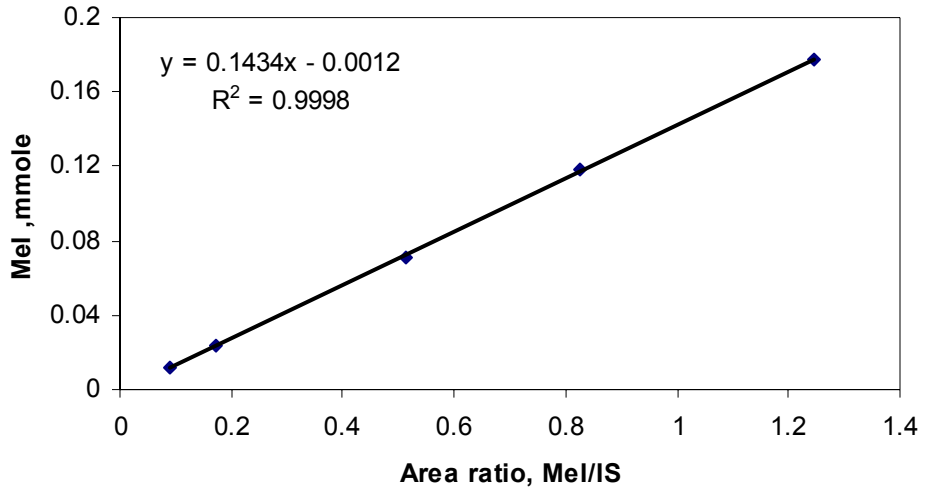

Figure 9.9 GC calibration line for methoxyl content analysis. (IS) internal standard, EtI.

9.5 NMR Spectra

NMR peak assignments (Table 9.1 and 9.2) and related lignin structures (Figure 9.10) are shown according to Capanema et al. [10], Balakshin et al. [11], and the references there in.

Table 9.1 NMR peak assignments of non-acetylated MWL [11].

Range (ppm)	Assignment
210-200	Non-conjugated CO
200-196	α–CO except **D**
196-193	CO in α–CO/β–*O*–4 (**D**), **L**
193-191	Ar-CHO (**M**)
182-180	C-4 in **I**
175-168	Aliphatic COOR
168 - 166	Conjugated COOR
162-160	C-4 in conjugated **H**-units
159-156	C-4 in non-conjugated **H**-units
156-151	C-3 in $\mathbf{T}_{et}$, C-3,5 in $\mathbf{R}_{et}$ and $\mathbf{S}_{et}$, C–α in **L**, C-3,6 in **I**, C-4 in conjugated CO/COOR ether units
106-103	C-2,6 in **S**-units
58-54	OMe, C-β in **J**, C-1 in **I**, C–γ in **P**
54-52	C-β in **E** and **F**
35-34	C-β in **Q**, C-α in **O**
32.5-31.5	C-α in **Q**
Clusters	
125-102	C_{Ar-H}
90-58	Alk-*O*-
90-77	Alk-*O*-Ar, α–*O*-Alk
77-65	γ–*O*-Alk, OH_{sec}
65-58	OH_{prim}

Table 9.2 NMR peak assignments of acetylated MWL [11].

Range (ppm)	Assignment
210-200	Non-conjugated CO
200-196	α–CO except **D**
196-193	CO in α–CO/β–*O*–4 (**D**), **L**
193-191	Ar-CHO (**M**)
182-180	C-4 in **I**
175-169.6	Primary aliphatic OH, aliphatic COOR
169.6-168.6	Secondary aliphatic OH
168.6-166	Phenolic OH, conjugated COOR
162-160	C-4 in conjugated etherified **H**-units
159-156	C-4 in non-conj. etherified **H**-units
162-148	All C-3 (except **E** and **H**-units), C-5 in **R** and **S**-units, C–α in **L**, C-6 in **I**, C-4 in conjugated CO/COOR etherified and **H**-units
106-103	C-2,6 in **S**-units
88-86	C-α in **E**
86-83	C-α in **F**, **N**
77-72.5	C-α in **A**, **J**, carbohydrates
60-59	C–γ in **P**
58-54	OMe, C-1 and C-β in **I**
50-48	C-β in **J**, **E**
35-34	C-α in **O**
32.5-31.5	C-α in **Q**
Clusters	
90-58	Alk-*O*-
90-77	Alk-*O*-Ar, α–*O*-Alk
77-65	γ–*O*-Alk, OH_{sec}
65-58	OH_{prim}

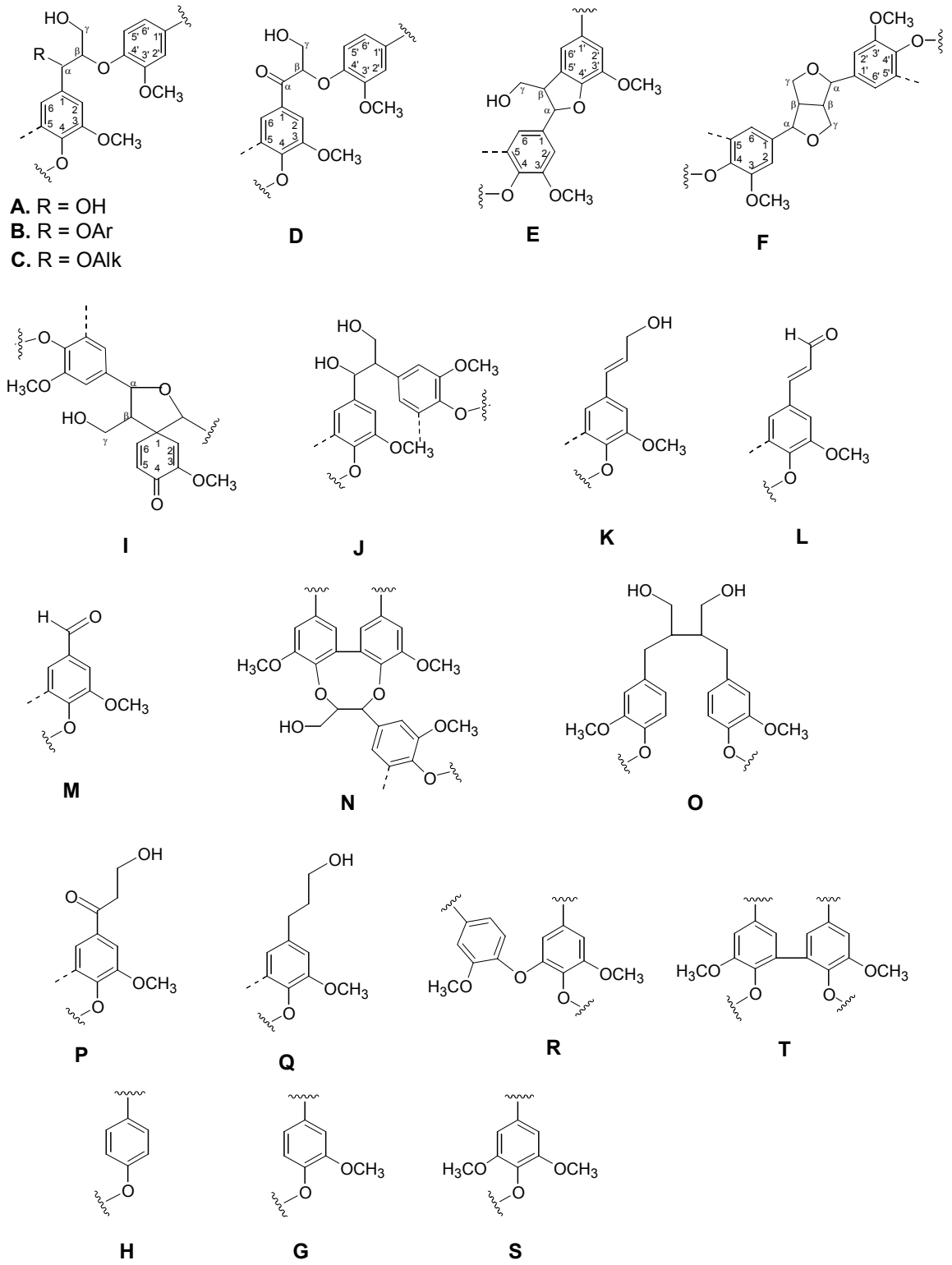

Figure 9.10 Lignin structures [11].

9.5.1 Phytotron Project

The group names are corresponded to Section 5.3 “Materials”.

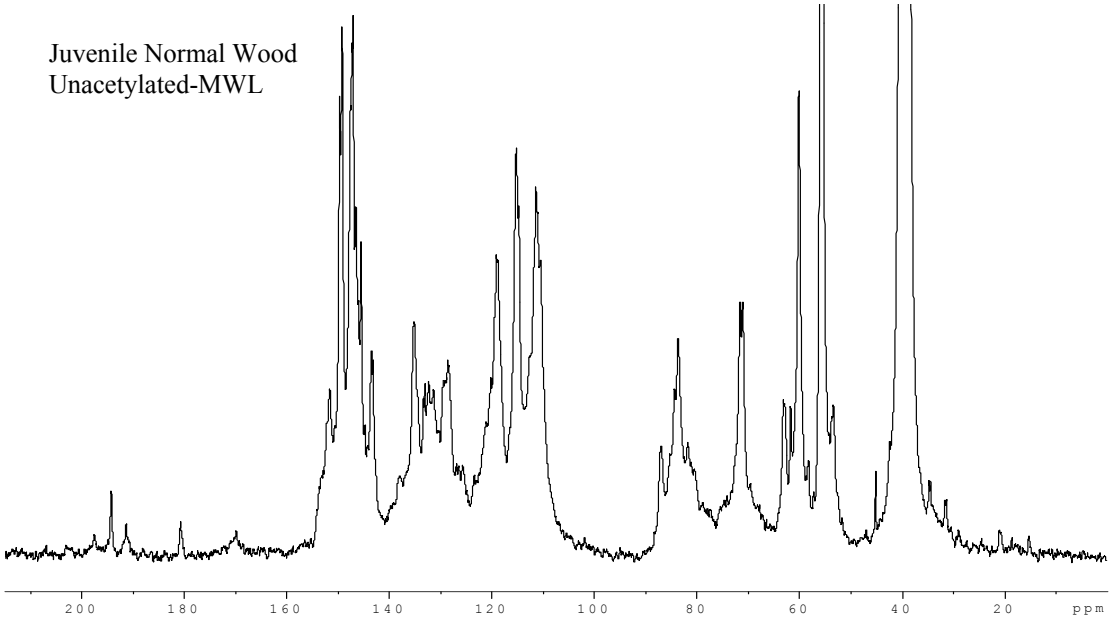

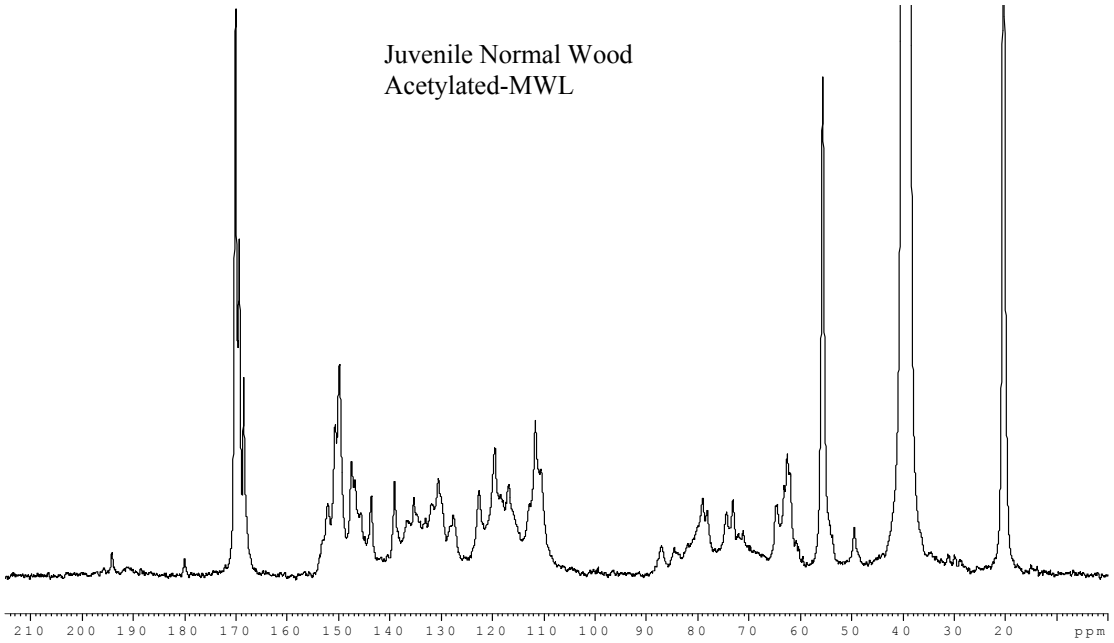

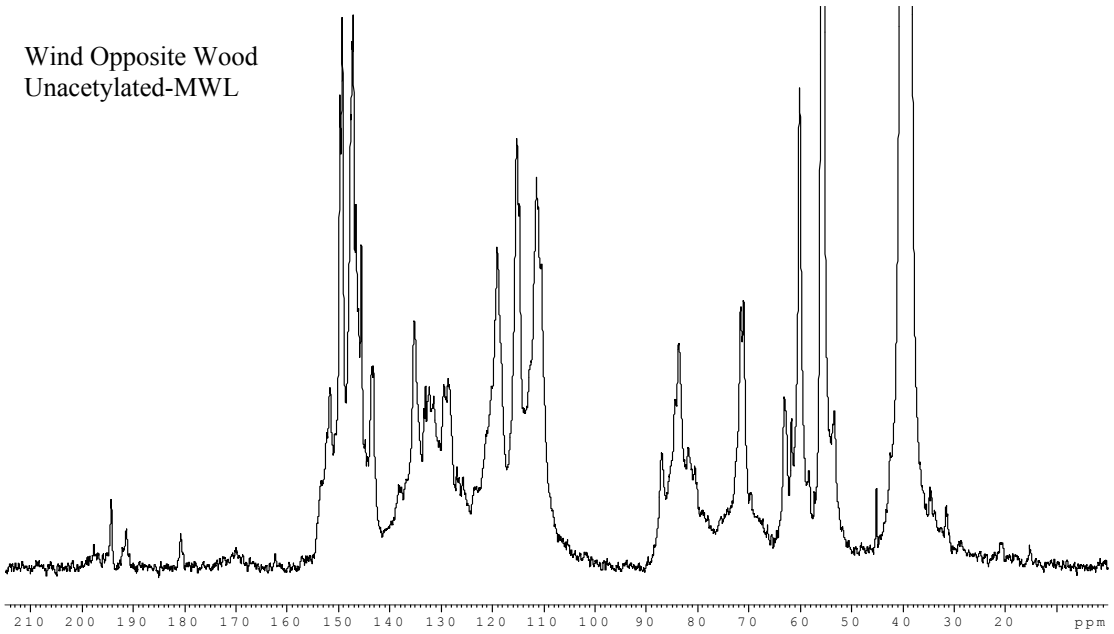
Wind Opposite Wood
Unacetylated-MWL
210 200 190 180 170 160 150 140 130 120 110 100 90 80 70 60 50 40 30 20 ppm

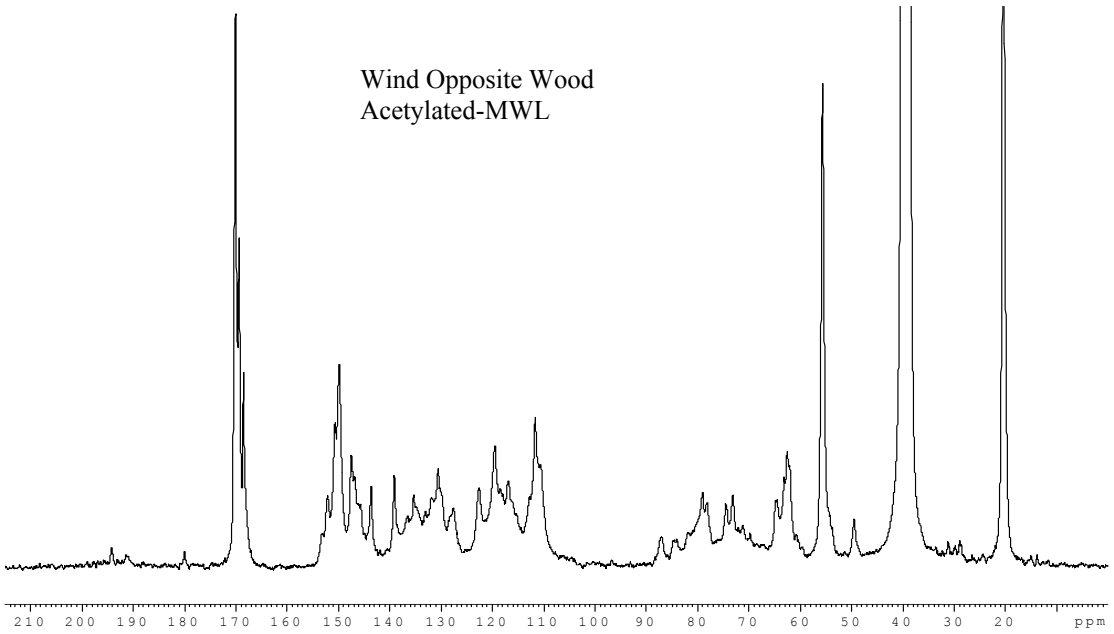
Wind Opposite Wood
Acetylated-MWL
210 200 190 180 170 160 150 140 130 120 110 100 90 80 70 60 50 40 30 20 ppm

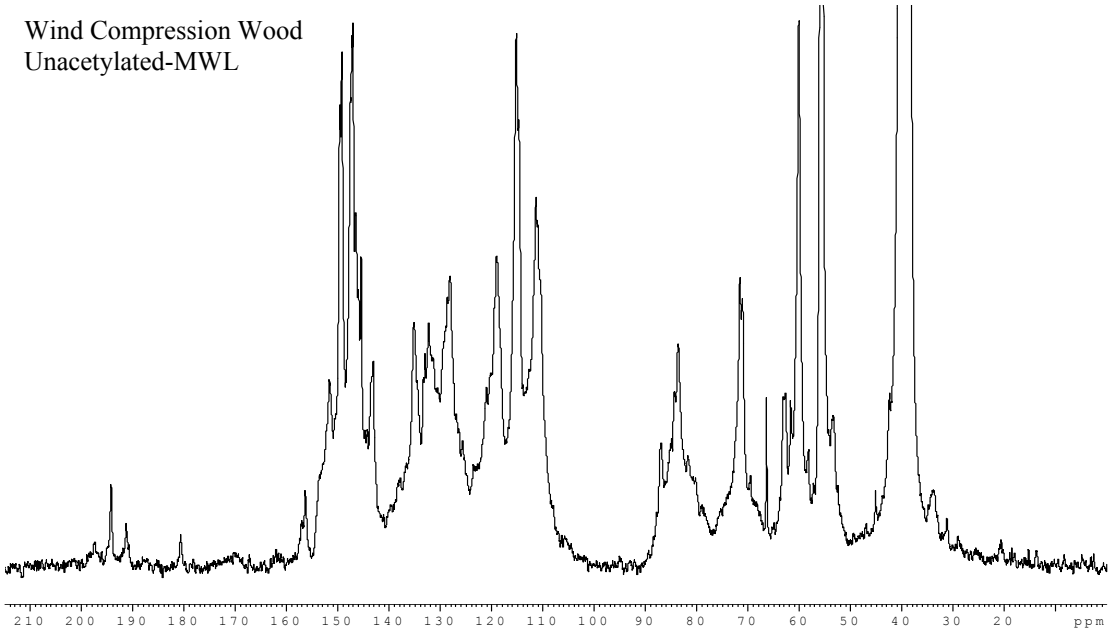
Wind Compression Wood
Unacetylated-MWL
210 200 190 180 170 160 150 140 130 120 110 100 90 80 70 60 50 40 30 20 ppm

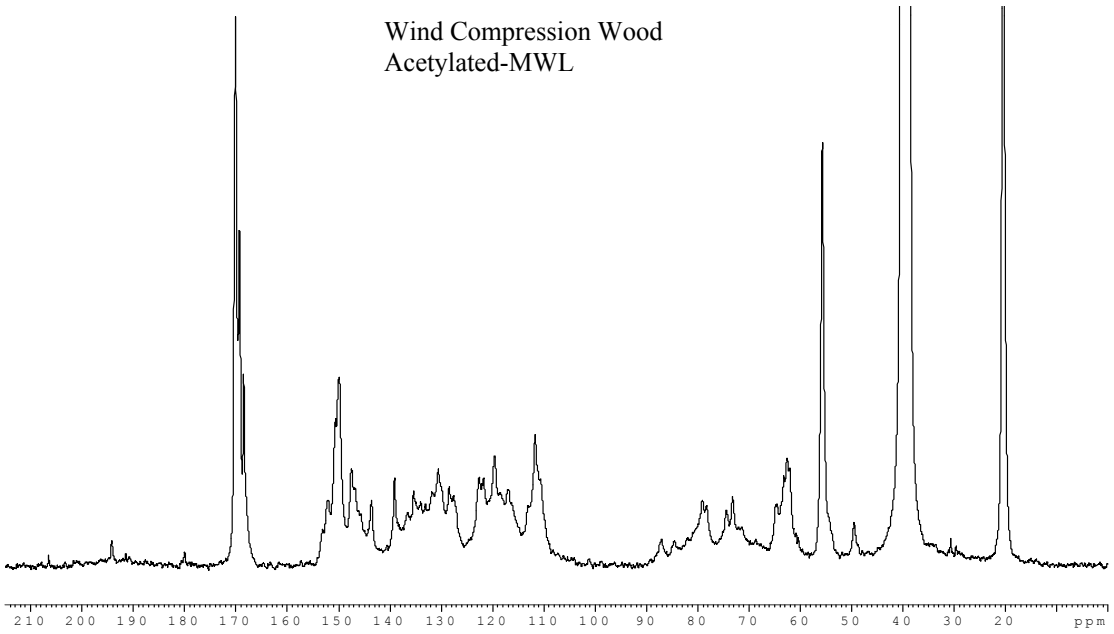
Wind Compression Wood
Acetylated-MWL
210 200 190 180 170 160 150 140 130 120 110 100 90 80 70 60 50 40 30 20 ppm

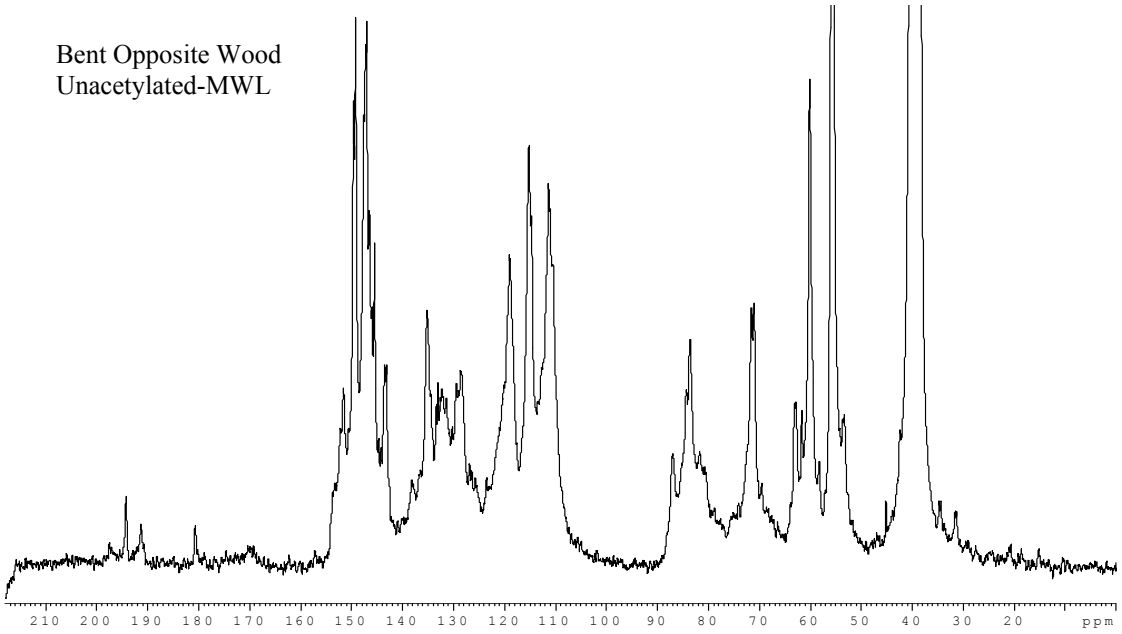
Bent Opposite Wood
Unacetylated-MWL
210 200 190 180 170 160 150 140 130 120 110 100 90 80 70 60 50 40 30 20 ppm

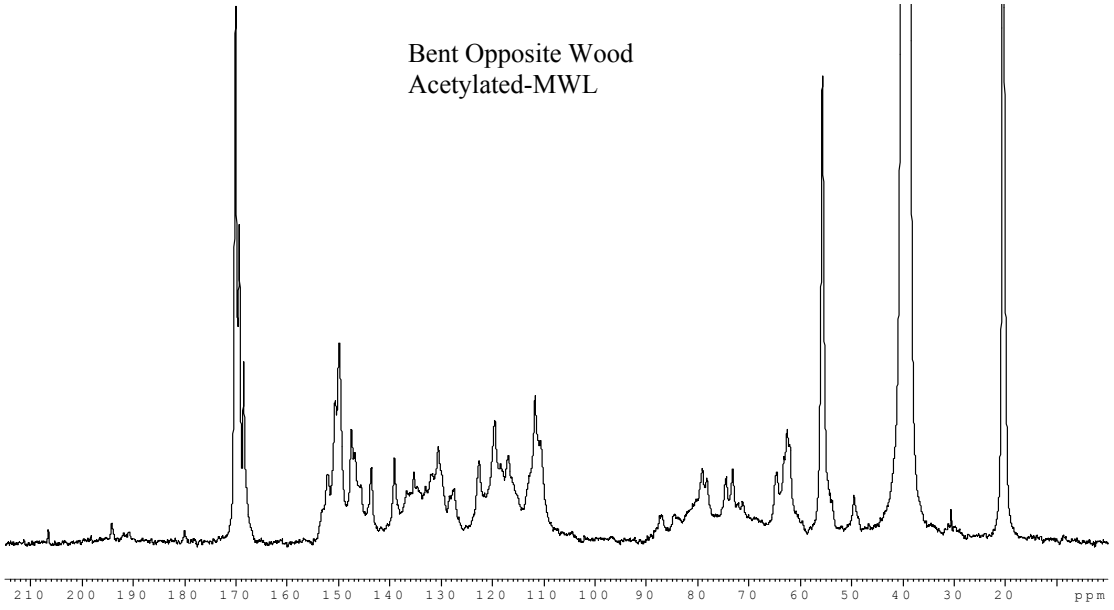
Bent Opposite Wood
Acetylated-MWL
210 200 190 180 170 160 150 140 130 120 110 100 90 80 70 60 50 40 30 20 ppm

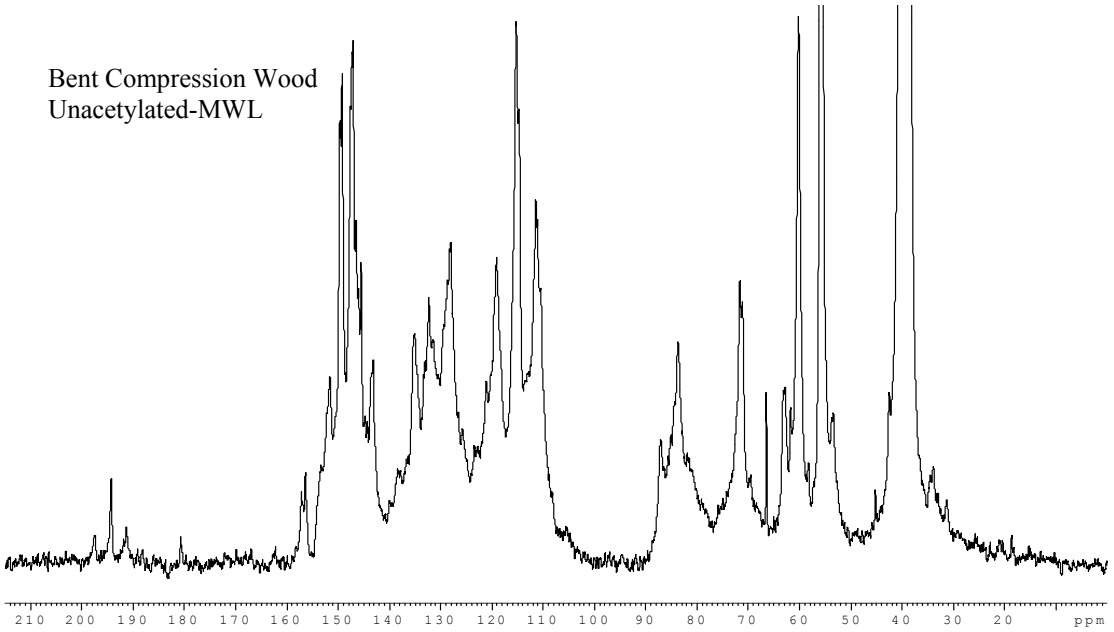
Bent Compression Wood
Unacetylated-MWL
210 200 190 180 170 160 150 140 130 120 110 100 90 80 70 60 50 40 30 20 ppm

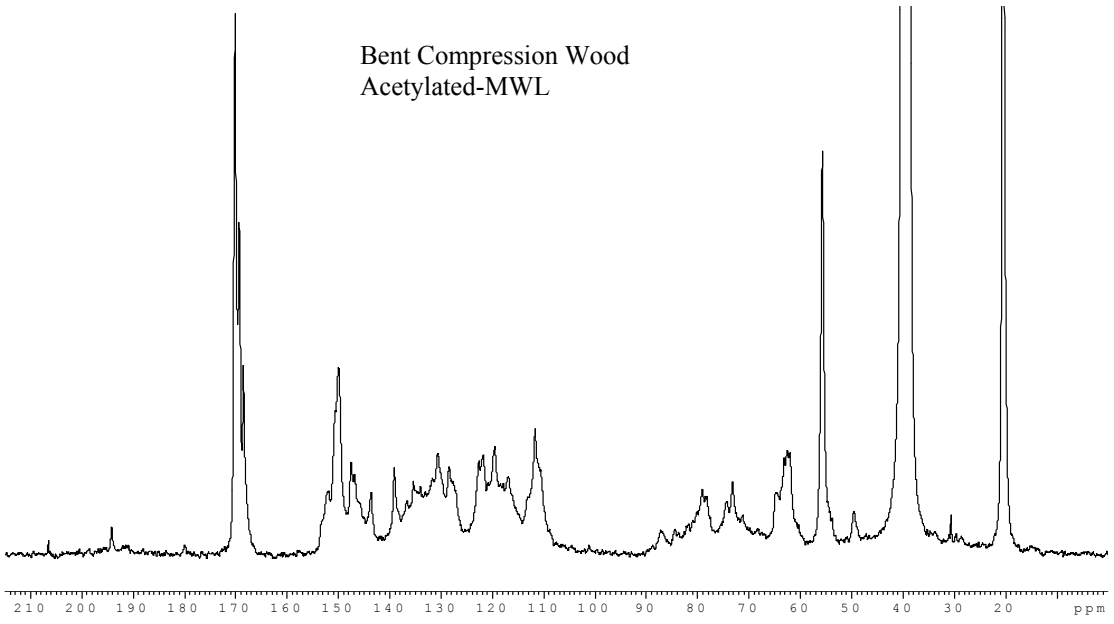
Bent Compression Wood
Acetylated-MWL
210 200 190 180 170 160 150 140 130 120 110 100 90 80 70 60 50 40 30 20 ppm

9.5.2 Bent Mature Pine Project

The group names are corresponded to Section 7.3 “Materials”.

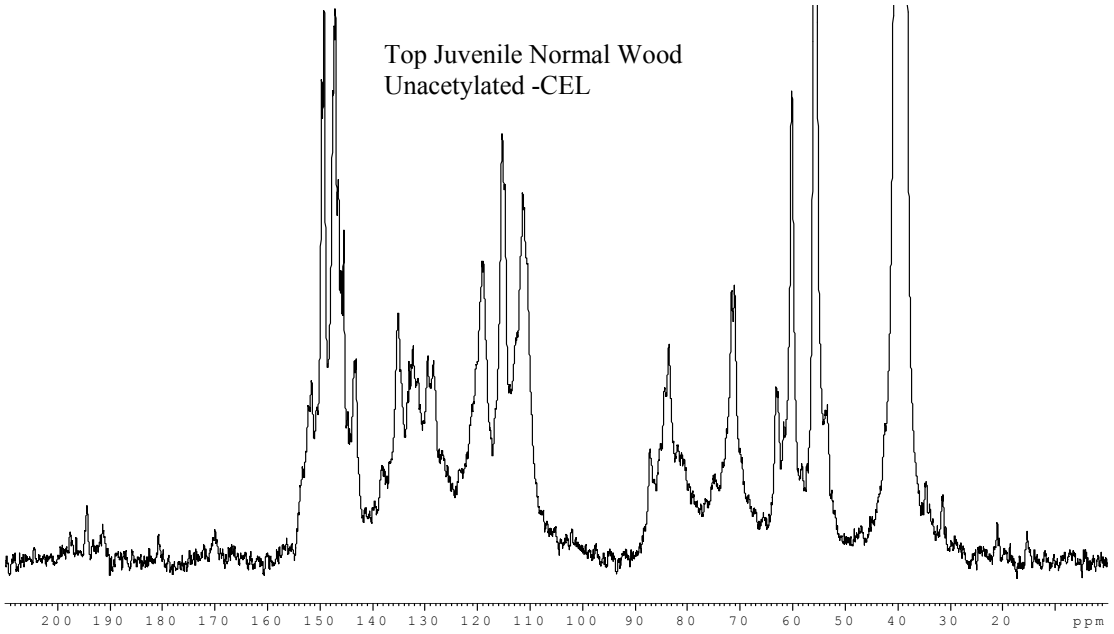

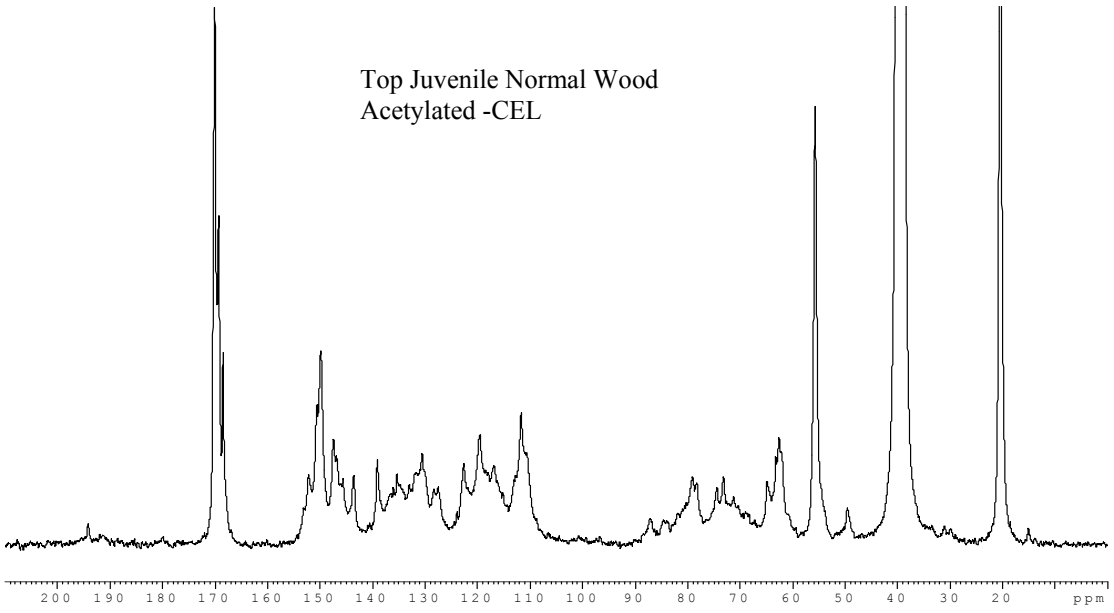

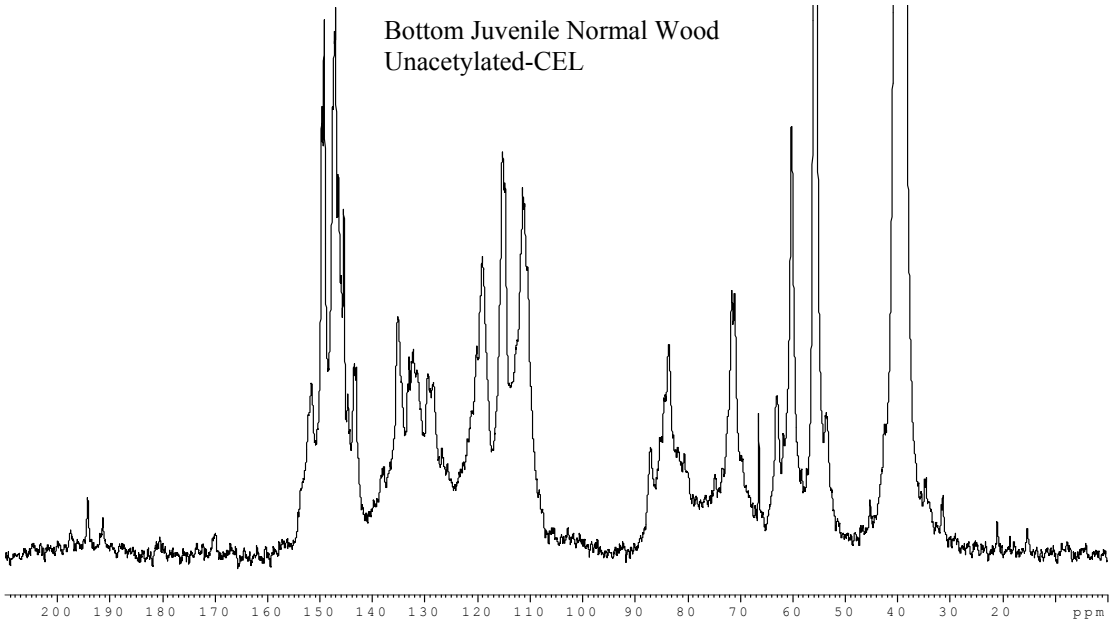
Bottom Juvenile Normal Wood
Unacetylated-CEL
200 190 180 170 160 150 140 130 120 110 100 90 80 70 60 50 40 30 20 ppm

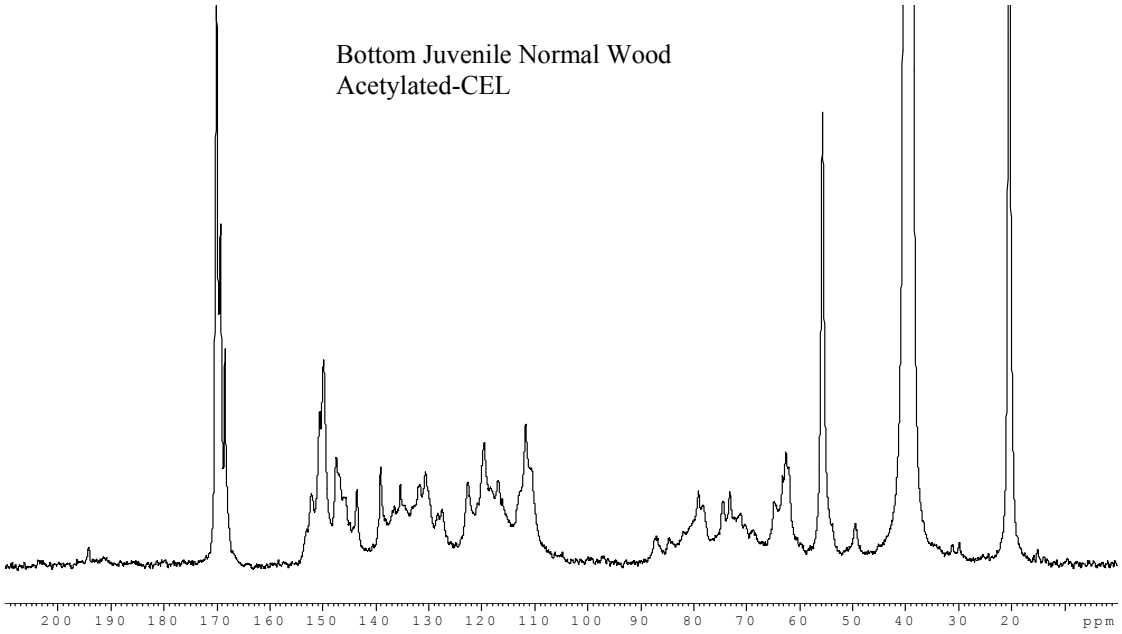
Bottom Juvenile Normal Wood
Acetylated-CEL
200 190 180 170 160 150 140 130 120 110 100 90 80 70 60 50 40 30 20 ppm

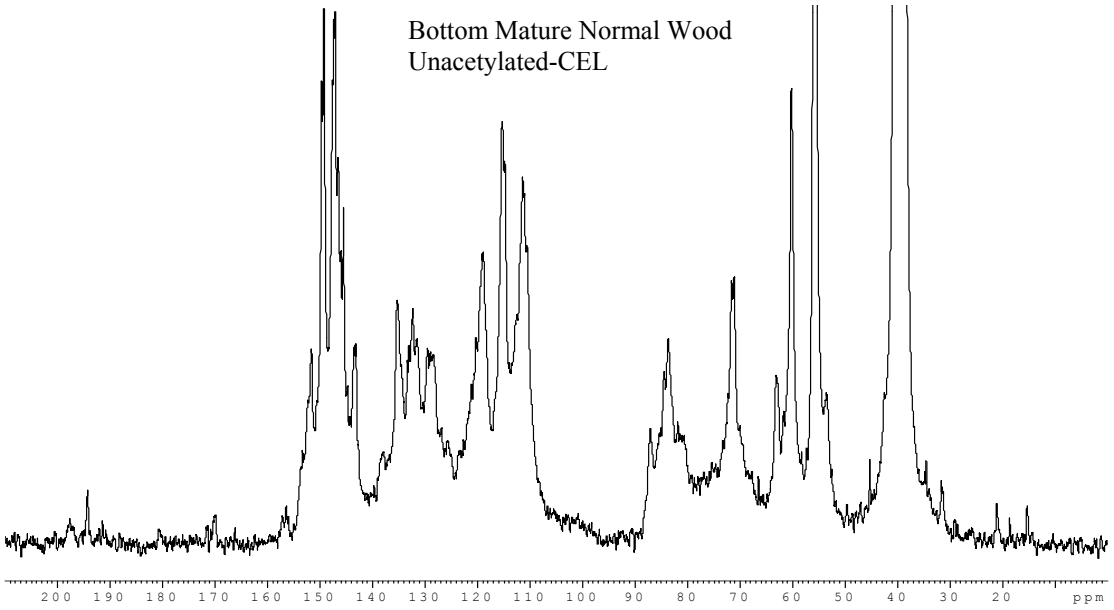
Bottom Mature Normal Wood
Unacetylated-CEL
200 190 180 170 160 150 140 130 120 110 100 90 80 70 60 50 40 30 20 ppm

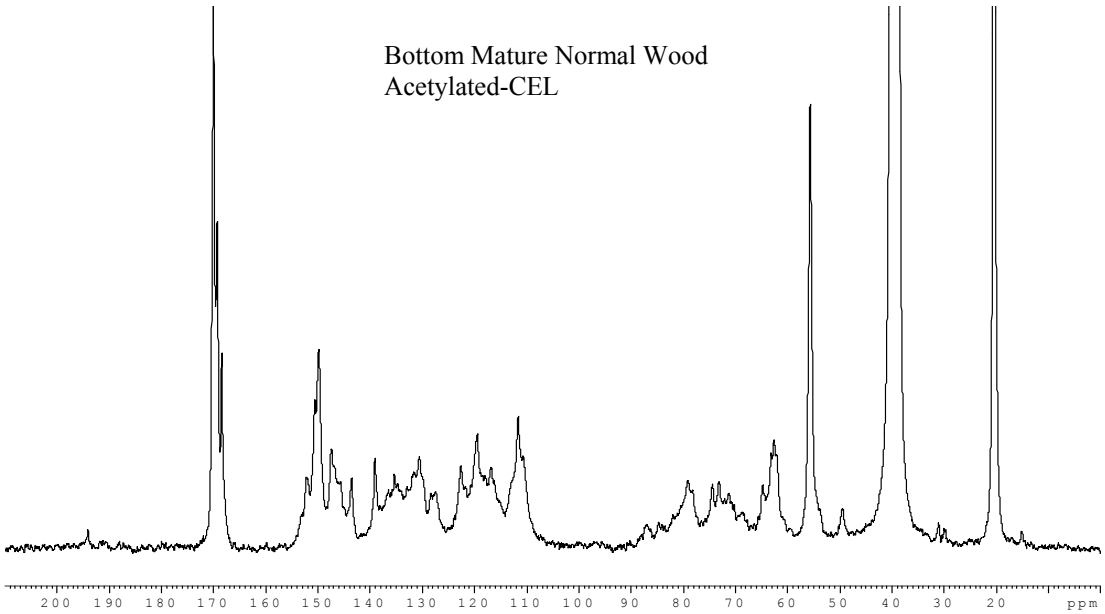
Bottom Mature Normal Wood
Acetylated-CEL
200 190 180 170 160 150 140 130 120 110 100 90 80 70 60 50 40 30 20 ppm

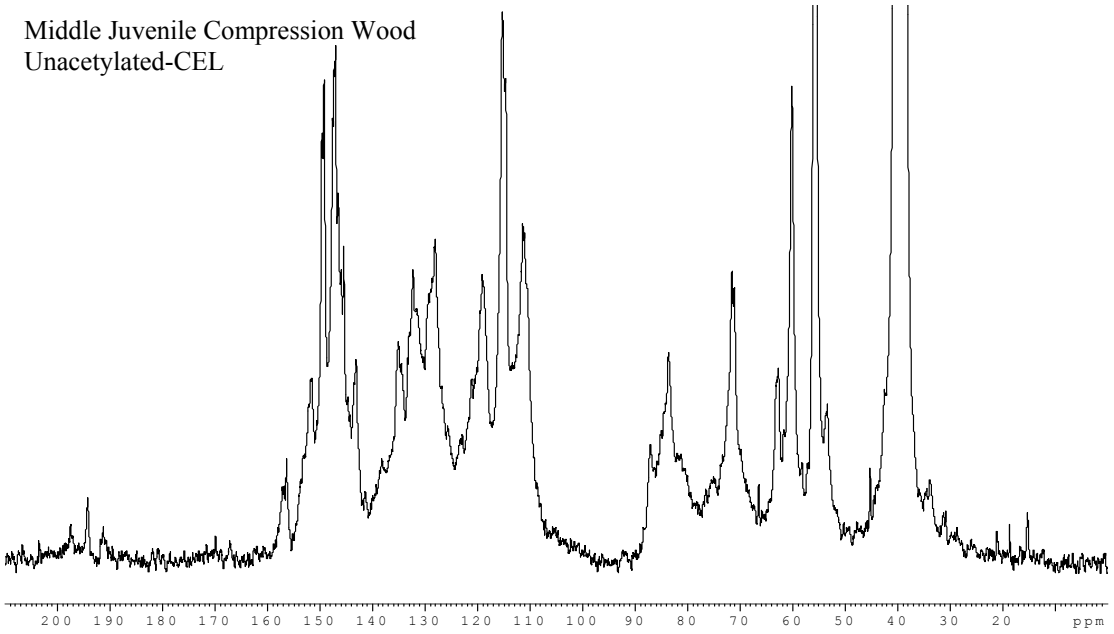
Middle Juvenile Compression Wood
Unacetylated-CEL
200 190 180 170 160 150 140 130 120 110 100 90 80 70 60 50 40 30 20 ppm

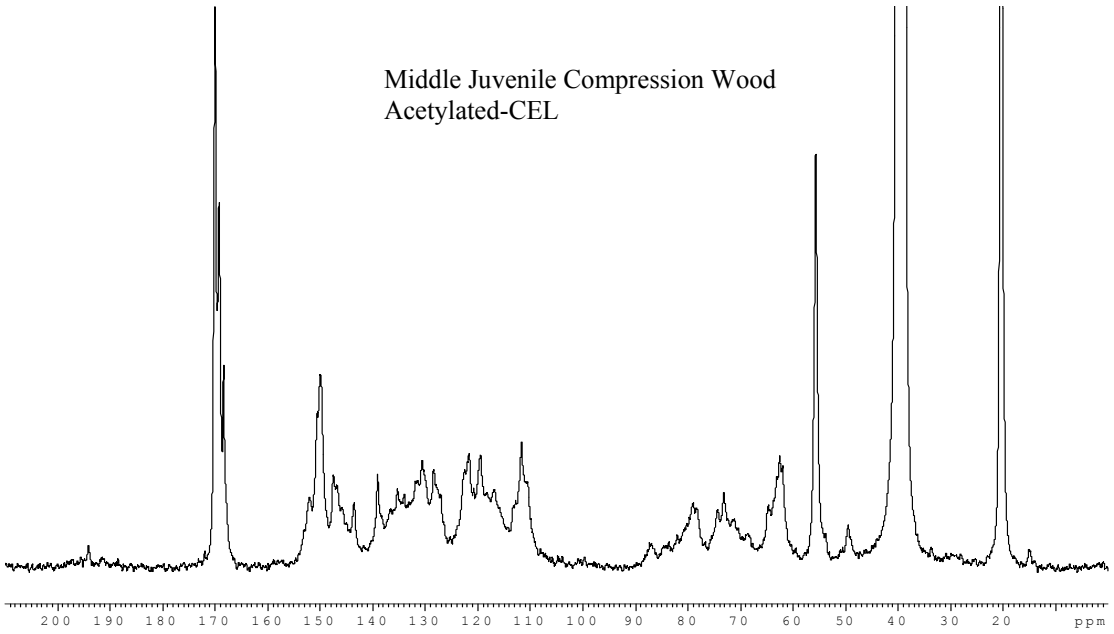
Middle Juvenile Compression Wood
Acetylated-CEL
200 190 180 170 160 150 140 130 120 110 100 90 80 70 60 50 40 30 20 ppm

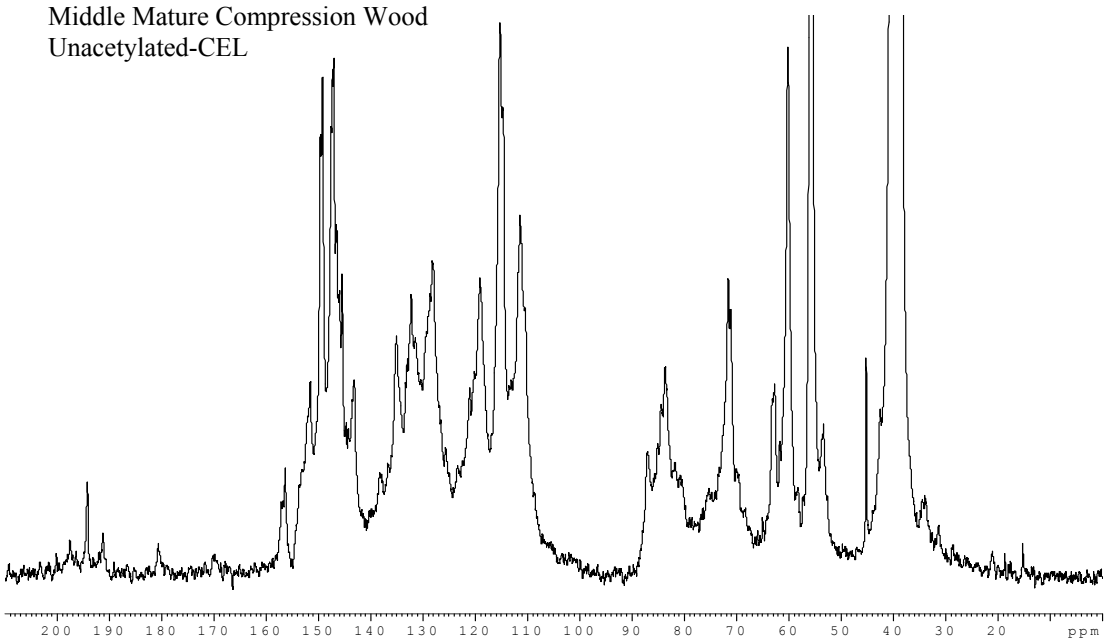
Middle Mature Compression Wood
Unacetylated-CEL
200 190 180 170 160 150 140 130 120 110 100 90 80 70 60 50 40 30 20 ppm

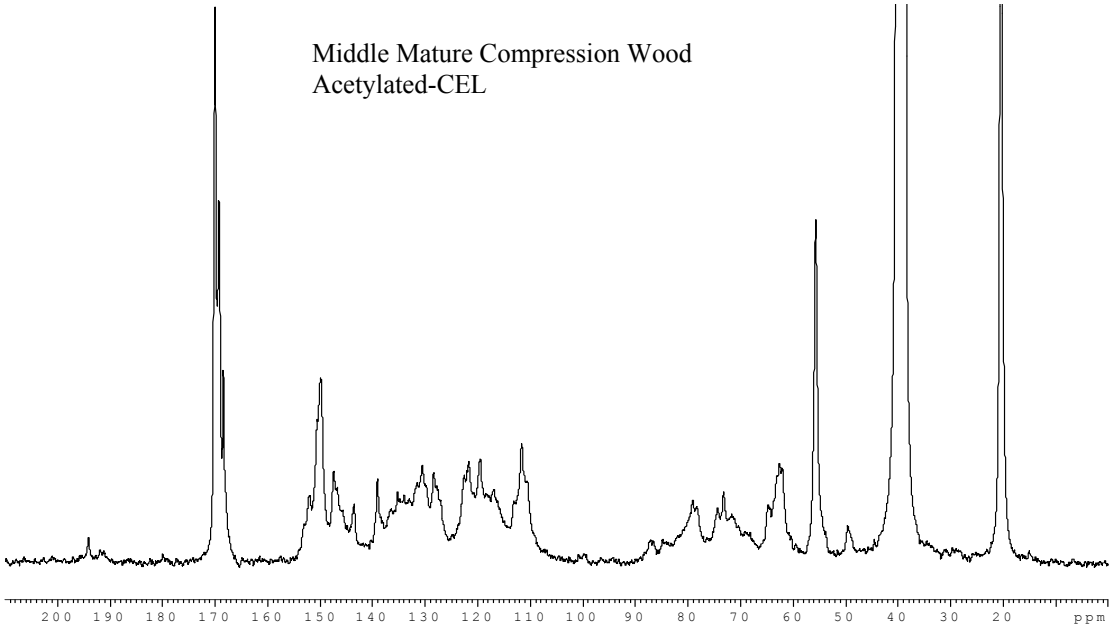
Middle Mature Compression Wood
Acetylated-CEL
200 190 180 170 160 150 140 130 120 110 100 90 80 70 60 50 40 30 20 ppm

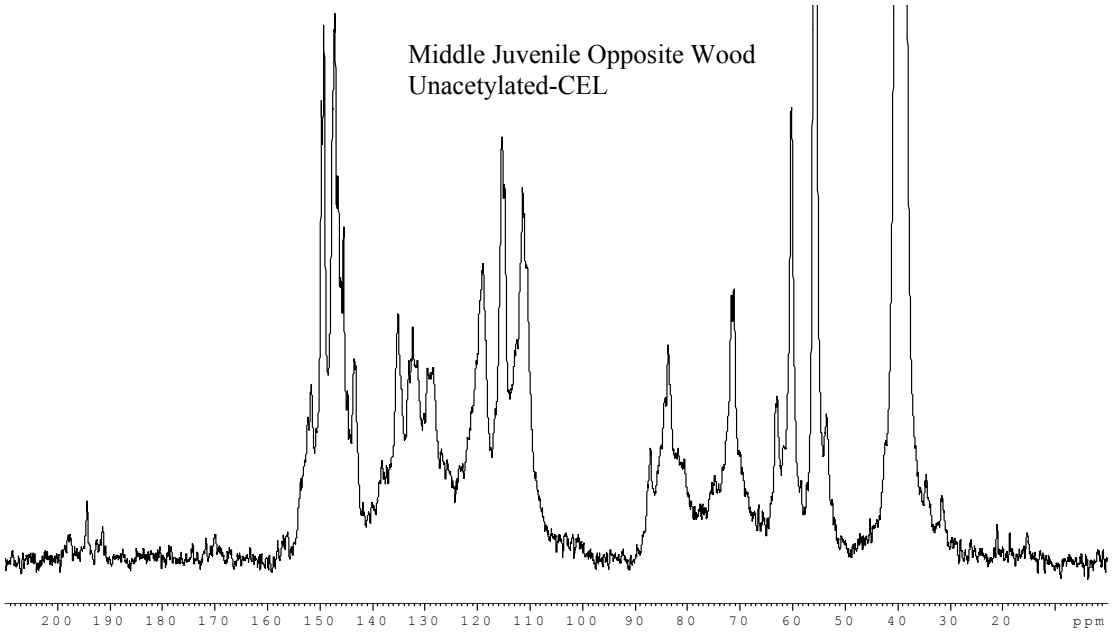
Middle Juvenile Opposite Wood
Unacetylated-CEL
200 190 180 170 160 150 140 130 120 110 100 90 80 70 60 50 40 30 20 ppm

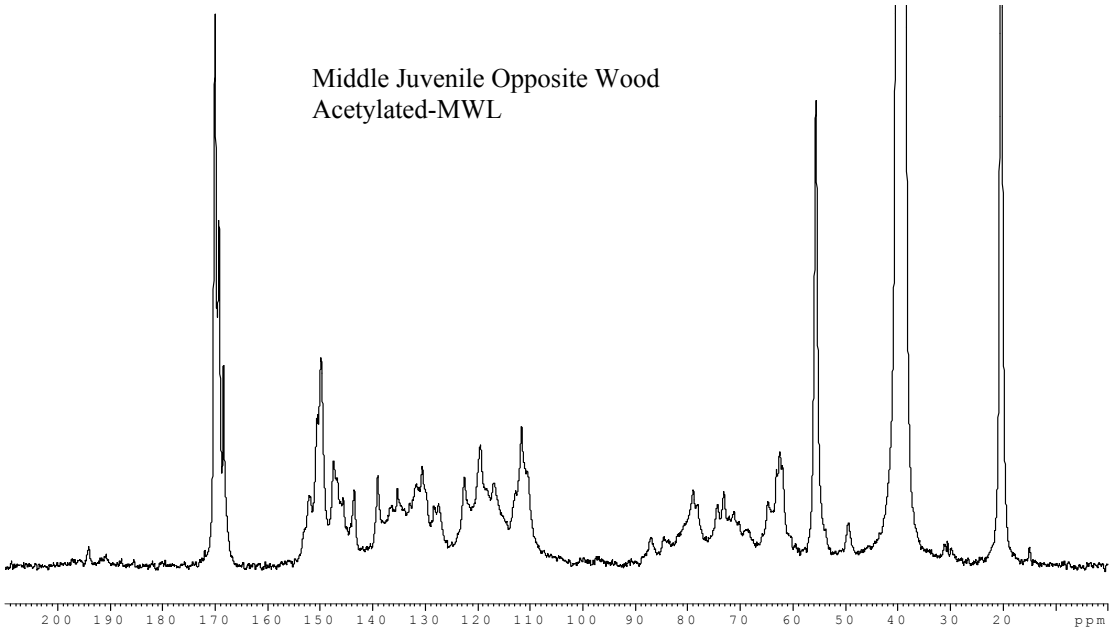
Middle Juvenile Opposite Wood
Acetylated-MWL
200 190 180 170 160 150 140 130 120 110 100 90 80 70 60 50 40 30 20 ppm

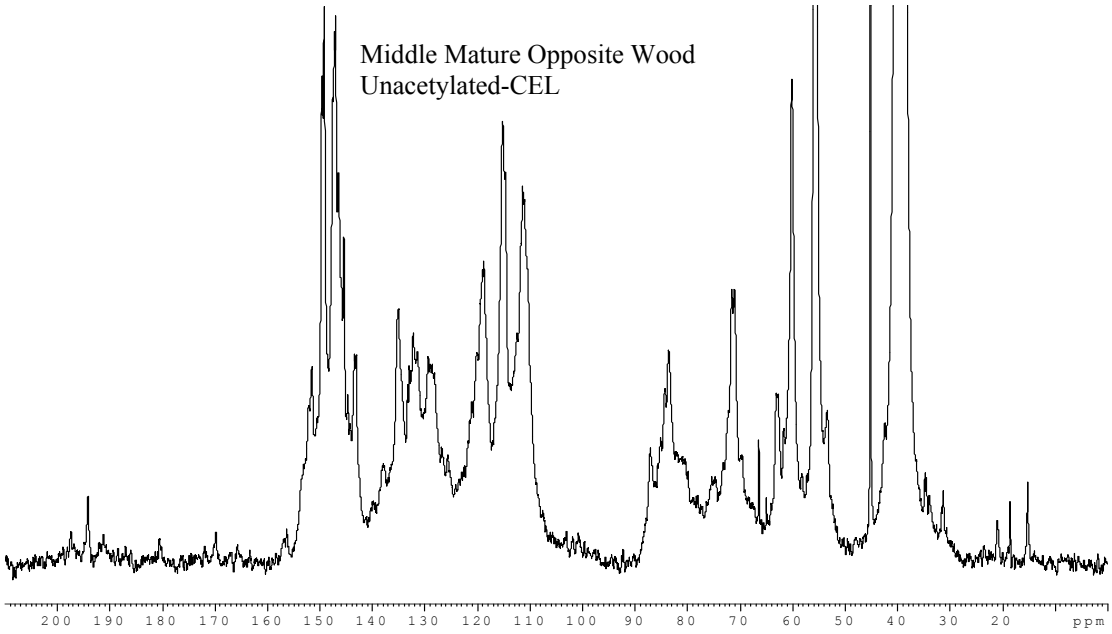
Middle Mature Opposite Wood
Unacetylated-CEL
200 190 180 170 160 150 140 130 120 110 100 90 80 70 60 50 40 30 20 ppm

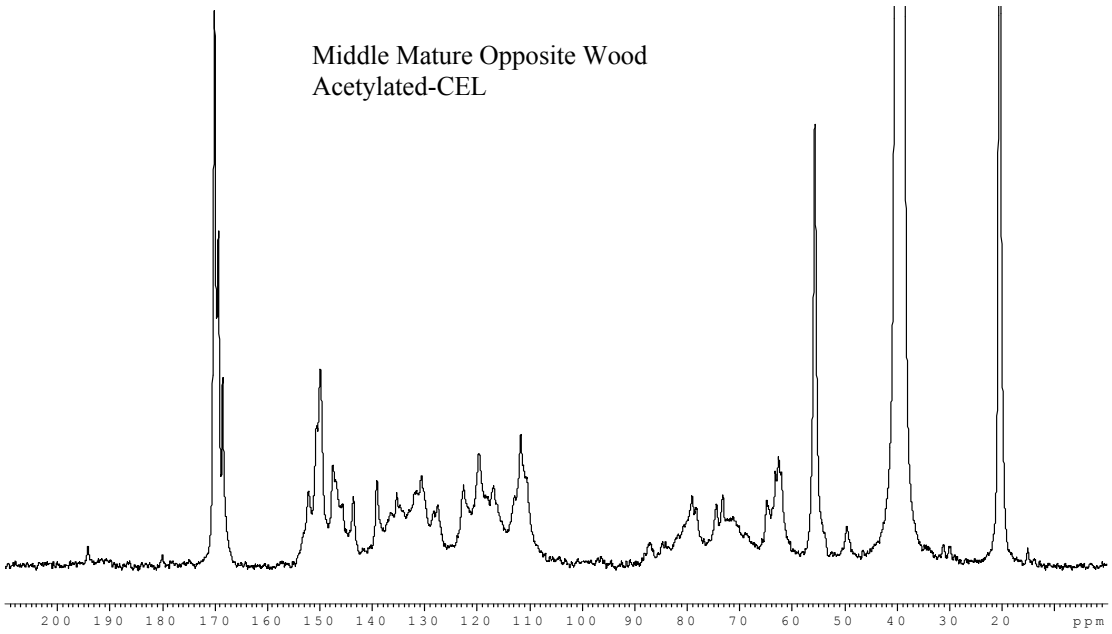
Middle Mature Opposite Wood
Acetylated-CEL
200 190 180 170 160 150 140 130 120 110 100 90 80 70 60 50 40 30 20 ppm

9.6 References

[1] Akiyama, T.; Matsumoto, Y.; Okuyama, T.; Meshitsuka, G. Ratio of *erythro* and *threo* form of β-O-4 structures in tension wood lignin. *Phytochem.* **2003**, *64*, 1157-1162.

[2] Akiyama, T.; Sugimoto, T.; Matsumoto, Y.; Meshitsuka, G. Erythro/threo ratio of β-O-4 structures as an important structural characteristic of lignin. I: Improvement of ozonation method for the quantitative analysis of lignin side-chain structure. *J. Wood Sci.* **2002**, *48*, 210-215.

[3] Chen, C.L. Nitrobenzene and cupric oxide oxidation. In *Methods in Lignin Chemistry*; S.Y. Lin and C.W. Dence, Eds.; Springer-Verlag: Berlin, 1992; pp 301-321.

[4] Katahira, R.; Nakatsubo, F. Determination of nitrobenzene oxidation products by GC and 1H-NMR spectroscopy using 5-iodovanillin as a new internal standard. *J.Wood Sci.* **2001**, *47*, 378-382.

[5] Yeh, T.F.; Yamada, T.; Capanema, E.; Chang, H.M.; Chiang, V.; Kadla, J.F. Rapid screening of wood chemical component variations using transmittance near infrared spectroscopy. *J. Agric. Food Chem.* **2005**, 3328-3332.

[6] Blakeney, A.B.; Harris, P.J.; Henry, R.J.; Stone, B.A. A simple and rapid preparation of alditol acetates for monosaccharide analysis. *Carbohyd. Res.* **1983**, *113*, 291-299.

[7] Coimbra, M.A.; Delgadillo, I.; Waldron, K.W.; Selvendran, R. Isolation and analysis of cell wall polymers from olive pulp. In *Modern Methods of Plant Analysis*; H.F. Linskens and J.F. Jackson, Eds.; Springer-Verlag: Berlin, 1996; pp 33-44.

[8] Baker, S.M. Rapid methoxyl analysis of lignins using gas chromatography. *Holzforschung* **1996**, *50*, 573-574.

[9] Goto, H.; Koda, K.; Matsumoto, Y.; Meshitsuka, G. Precise determination of methoxyl content as an important indication of the extent of lignin oxidation remaining in bleached pulp. *11th International Symposium on Wood and Pulping Chemistry, Nice, France*; Vol. III, pp 417-420.

[10] Capanema, E.A.; Balakshin, M.Y.; Kadla, J.F. A comprehensive approach for quantitative lignin characterization by NMR spectroscopy. *J. Agric. Food Chem.* **2004**, *52*, 1850-1860.

[11] Balakshin, M.Y.; Capanema, E.; Goldfarb, B.; Frampton, J.; Kadla, J.F. NMR studies on Fraser fir *Abies fraseri* (Pursh) Poir. lignins. *Holzforschung* **2005**, *59*, 488-496.